Estimation of Uncertain Vehicle Center of Gravity using Polynomial Chaos Expansions

Darryl Price

Thesis submitted to the Faculty of Virginia Polytechnic Institute and State University
in partial fulfillment of the requirements for the degree of

Master of Science
in
Mechanical Engineering

Dr. Steve Southward, Chairman
Dr. Adrian Sandu
Dr. Corina Sandu

June 3, 2008
Virginia Polytechnic Institute and State University
Blacksburg, Virginia

Keywords: polynomial chaos expansion, center of gravity, 8-post test, Galerkin method

Estimation of Uncertain Vehicle Center of Gravity using Polynomial Chaos Expansions

Darryl Price

Abstract

The main goal of this study is the use of polynomial chaos expansion (PCE) to analyze the uncertainty in calculating the lateral and longitudinal center of gravity for a vehicle from static load cell measurements. A secondary goal is to use experimental testing as a source of uncertainty and as a method to confirm the results from the PCE simulation. While PCE has often been used as an alternative to Monte Carlo, PCE models have rarely been based on experimental data. The 8-post test rig at the Virginia Institute for Performance Engineering and Research facility at Virginia International Raceway is the experimental test bed used to implement the PCE model. Experimental tests are conducted to define the true distribution for the load measurement systems' uncertainty. A method that does not require a new uncertainty distribution experiment for multiple tests with different goals is presented. Moved mass tests confirm the uncertainty analysis using portable scales that provide accurate results.

The polynomial chaos model used to find the uncertainty in the center of gravity calculation is derived. Karhunen-Loeve expansions, similar to Fourier series, are used to define the uncertainties to allow for the polynomial chaos expansion. PCE models are typically computed via the collocation method or the Galerkin method. The Galerkin method is chosen as the PCE method in order to formulate a more accurate analytical result. The derivation systematically increases from one uncertain load cell to all four uncertain load cells noting the differences and increased complexity as the uncertainty dimensions increase. For each derivation the PCE model is shown and the solution to the simulation is given. Results are presented comparing the polynomial chaos simulation to the Monte Carlo simulation and to the accurate scales. It is shown that the PCE simulations closely match the Monte Carlo simulations.

ACKNOWLEDGEMENT

I would first like to thank my advisor, Dr. Steve Southward, whose help and guidance throughout my time as a master's student has been invaluable. Though always juggling more projects and work than I can imagine, Dr. Southward was always able to find time for me and his other students. The use of the 8-post rig has been a unique research opportunity. Also, taking the driving simulator for a few spins at the VIPER Grand Opening surpassed all my years of *Gran Turismo* experience.

I want to thank the NASA-VIPER program for supporting my research at Virginia Tech. Dr. Adrian Sandu and Dr. Corina Sandu have been very kind to be a part of my committee and helpful as I learned polynomial chaos theory. I want to thank the other professors of CVeSS who taught me academic knowledge and industry skills. Thank you Dr. Ahmadian for bringing me into the CVeSS organization. Thanks to everyone on the NASA-VIPER team who have answered technical questions and provided help. I want to thank all my fellow grad students at CVeSS for keeping life interesting on a daily basis and providing help and tips to make a rough road a bit easier. I want to thank Parham Shahidi for making the many trips to Danville, VA with me and making the ride much more enjoyable and easier. I want to thank Sue Teel always being understanding and helpful the many times I would bother her for help with paperwork, copier problems, and other miscellaneous office troubles. I want to thank the many other people at CVeSS who have made these years at Virginia Tech a positive experience in my life.

I also want to thank my best friends, Brent, Page, and Matt (K104), who have always provided much needed great stress relief and support. They've given me so many unforgettable experiences and I look forward to many more. I want to thank Christine, who has helped me through many tough times. She is remarkable. No matter the situation, she makes it better. Christine also makes the best blackberry-raspberry cobbler in the world.

I want to thank my parents, Larry and Sandy, and my family for all their support in life and school. Without them, I would not have all the opportunities in life that I before me today. My parents have helped me in every way they could. I will never be able to repay them for all the opportunities they have given me. I am indebted to the rest of my family as well for their support in my endeavors. Lastly, I want to thank my nephews, Ethan and Caden, for always smiling and being full of energy.

CONTENTS

LIST OF NOMENCLATURE

W	total weight of the vehicle [lbs]
W_F	weight of the front axle [lbs]
CG	center of gravity of the vehicle
h	height of the center of gravity [in]
a	distance of the front wheels to the CG [in]
b	distance of the rear wheels to the CG [in]
h_1	height of the centerline of the vehicle [in]
b_1	distance of the rear of the vehicle to the lifted CG [in]
l_1	wheelbase with rear of vehicle lifted [in]
l	wheelbase of vehicle [in]
θ	angle of vehicle above horizontal [radians] b
R_L	radius of tire [in]
ζ	random variable
ϕ	basis function for single uncertain distribution
n	order of polynomial chaos function
L	wheelbase of vehicle [in]
T	track of vehicle [in]
x	longitudinal CG coordinate [in]
y	lateral CG coordinate [in]
LF	left front wheel
RF	right front wheel

LR	left rear wheel
RR	right rear wheel
F_1, F_2, F_3, F_4	load at each wheel (LR, LF, RF, RR) [lbs]
M_x	moment in the longitudinal direction [lbs-in]
M_y	moment in the lateral direction [lbs-in]
α, β	parameters to define beta distribution
a, b, c, d	polynomial chaos coefficients for each force
s	order of single PCE input
w	weighting function
δ	precomputed matrix of integrals
ψ, γ, χ, τ	coefficients for matrices
p	probability
Φ	basis function for multiple varibles

LIST OF TABLES

LIST OF FIGURES

1. INTRODUCTION

This chapter discusses the motivation behind the research. The objectives of the research are discussed next, and the chapter ends with an outline of the remainder of the thesis.

1.1 Motivation

In research and design it is necessary to know the confidence one has in a measurement, a parameter, or a design. If not properly analyzed and considered, an uncertain parameter can have unforeseen impacts on other parameters or dynamics of the system. There are various methods of analyzing these uncertainties. One common method is the Monte Carlo simulation.

The Monte Carlo simulation finds the uncertain parameters uncertainty distribution through trial events. As long as each parameter is represented with its proper uncertainty distribution and enough attempts are made, the correct uncertain parameter distribution can be attained. It requires thousands to millions of trials may be needed to find a good approximation of the true distribution And may take a lot of computational power and time.

To analyze uncertainties the NASA-VIPER research team has been implementing other methods, one of which, is the polynomial chaos approach. There are several polynomial chaos approaches including collocation and the Galerkin method, each of which, has distinct advantages and will be discussed later.

Polynomial chaos has been shown to work for dynamic and static simulations, but rarely have the simulations been directly related to real world tests. The direct correlation between reality and simulation must exist for the simulation to be useful. This study will use the 8-post rig at the Virginia Institute for Performance Engineering and Research

(VIPER) Lab to test the validity of the polynomial chaos approach against real world results.

The VIPER Lab has recently built an 8-post rig at its facility at VIR (Virginia International Raceway). An 8-post rig is a vehicle dynamics rig that is used to analyze a vehicle’s suspension dynamics. The rig has the ability to put the vehicle through numerous tests to determine the vehicle’s ability to negotiate different road or terrain conditions. This is done through its four wheel shakers and four aero loaders. The wheel shakers are hydraulically driven and provide the road input. The four aero loaders are pneumatically powered and can provide other forces to the vehicle chassis such as: inertial forces from braking, cornering, and accelerating and aerodynamic forces. The 8-post rig has been designed to operate with race vehicles to vehicles larger than a military Humvee. The equipment is designed to operate under dynamic situations and therefore measures high loads. This brings into question the accuracy of the load cells on the rig. Each load cell system is built to handle loads as high as 10,000 lbs to accommodate the dynamic forces of a heavy vehicle, while a static center of gravity test may measure loads as small as 400 pounds to a wheel.

An important parameter to vehicle characteristics is its center of gravity. It would be useful to find this parameter by using the load cell system on the 8-post rig since this rig is used to define many vehicle parameters. However, the uncertainties for a lighter vehicle sitting statically may be significant. Each wheel pan would be working around 5% of total capacity for a vehicle that weighs a ton. The uncertainties in these measurements create a useful test bed to implement polynomial chaos theory to an experimental situation.

1.2 Objective

The objective of this study is to setup a method to use polynomial chaos expansion to analyze the uncertainties in a real world situation based upon the calculation of a known parameter. This objective will be achieved by using VIPER's 8-post rig as a test bed. The method in achieving this goal is to use polynomial chaos expansion to propagate the uncertainty in the wheel load through the center of gravity equation. A distribution will be found to represent the wheel load uncertainty from vehicle testing and used in the PCE model. The simulation will be confirmed through a Monte Carlo Simulation and with accurate portable wheel scales.

1.3 Outline

The following thesis begins with a background of the subjects in the study. This includes a literature review of techniques used to find the center of gravity of a vehicle as well as other studies using polynomial chaos expansion theory. Chapter four details the 8-post rig at the VIPER facility and describes the experimental testing and the results from those tests. Chapter five derives the polynomial chaos expansion model for two separate uncertain wheel loads. Then the results of simulations are shown to show how an uncertainty impacts the center of gravity uncertainty. Also, results from the 8-post experiment are used for some of these simulations. Chapter six derives the polynomial chaos expansion model for multiple uncertain wheel loads using data collected in the experimental testing is used in the polynomial chaos simulations. The results from these simulations are discussed in chapter six as well. The thesis concludes with the results and recommendations in chapter seven.

2. LITERATURE REVIEW

This section presents the results of previous literature in the areas of vehicle center of gravity calculation and error analysis and polynomial chaos theory. The differences between previous literature and those presented in this paper are also discussed.

2.1 Center of Gravity Calculation

Locating the center of gravity of a vehicle is important for anticipating the vehicle's behavior in different situations. The easiest way to find the lateral and longitudinal coordinates of the center of gravity is to place the vehicle on four individual level scales. First, the track and the wheelbase of the vehicle are recorded. Then the weight at each wheel is recorded. The weight from each wheel and geometry are used in moment calculations to find the center of gravity in the longitudinal and lateral equations. This method is shown in more detail in Milliken's Race Car Vehicle Dynamics [1] and is discussed more in Chapter 3.

The most difficult center of gravity coordinate to attain in a vehicle is the height. There are multiple methods to attain this parameter, one of which, is to lift the rear axle of the vehicle so the front to rear wheel centerline creates a certain angle, θ, with the horizontal. A diagram of this is shown in the following figure which was reproduced with permission from Milliken.

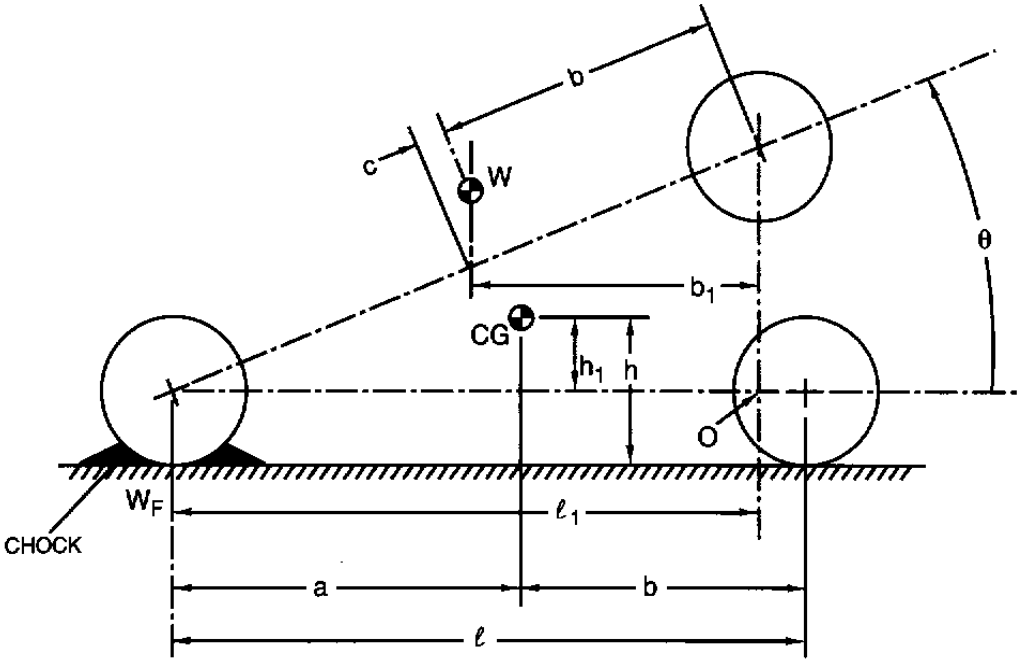

Figure 2.1: Modified Reaction Method for Locating Vehicle CG Height (Milliken, 1995)

The new configuration will cause a shift in vehicle weight towards the front wheels thus presenting a new center of gravity position. Knowledge of the vehicle parameters such as wheelbase (l), radius of front (R_{LF}) and rear wheels (R_{LR}), total weight of vehicle (W), and longitudinal distance of the center of gravity (a)of the vehicle are required. Special care must be taken in these tests such as the suspension motion must be locked. This prevents the suspension from impacting the results through stiction in the springs and damper.. The solution for vehicle height is given by equation (2.1).

$$h = R_L + \left(\frac{W_F l - Wb}{W \tan\theta} \right) \tag{2.1}$$

R_L is the radius of the front tires, W is the total weight of the vehicle, and W_F is the weight of front of the vehicle during the test. A more complex equation is required if the front and rear wheels have different radii. A more in depth look at this method can be found in references [1, 3, and 4].

The above method of finding the center of gravity height can be used on a four post rig. The accuracy of test depends on the θ that is achieved in tilting the vehicle. In general a greater θ will achieve better accuracy. High accuracy can be achieved if the vehicle can be tilted forty degrees or more. More accurate results are produced for heavy vehicles, ones that weigh more than 1500 kg, than lighter ones. One advantage of using this method is that it requires very little specialty equipment. One simply needs vehicle scales and a way to lift the rear of the vehicle. If the vehicle can be lifted to high angles, forty degrees or more, accuracy of $(\pm 2\%)$ can be attained for large vehicles. Other more difficult methods to locating the center of gravity height require special rigs.

Four different methods of finding center of gravity height are compared to each other in *Error Analysis of Center-of-Gravity Measurement Techniques* by Shapiro, Dickerson, et al [3]. The modified reaction method has already been discussed. The null point method requires a platform that has two parallel knife edges several inches apart from each other. In this method the vehicle is placed so the center of gravity is between the two knife edges. The vehicle is then tilted in either direction until the vehicle balances on one knife edge. This indicates when the vehicle CG has rotated outside the stable zone between the knife edges. Therefore, the CG height can be calculated from the two tilt angles. This method is more accurate than the modification reaction method, but requires a special rig.

Another method is the weight balance method. This method balances the vehicle on a rotating platform. Then a known mass is added to the platform to provide a torque. The amount the platform rotates will allow the height of the vehicle CG to be derived. Like the null point method, the weight balance method is very accurate, but requires a special rig [2]. The last method analyzed is the pendulum method. This method swings the vehicle at the end of a pendulum. Then the length of the pendulum arms is changed. Once again the vehicle is swung on the pendulum. The change in the period of the oscillation will allow the center of gravity of the vehicle to be attained. The advanced rig for this test does not provide significant increases in accuracy over the modified reaction method.

The goal of this thesis is to use polynomial chaos expansions to analyze the uncertainty in the load cell measurement system in the 8-post rig. Therefore, the distribution of the output from the load cell system will be used to analyze the uncertainty in the load measurement system. This information will be propagated through the perfect center of gravity calculation process to impact the lateral and longitudinal center of gravity coordinates of a vehicle.

2.2 Polynomial Chaos Expansion

Polynomial chaos expansion is a method that can be used to represent random variables as functions. The random variable can be represented by orthogonal polynomial chaos series. This series is constructed in the much the same way that the Fourier series is constructed except the functions are an orthogonal set of polynomials instead of complex combinations of sines and cosines. The series for polynomial chaos is created by the Karhunen-Loeve Expansion [7, 8, 11, 13, 15, 16].

$$\omega(x,\theta) = \sum_{n=0}^{\infty} \sqrt{\lambda_n} \xi_n(\theta) f(x) \tag{2.2}$$

This expansion was derived independently by Karhunen in 1947, Loeve in 1948, and Kac and Siegert in 1947. $\xi_n(\theta)$ is a set of random variables, λ_n is a constant, and $f(x)$ is an orthonormal set of deterministic functions, also know as basis functions [8].

The basis functions $\phi_j(\xi(\theta))$ are Askey-Weiner polynomial chaos expansions. They are in terms of the random variable, ξ. Multiple orthogonal polynomial sets are known that can represent different distributions. While theoretically any orthogonal polynomial set can represent any distribution, different sets more naturally represent a certain distribution as shown in Table 2.1. These sets also converge faster to the solution because they require less polynomials to represent the distribution [7-9].

Table 2.1: Askey-Weiner Polynomial Chaos Basis Function Sets [9]

Distribution	**Orthogonal Basis Function Set**
Gaussian	Hermite
Gamma	Laguerre
Uniform	Legendre
Beta	Jacobi
Poisson	Charlier
Negative Binomial	Meixner
Binomial	Krawtchouk
Hypergeometric	Hahn

The highlighted uniform and beta distributions in Table 2.1 are used in for this study. The uniform distribution can be represented by the Legendre polynomials. The uniform distribution only needs two of these polynomials to represent the distribution [7, 8, 10].

$$\phi_n(\zeta) = \left(\frac{1}{2^n(n!)}\right)\frac{\partial^n}{\partial\zeta^n}\left(\zeta^2 - 1\right)^n = \begin{cases} 1 & n = 0 \\ \zeta & n = 1 \\ 1/2\left(3\zeta^2 - 1\right) & n = 2 \\ \vdots & \vdots \end{cases} \tag{2.3}$$

The beta distribution is best represented by Jacobian polynomials. These polynomials are chosen by α and β that define the beta distribution. The Askey-Weiner polynomials and Karhunen-Loeve expansions can be placed into ODE's, state-space models and other processes to represent uncertain variables or distributions as functions. There are two methods for solving these functions, Galerkin and Collocation [7, 8, 14, 15].

The overall differences in these methods are the Galerkin method provides an analytical result, but the Collocation method decreases the computational requirements in plotting the distribution and does not provide as an exact of a solution. The Galerkin method can efficiently solve for the analytical results, but the distributions can take longer to compute than the collocation method. The collocation method decreases the number of runs the solution must take by using pseudo-spectral methods. This method does not provide an analytical solution and requires some guess work in choosing collocation points. Still, it can significantly reduce the processing time over Monte Carlo or Galerkin methods and provide a good result. Since our process is static, computation time was less of a focus than arriving at a true solution. Therefore, the Galerkin method is used in this study. It should be noted that solving for the analytical equation via the Galerkin method is very fast, but plotting the solution is not as fast as the collocation method [7, 14].

3. PROBLEM DEFINITION

This section will define the problem and derive the equations used to find the center of gravity of a vehicle in the lateral and longitudinal directions. Polynomial chaos expansions will be used to analyze uncertain variables in the center of gravity equation in later chapters.

3.1 Calculation of Vehicle Center of Gravity

The longitudinal and lateral center of gravity positions of a vehicle can be determined by knowing the effective normal forces of the vehicle at each wheel. This method is used as the simplest method to find the lateral and longitudinal center of gravity of a vehicle. It assumes the vehicle is completely static while the forces are measured. Any movement would create dynamic forces that would significantly impact the accuracy of the test.

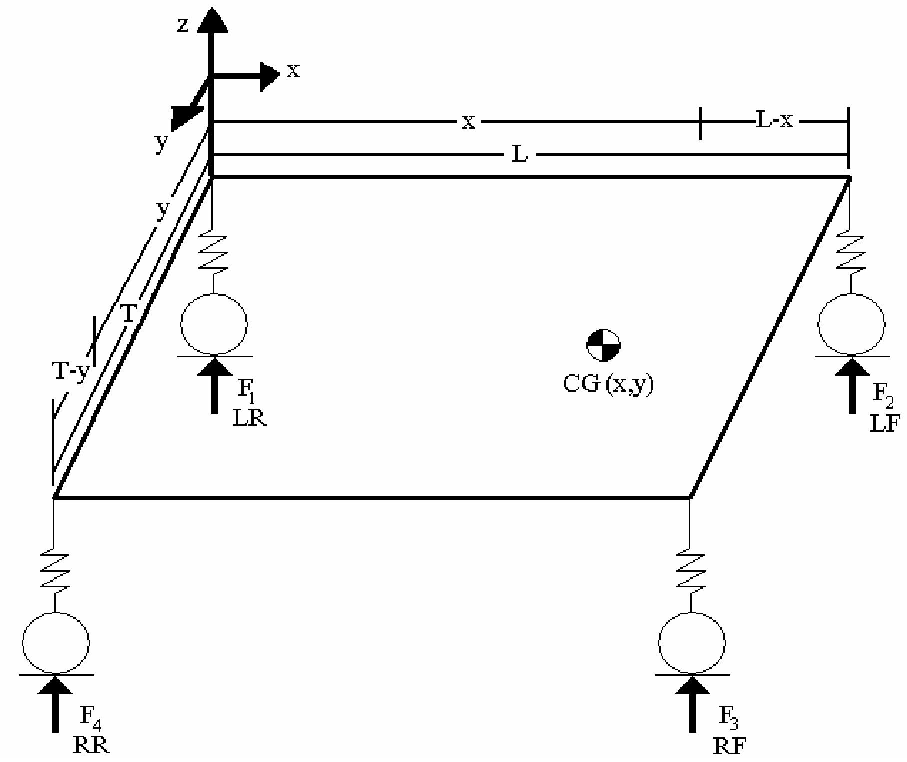

Figure 3.1: Force Diagram of Vehicle

Figure 3.1 shows the force diagram of a stationary vehicle. F_1, F_2, F_3, F_4 are the normal forces at each wheel of the vehicle, *x* and *y* relate to the center of gravity, CG, coordinates of the vehicle, and *L* and *T* are the wheelbase and track of the vehicle. Static force and moment equations can be used to find the center of gravity coordinates independently of each other.

$$\begin{aligned} \sum M_x &= (F_2 + F_3)(L - x) - (F_1 + F_4)x = 0 \\ \sum M_y &= (F_1 + F_2)y - (F_3 + F_4)(T - y) = 0 \end{aligned} \tag{3.1}$$

Solving for x and y.

$$\begin{aligned} &(F_2 + F_3)L - (F_2 + F_3)x - (F_1 + F_4)x = 0 \\ &(F_1 + F_2)y - (F_3 + F_4)T + (F_3 + F_4)y = 0 \end{aligned} \tag{3.2}$$

$$\begin{aligned} (F_1 + F_2 + F_3 + F_4)x &= (F_2 + F_3)L \\ (F_1 + F_2 + F_3 + F_4)y &= (F_3 + F_4)T \end{aligned} \tag{3.3}$$

$$\begin{aligned} x &= \frac{(F_2 + F_3)L}{(F_1 + F_2 + F_3 + F_4)} \\ y &= \frac{(F_3 + F_4)T}{(F_1 + F_2 + F_3 + F_4)} \end{aligned} \tag{3.4}$$

Equation (3.4) is used to find the longitudinal and lateral center of gravity positions of a vehicle. The vertical CG position is found through other methods such discussed in the literature review. From the above derivation, it is clear that the lateral CG equation is nearly identical with the longitudinal CG equation. The differences between the two equations are the two different forces and the multiplication by different lengths in the numerator. The reasons for the differences in the equations are strictly due to the geometry of the vehicle.

3.2 Process Definition

Parameters within equation (3.4) can have uncertain values, but the process itself is perfectly deterministic. The wheelbase, L, and track, T, of the vehicle are set and well known due to the geometry of the chassis. The four force inputs are impacted by changes in the position of the mass or if it is added or subtracted from the vehicle. This process looks like the system below.

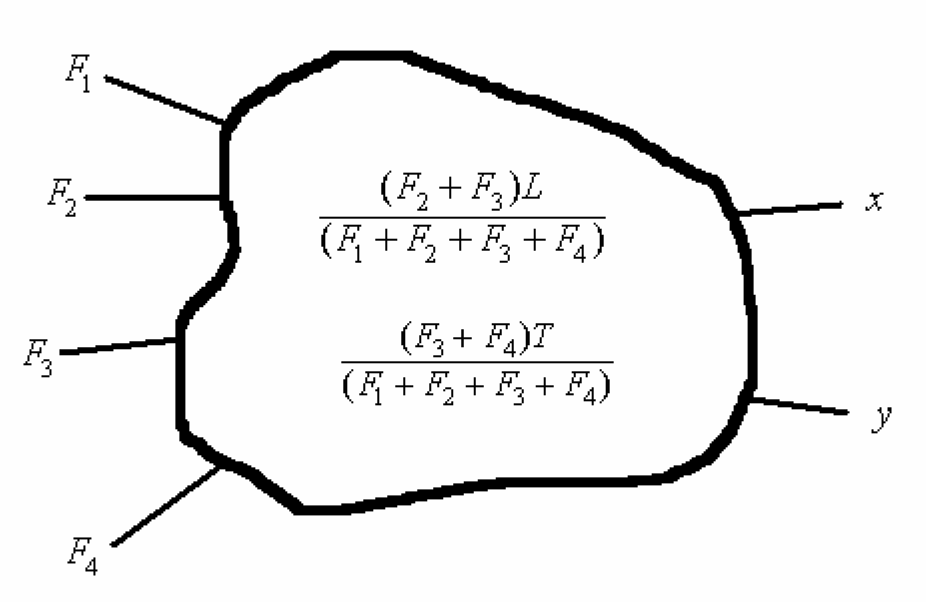

Figure 3.2: Lateral and Longitudinal CG Calculation Process

The process shown above has no uncertainty included in the system. This would be the ideal case and is often assumed while calculating the CG of a vehicle. In the real world, there are no certain measurements. While engineers strive to ensure that the uncertainty from measurement devices is negligible, there will be cases where this assumption is not applicable. The wheelbase and track of the vehicle can be measured very accurately with simple equipment. Significant error can be found while measuring the four normal forces if the load cells are made to perform an array of tasks beyond simply weighing vehicles in the same mass range. Uncertainties from the four wheel loads will be analyzed using polynomial chaos in the following sections.

4. UNCERTAINTY CHARACTERIZATION: 8-POST TEST RIG

The VIPER 8-post rig at Virginia International Raceway (VIR) is a one of a kind shaker for testing vehicle suspension performance under a controlled laboratory environment. This rig has 4-hydraulic shakers, one for each wheel, that can independently input a displacement and velocity into each wheel of the vehicle. It also has four pneumatic loaders, also known as aero loaders, that can apply other forces to the vehicle chassis to simulate aerodynamic forces as well as vehicle inertial forces.

An important first step in characterizing a vehicle's performance is to find the center of gravity of that vehicle. The 8-post test rig has a load measurement system for each wheel. This provides the information needed to solve for the lateral and longitudinal CG positions of the vehicle, equation (3.4). The problem for this rig is the significant amount of uncertainty in the measurement of the loads at each wheel.

There are several reasons for the uncertainty in the load measurement system. The four load measurement systems, one for each wheel, are composed of the following components: four load cells, data distribution and summing system, and data acquisition system. Each of these components introduces uncertainty to the load measurement system and further complicates the uncertainty's distribution. Each of the four load cells within the wheel pan has a load capacity of 10,000 lbs, so the system can meet the demands of large vehicles under dynamic conditions. Testing large off road vehicles on the 8-post rig can cause very large loads under dynamic conditions. The large range due to this fact causes problems for the accuracy of the system for many typical cars and motorsport vehicles. For these cars the load measurement system can be working under 5% of the total capacity of the system during static conditions, the same conditions a center of gravity test would be taken under. If the load measurement system is accurate to even 0.1% of its total capacity the error range would be 10 lbs, with 1% accuracy error would be 100 lbs. This is just the uncertainty created by the load sensors. Since each load pan has four load sensors as shown in the figure below, there must be a data distribution and acquisition system for each measurement system. *A, B, C,* and *D* represent each of the four wheel load sensors.

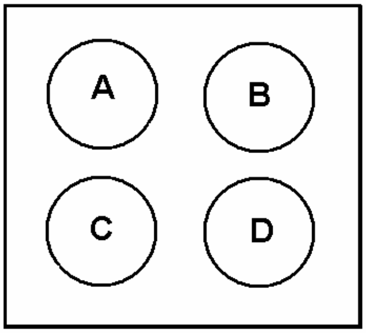

Figure 4.1: Wheel Pan with Four Load Sensors

The data distribution impacts the uncertainty in that it sums the four load sensors together. Also, the actual digital resolution can impact the uncertainty of the load measurement system. The data distribution and acquisition methods are largely unknown due to the black box system, the analytical characterization of uncertainty in the measurement is unclear. Therefore, a test would provide the best means to characterize the uncertainty in the measurement.

4.1 Characterization of Load Measurement System Uncertainty

Characterizing the uncertainty of the load measurement system involves taking multiple load measurements of the vehicle on the 8-post rig. The vehicle used is a retired NASCAR Sprint Cup car that was donated by Petty Racing.

Figure 4.2: NASCAR Cup Car used for Uncertainty Characterization (Car donated by Petty Racing Team, permission to use photo granted)

This car was one of two donated by the Petty Racing Team. It is missing the engine and transmission, but the chassis and suspension are complete. The lack of engine and transmission will impact the total weight of the vehicle and move the weight distribution towards the rear of the vehicle. The impact on our tests for this situation is simply that the measurements will be taken on a vehicle lighter than a typical cup car and not fall within a typical CG location.

The goal of this test is to characterize the uncertainty of each wheel's load measurement system by simulating the center of gravity under normal conditions. The CG test could be run either before or after dynamic tests with the vehicle wheels located anywhere safely on the wheel pan. Enough tests would also be conducted to get an adequate approximation of the distribution of the load uncertainty.

Figure 4.3: Load Measurement Output Display

In order to accomplish these goals the following procedure was taken. First, the vehicle was be placed on the 8-post rig ensuring that all wheels are on the wheel pan with no weight being held by any other object or platform. Then a measurement was taken from the measurement panel seen in Figure 4.3. The top four display outputs relate to the wheels as an overhead view with the front of the car at the top of the display so the LF wheel is the top left output. The bottom two outputs relate to relative weight distributions. Several different methods were used to move the vehicle on and off the 8-post test rig. The vehicle was either rolled on and off the 8-post rig or hydraulic jacks were used to lift each side of the vehicle and lower it back onto the rig. This put a bit of randomness into the vehicle positioning on the wheel pan. After the vehicle was moved on and off, the suspension was depressed at all four corners to remove stiction in the suspension.

This process was repeated until fifty measurements had been taken for the load at each wheel. Fifty measurements should provide enough data to attain a distribution for each load measurement system. The last step in this process is to have an actual value for the wheel loads in order to have a direct comparison between that and the load measurement system's distribution.

Longacre Computerscales DX was used to find a much more accurate "true" value for the vehicle weight at each wheel. These scales are specifically designed specifically to measure the weight of a vehicle to find vehicle characteristics such as the center of gravity. Therefore, they are very accurate within the range of a vehicle's weight. Each of the four scales has a maximum weight capacity of 1500 lbs and accuracy within a pound of the true value.

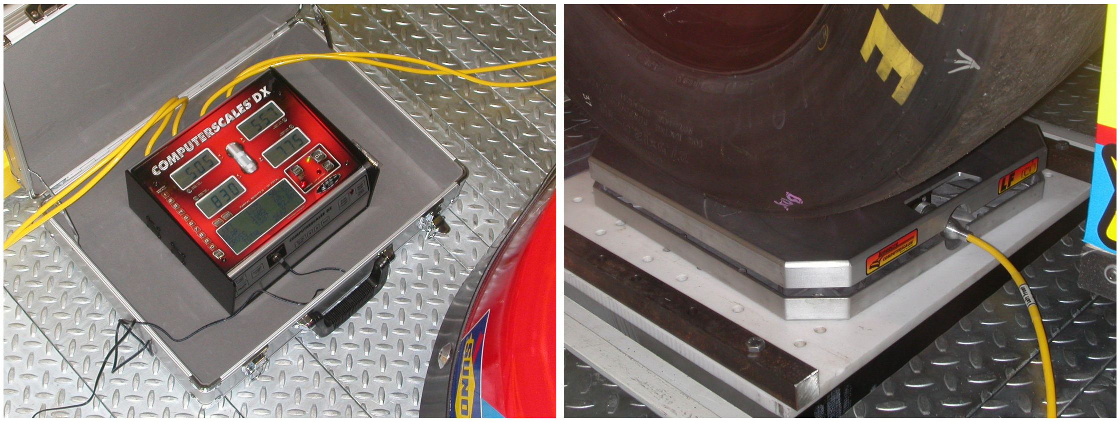

Figure 4.4: Longacre Computerscales DX

The procedure for weighing a vehicle with Longacre Computerscales DX [19]:

- Set scale pads next to wheels.
- Place control box in convenient place, uncoil cables, and plug into pads.
- Turn on computerscales box and allow to warm up.
- Zero all 4 pads.
- Lift vehicle and place pads under each wheel.
- Shake each corner of the vehicle to remove stiction in the shock absorbers.
- Record vehicle weight at each wheel.

4.2 Load Measurement System Distribution Results

The first test was conducted to characterize the distributions of the four force measurement systems. From that information, the ideal polynomial chaos basis functions can be chosen to best fit the distribution.

The following distribution histograms were created by finding the minimum and maximum recorded forces for each wheel load cell. This range was divided into equal histogram bins and the number of force records was counted in each bin. The vehicle weight from the accurate Longacre Computerscales DX is included in the figure to give a comparison of the vehicle load cell distributions to the portable scales weight.

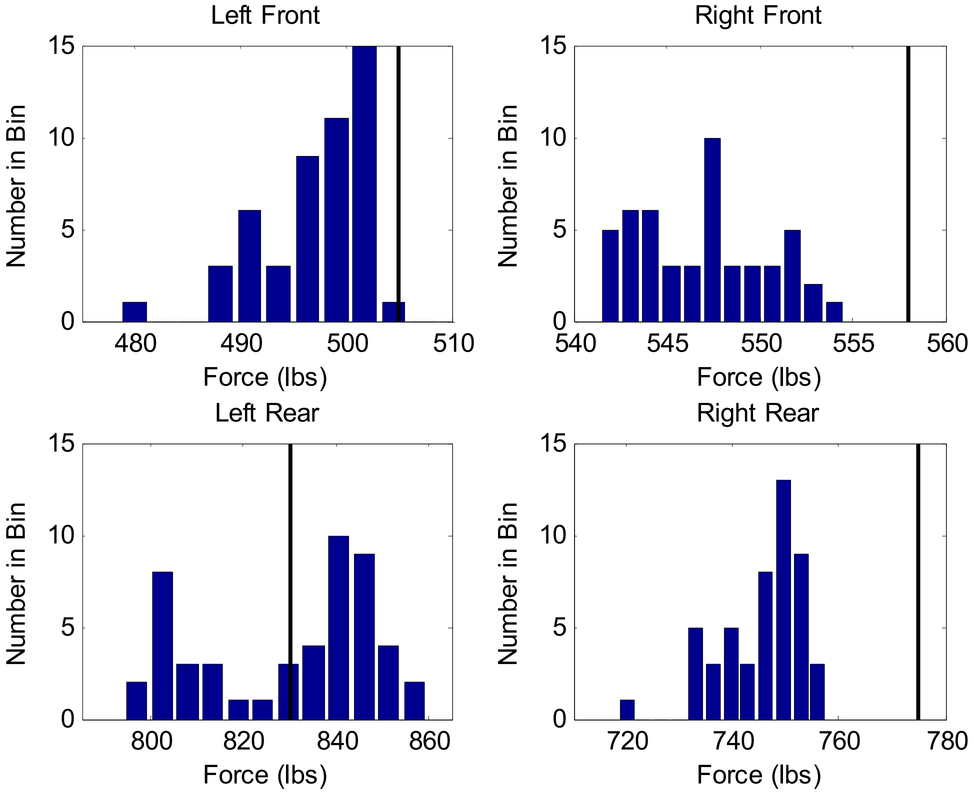

Figure 4.5: Force Distributions from Test 1

From the above figures, the left front and right rear distributions appear to resemble a skewed Gaussian distribution. The force clearly has a greater possibility of occurring at the high end of the force range than in the center. Also, the force tapers off on the lower side for each wheel and the left front and right rear wheels have a point 10-15 lbs lower than the rest. The right front wheel distribution has a less distinctive distribution. One could draw the conclusion that this distribution is uniform with merely more hits on one number in the center by chance or that the distribution is Gaussian. The left rear load distribution is also not distinctive. Analyzing this distribution one can arrive at one of two conclusions: the distribution consists of two peaks or the distribution is a skewed Gaussian distribution like the left front and right rear distributions. To arrive at the second conclusion, to the test would be consided imperfect; therefore, it is possible for the data to land in one position more than another just for this test, thus skewing results. Based on the data from the left front and right rear, the left rear distribution is also a skewed Gaussian distribution with a testing error within the second bin.

The actual load at each wheel reveals that there is also a bias error in the load measurement system. This error causes the system to underestimate the vehicle's weight at three of the four wheels. The distributions for the LF, RF, and RR do not include the actual load for these wheels. The left rear distribution does include it, but this distribution is the largest of the four at sixty pounds. The bias of the load measurement system should be factored into the final solution of the distribution. Table 4.1 provides an overview of many of the statistical properties of each distribution without modification for the bias error. It also includes the true measure of the load at each wheel.

Table 4.1: Distribution Statistics

	Mean (lbs)	Median (lbs)	Range (lbs)	Variance(lbs)	Actual (lbs)
LF	497.6	500	47	58.4	505
RF	547.6	548	12	10.5	558
LR	833.2	841	60	354.4	830
RR	746.9	749	36	58.6	775

A skewed Gaussian distribution is defined as a probability from negative infinity to positive infinity. The force measurement system will never grow that far out of range of the actual measurement. If it did, the measurement would be rejected as incorrect or an outlier. A more realistic distribution would have limits outside the measurement range to limit the possible measurements from attaining impossible or clearly incorrect values. In order to create a more realistic distribution, a beta distribution is used.

Beta distributions are characterized by the coefficients α and β. The general shape of a beta distribution is defined via α and β in the following table.

Table 4.2: Beta Distribution General Shape

$\alpha < 1$	$\beta < 1$	U-shaped Distribution
$\alpha < 1$	$\beta \geq 1$	Decreasing
$\alpha = 1$	$\beta > 1$	Decreasing
$\alpha = 1$	$\beta > 2$	Convex
$\alpha = 1$	$\beta = 2$	Straight Line
$\alpha = 1$	$1 < \beta < 2$	Concave
$\alpha = 1$	$\beta = 1$	Uniform Distribution
$\alpha > 1$	$\beta > 1$	Unimodal

The reverse of the distributions in Table 4.2 can be attained by switching α and β. From this table a unimodal distribution would best characterize the load measurement system's distribution. The unimodal distribution can be varied by choosing any combination of α and β greater than one.

A (5,2) beta distribution was chosen to best fit the overall data collected. This distribution does not need to perfectly fit the data since the polynomial chaos basis functions allows precise alteration in the shape of the distribution to model the collected data. The orthogonal polynomial basis functions will be chosen based on this distribution.

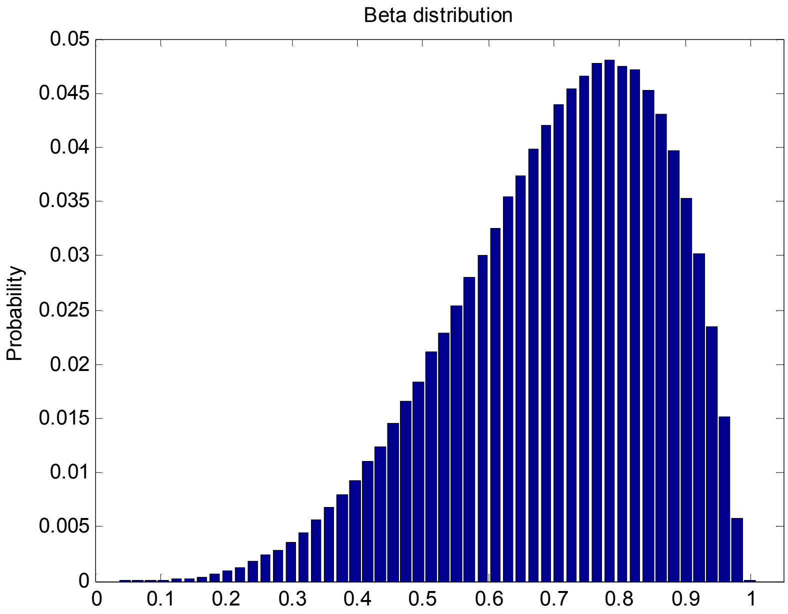

Figure 4.6: Beta (5,2) Distribution

The next step in the application of this distribution to the data from test one involves choosing the coefficients to the orthogonal polynomial basis functions. Choosing the orthogonal basis functions will be discussed in chapter 5, but for now it will be stated that Mathematica was used to find the jacobian basis functions.

$$\phi_n = \left\{ \begin{array}{c} 1 \\ (3/2)(-1+3\zeta) \\ (1/4)(-1-30\zeta+55\zeta^2) \\ (1/4)(7-11\zeta-99\zeta^2+143\zeta^3) \\ \vdots \end{array} \right\}. \tag{4.1}$$

These basis functions can define the distributions for each parameter via the following equations. Equation (4.2) relates the forces to the proper wheel locations as indicated previously in Figure 4.9.

$$\begin{aligned}\widehat{F}_1(\zeta_1) &= \sum_{i=1}^{s} a_i\phi_i(\zeta_1)\\ \widehat{F}_2(\zeta_2) &= \sum_{i=1}^{s} b_i\phi_i(\zeta_2)\\ \widehat{F}_3(\zeta_3) &= \sum_{i=1}^{s} c_i\phi_i(\zeta_3)\\ \widehat{F}_4(\zeta_4) &= \sum_{i=1}^{s} d_i\phi_i(\zeta_4)\end{aligned} \tag{4.2}$$

The basis functions are given to the 7th order in the appendix. The coefficients (*a,b,c,d*) of these basis functions are chosen to create an accurate representation of the collected data. s is the highest order of the basis functions used to define the input distributions.

It is known that the data is imperfect, but ultimately captures the trend of the real world distribution. Therefore, the goal is to not to exactly recreate these distributions precisely, but to create distributions that capture the overall trend of the real distributions.

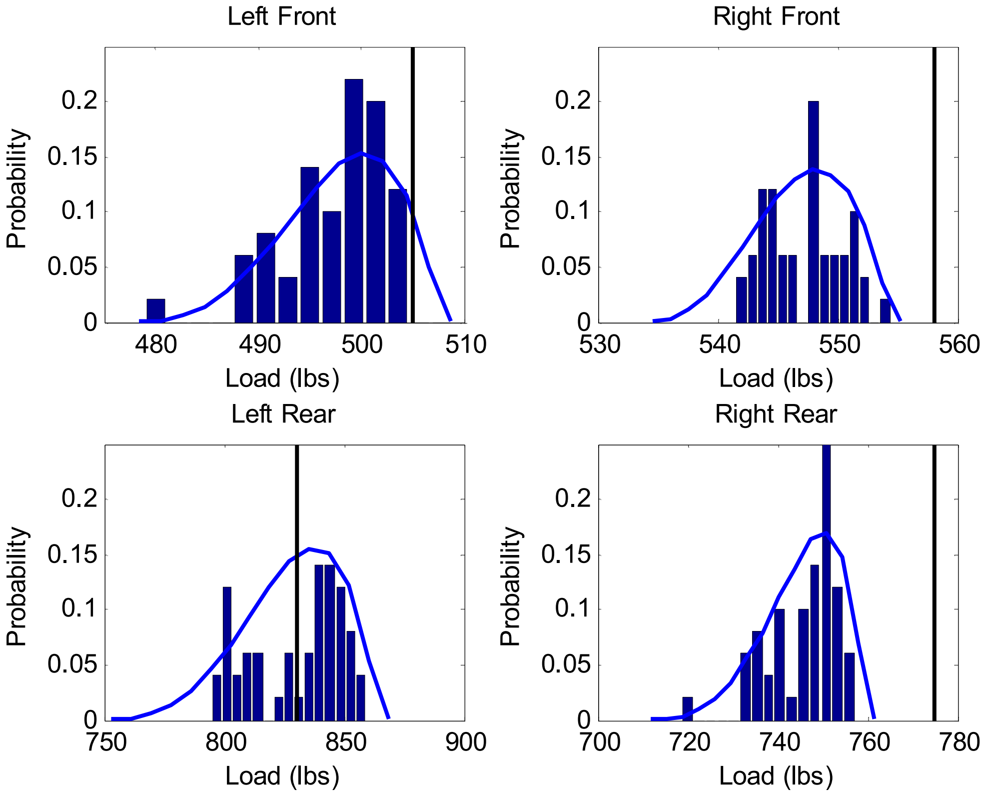

Figure 4.7: Experiment Data vs Polynomial Chaos Estimated Distributions

In the figure above, the histogram bar plots are the experimental data and the blue curved lines represent the estimated polynomial chaos distribution for each wheel load cell. The wheel load from the portable scales is represented by the black line. These polynomial chaos distributions provide an accurate representation of the true data. The *LR* and *RR* distributions closely match the beta distribution however it can be seen that these distributions do not include the true wheel load found from the Longacre Computerscales DX. The following table gives the coefficients of the polynomial basis functions for the four distributions.

Table 4.3: Polynomial Coefficient Values to Define Input Distributions

		Polynomial Coefficient Values						
Wheel Location	**Force Label**	**Zeroth order**	**1st order**	**2nd order**	**3rd order**	**4th order**	**5th order**	**6th order**
LF	**F2**	529.25	3	0.25	0.05	0	0	0
RF	**F3**	467.5	6	0.25	0	0	0	0
LR	**F1**	708	25	0.5	0	0	0	0
RR	**F4**	690	12	0.25	-0.1	0	0	0

A bias error in the input distributions exists, preventing them from including the true value of the wheel load. Bias error is different from random error in that it is repeatable. The simplest way to take into account the bias value is to shift the PCE distribution to center over the true value. This can be done by changing the first coefficient which only multiplies by one. The bias error can be calculated by finding the difference between the actual value and the highest value found from the experiment.

$$Error_{bias} = \left(\frac{F_{actual} - F_{highprob}}{F_{median}} \right) \tag{4.3}$$

To adjust the distribution to account for the bias error, the median value is multiplied by the bias error plus one.

$$F_{shifted} = F_{highprob}\left(Error_{bias} + 1\right) = F_{actual} \tag{4.4}$$

Accounting for the bias error in the polynomial chaos functions involves, adding the difference between the F_{actual} and $F_{highprob}$ to the first coefficient in the PCE model.

$$a_{adjusted} = a_0 + \left(F_{actual} - F_{highprob}\right) \tag{4.5}$$

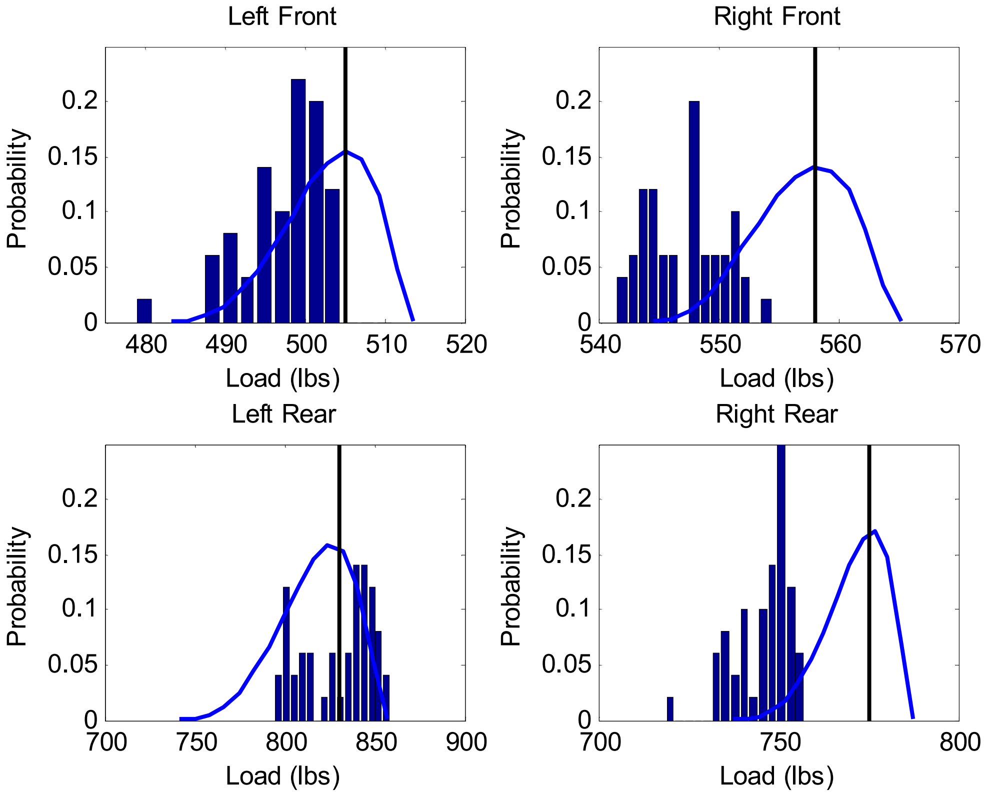

Figure 4.8: Bias Corrected Distributions

Figure 4.8 shows the PCE model distribution shifted to have the greatest probability at the portable wheel scales. The actual shape of this distribution has not been changed from the initial distribution test since only the first polynomial chaos coefficient has been changed.

The bias error will not be included in the moved mass tests. However, the method should be noted in case one is dealing with a system with improper calibration to cause a bias error.

4.3 Moved Mass Test

The second test was completed while the vehicle was in a slightly different configuration. The aero loaders were not attached to the vehicle in the distribution test. However, for the moved mass tests all four aero loaders were attached, two on each side of the vehicle. The aero loaders force output is set to zero, but this force can vary as much as thirty pounds. Therefore, the previous distribution test may not provide the correct distribution for the moved mass tests. The aero loaders can add a significant amount of uncertainty to the system which is considered in the tests. It is assumed that the distribution is uniform, but an analysis describing the distribution includes the previously described tests. These distributions will be described in the results section of this chapter.

The goal of this test is to create a real world situation to which the polynomial chaos expansion method can be applied. Multiple mass distributions were created to ensure that the method works for many situations. To create multiple center of gravity locations, lead shot bags will be moved around the vehicle to create a different center of gravity. Data is then collected to determine the range of the force distribution for each different moved mass test. Once the range is known, the distribution can either be recreated from the information collected from the initial distribution shapes or from an assumed uniform distribution. The actual loads at each wheel can be checked with the Longacre Computerscales DX system.

The procedure for this test is to first record the weight of the vehicle without the sixteen twenty-five pound lead shot bags. The output for each wheel load cell is observed for thirty seconds. The output updates approximately every second to provide thirty outputs. The lowest output and the highest output are recorded to create a range of possible outputs from the wheel load system. After this is done, the vehicle is moved on and off the wheel loaders by jacking up each side of the vehicle. The vehicle is also depressed at each corner to remove stiction in the suspension. The outputs are recorded as previously stated. This will test the system's variability between placements on the rig. The vehicle is moved on and off the wheel pan four times so that five outputs can be recorded for each moved lump mass test. For each mass distribution the vehicle is also weighed on the Longacre Computerscales DX system to provide for an accurate weight at each wheel.

This process is repeated five times for each of the four different mass distributions. After the test with no added lead shot bags is complete, the lead shot bags are placed in the trunk of the vehicle, then half the weight is moved forward into the passenger area, and lastly the remaining lead shot bags are moved to the passenger area as well. The process is repeated for each of these mass distributions. This totals to four different mass distributions to test the system on.

There were four different locations that the weight was placed at within the vehicle. These locations are given in the following figure and table.

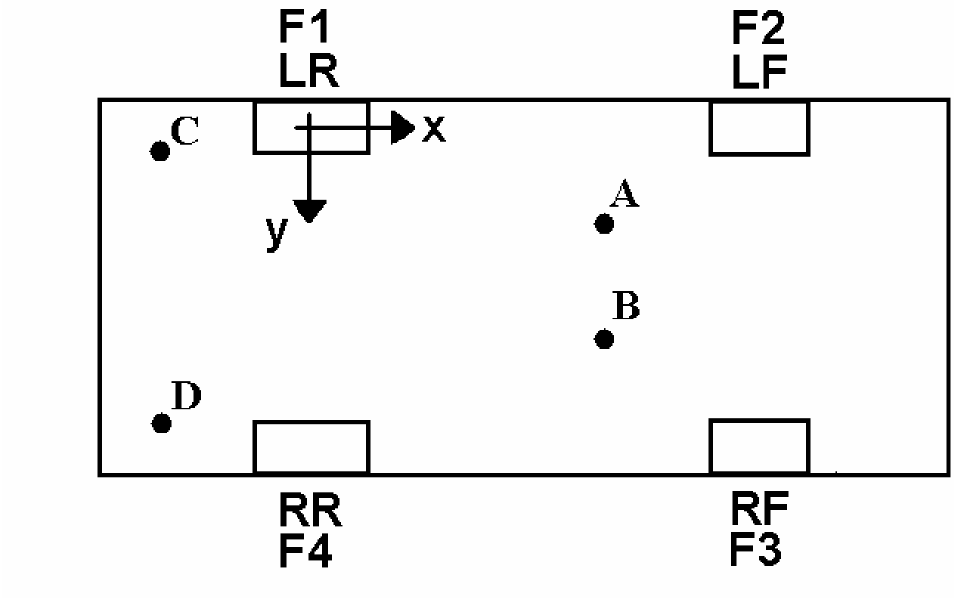

Figure 4.9: Locations of Lumped Masses

Table 4.4: Coordinates of Locations Points for Lumped Masses

Location	x (in)	y (in)
A	63	15
B	63	45
C	-36	4
D	-36	56

The lumped mass additions to the four different mass distribution tests are:

Table 4.5: Lump Mass Locations for Each Mass Distribution Test

	Location Weights (lbs)			
Test	**A**	**B**	**C**	**D**
1	0	0	0	0
2	0	0	200	200
3	100	100	100	100
4	200	200	0	0

These moved lumped masses could cause a significant shift in the location of the center of gravity. The results from these tests will be presented in the following section.

4.4 Moved Lump Mass Test Results

The moved lumped mass test was performed to test the polynomial chaos expansion's ability to estimate the center of gravity position based on results from the test data. The test data used in the polynomial chaos expansion is analyzed and coefficients for the polynomial chaos model are chosen in this section. The polynomial chaos results will be given in following chapters based on the test results in this section.

Also, the actual weight at each wheel is found by weighing the vehicle with the Longacre Computerscales DX, they are shown as black solid lines. The minimum and maximum range averages were found and are presented in this section. The maximum and minimum points for each record are shown as stem plots with the stems projecting from the corresponding average minimum or average maximum value. The output ranges from each of the four moved lump mass test are given in Figure 4.10 through Figure 4.13.

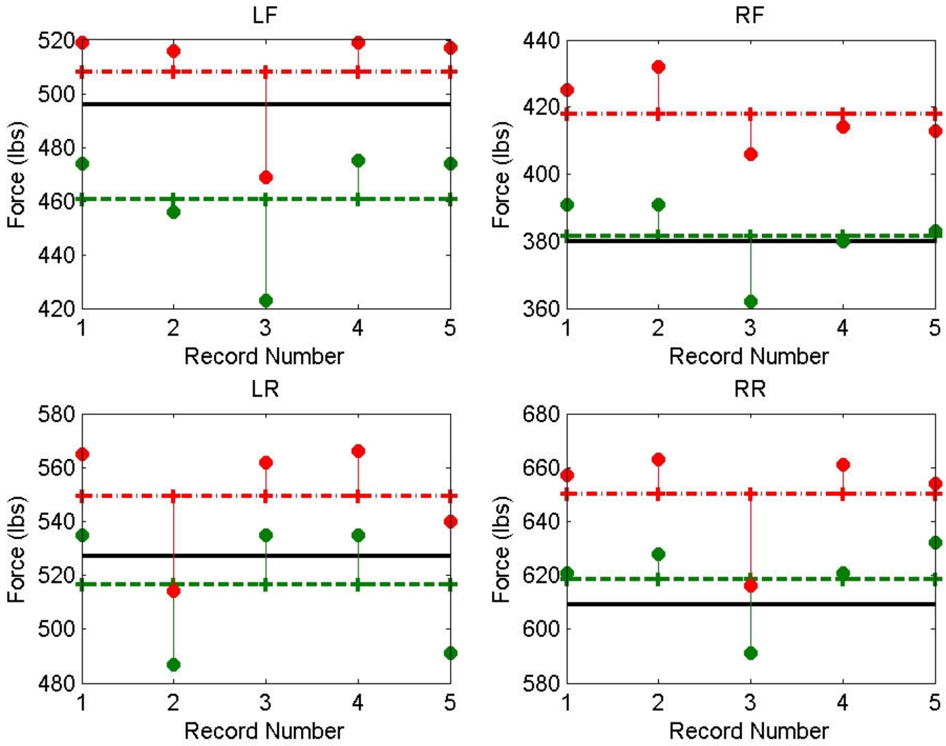

Figure 4.10: Moved Lump Mass Test 1

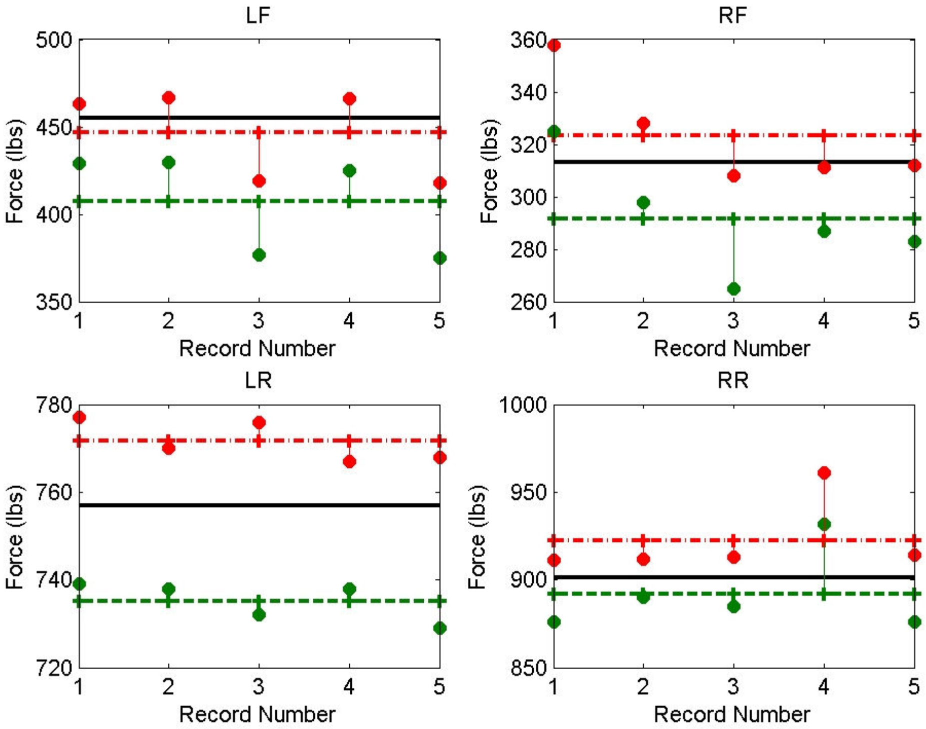

Figure 4.11: Moved Lump Mass Test 2

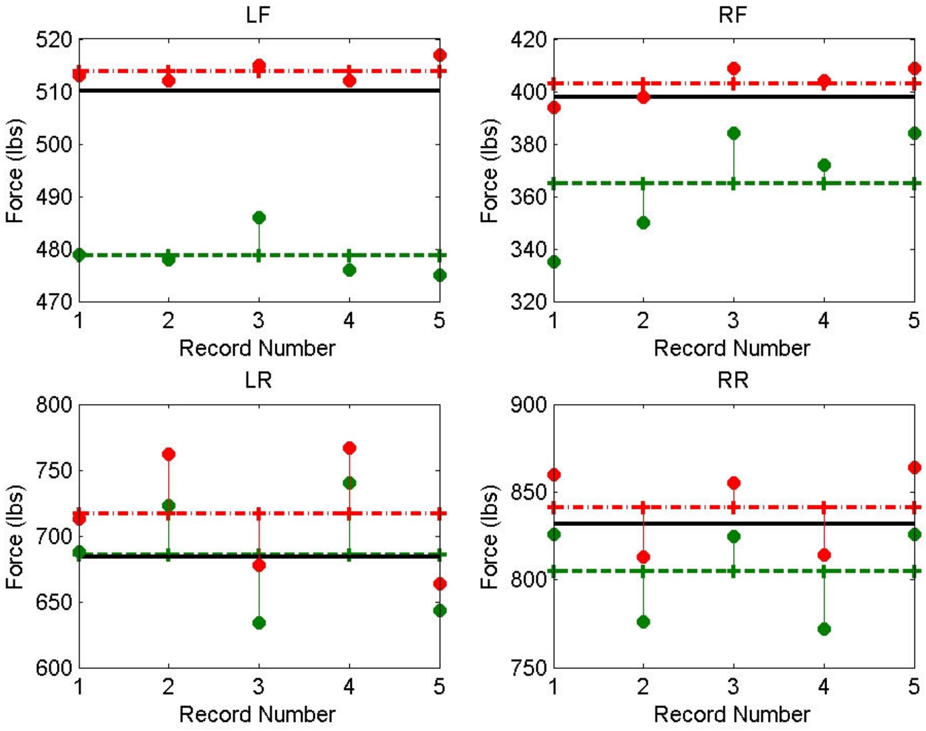

Figure 4.12: Moved Lump Mass Test 3

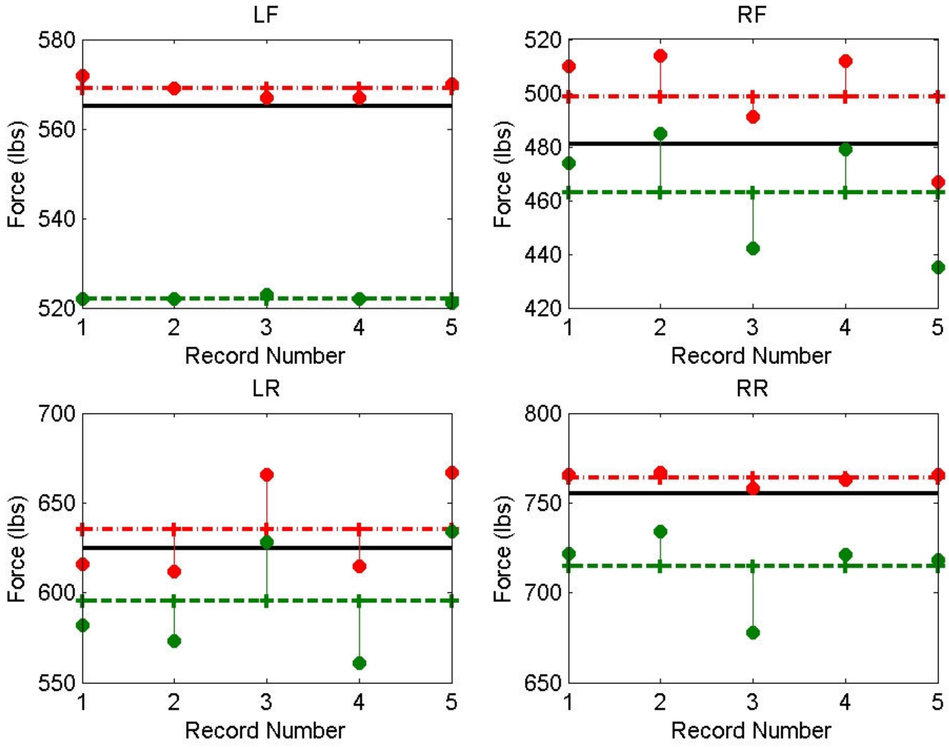

Figure 4.13: Moved Lump Mass Test 4

As seen from the above data there appears to be several different kinds of uncertainty in the load measurement. The output range varies which is shown by the minimum force and maximum forces. This range is generally thirty and forty pounds, but in several cases was as great as fifty or sixty pounds. A table of the range for each record and the average range for each test is given in Table 4.6. There are several possible causes for this uncertainty. The first is noise within the load cell measurement system. This can be caused from noise within the electronics or the accuracy of the load cells.

Table 4.6: Range Between Minumum and Maximum Force Outputs for each Record

	LF Record Range (lbs)						RF Record Range (lbs)					
Test	**1**	**2**	**3**	**4**	**5**	**Mean Range**	**1**	**2**	**3**	**4**	**5**	**Mean Range**
1	45	60	46	44	43	47.6	34	41	44	34	30	36.6
2	34	37	42	41	43	39.4	33	30	43	24	29	31.8
3	34	34	29	36	42	35	59	48	25	32	25	37.8
4	50	47	44	45	49	47	36	29	49	33	32	35.8

	LR Record Range (lbs)						RR Record Range (lbs)					
Test	**1**	**2**	**3**	**4**	**5**	**Mean Range**	**1**	**2**	**3**	**4**	**5**	**Mean Range**
1	30	27	27	31	49	32.8	36	35	25	40	22	31.6
2	38	32	44	29	39	36.4	35	22	28	29	38	30.4
3	25	39	44	27	21	31.2	34	37	30	42	38	36.2
4	34	39	38	54	33	39.6	44	33	80	42	48	49.4

The second source of uncertainty is developed each time the vehicle moves on and off the wheel pan. There are several possible causes of this uncertainty, not all of which are due to the wheel load measurement system. First, the vehicle shocks are actually sticking and preventing the vehicle from getting accurate center of gravity measurements. This effect can be seen clearly in the LR and RR wheel loads in Test 3, Figure 4.12. The weight appears to shift back and forth between the two rear wheel loads. Other possible causes include, a shift in the load cells between tests, the four load sensors being incorrectly calibrated within the load cell, or changes in the aero loaders force due to the vehicle being lifted. This would cause different force outputs as the wheel is moved over the wheel pan. The combined range from both sources of uncertainty can create a much lbroader range than that from the noise uncertainty as shown in Table 4.6. Since these uncertainties are likely not due to the load measurement system, but stiction in the suspension of the vehicle and aero loaders they will not be used in the PCE model. The mean of the five records will be used to lower the impact of the uncertainty between tests. The exact cause of these uncertainties is not further explored since the goal of these tests are just to provide a test bed for the Galerkin polynomial chaos method. It should also be noted that the scale does not actually prevent the error from the aero loaders and the stiction in the shocks of the vehicle from occurring; therefore, it can not be taken as the true value for the load.

Table 4.7: Total Wheel Load Range for each Lumped Mass Test

	Total Range (lbs)			
Test	**LR**	**RF**	**LR**	**RR**
1	96	70	79	72
2	92	93	48	85
3	42	74	133	92
4	51	79	106	89

Polynomial chaos expansion coefficients can be created for each moved mass location based on the data collected in the moved mass and the distribution tests. As stated earlier, characterization of the moved mass distribution can be accomplished by assuming a uniform distribution over the range or using the beta distribution that was found in the distribution test. The previous test did not include the aero loaders; therefore, its distribution can not be justifiably correct here. To show that polynomial chaos works with any distribution, both distributions will be considered.

The uniform distribution will be simpler to model from the data collected than the beta distribution. A uniform distribution is defined with the average wheel load and the determined range as the coefficients of the polynomial chaos expansion. The range is presented as the mean range in Table 4.6 and the average wheel load value is given in the following table.

Table 4.8: Average Wheel Load for each Moved Mass Test

	Average (lbs)			
Test	**LF**	**RF**	**LR**	**RR**
1	484.2	399.7	533	634.4
2	426.9	307.9	753.4	907
3	496.3	383.9	701.2	823.1
4	545.5	480.9	615.4	739.3

A uniform distribution can be defined with the Karhunen-Loeve Expansion as

$$F = \sum_{i=0}^{1} a_i \phi_i \left(\zeta \right) = a_0 + a_1 \zeta \tag{4.6}$$

where a_o is the average value and a_1 is the range of the uniform distribution [10].

The beta distribution is not simple to model the uniform distribution because the beta distribution requires multiple polynomials to define it. Based on the previous distribution and the information collected in the moved mass test a solution can be found. However, this distribution may not be correct due to the changes in the experimental setup. The beta distribution is performed to further understand the ability of applying experimental data to any type of distribution without running a full distribution test each time.

The distribution test found the polynomial coefficients for a beta distribution to the 3rd order polynomial. If it is assumed that the shape of the load uncertainty distribution does not significantly change, the first two polynomial coefficients can be adjusted creating a solid model for the distribution. The first two polynomial coefficients will not directly convert as seen in the uniform distribution using the Legendre polynomials. The method for determining the zeroth and first order polynomial coefficients for the beta distribution is dependent on the boundary conditions of the moved mass tests.

The boundary value method for solving the polynomial coefficients is done with the knowledge of the range of the test and from previous distributions. By knowing the test range, the maximum and minimum values of ζ can be inputted into the polynomial chaos expansion equation with the corresponding test values, $F_{\max}$ and $F_{\min}$. This creates two equations and two unknowns, allowing the determination of the zeroth and first order polynomials of the distribution. This process is shown in the following equations.

$$\begin{bmatrix} F_{\max} \\ F_{\min} \end{bmatrix} = \begin{bmatrix} C_1\phi_0\left(\zeta_{\max}\right) + C_2\phi_1\left(\zeta_{\max}\right) + P_2\phi_2\left(\zeta_{\max}\right) + \cdots + P_r\phi_r\left(\zeta_{\max}\right) \\ C_1\phi_0\left(\zeta_{\min}\right) + C_2\phi_1\left(\zeta_{\min}\right) + P_2\phi_2\left(\zeta_{\min}\right) + \cdots + P_r\phi_r\left(\zeta_{\min}\right) \end{bmatrix} \tag{4.7}$$

After restructuring to solve for the coefficients C_0 and C_1 the equation becomes:

$$\begin{bmatrix} F_{\max} \\ F_{\min} \end{bmatrix} = \left[\begin{bmatrix} \phi_0\left(\zeta_{\max}\right) & \phi_1\left(\zeta_{\max}\right) \\ \phi_0\left(\zeta_{\min}\right) & \phi_1\left(\zeta_{\min}\right) \end{bmatrix}\right] \begin{bmatrix} C_1 \\ C_2 \end{bmatrix} - \begin{bmatrix} P_2\phi_2\left(\zeta_{\max}\right) + \cdots + P_r\phi_r\left(\zeta_{\max}\right) \\ P_2\phi_2\left(\zeta_{\min}\right) + \cdots + P_r\phi_r\left(\zeta_{\min}\right) \end{bmatrix} \tag{4.8}$$

The coefficients can then be solved for by moving the other polynomial chaos coefficients to the other side of the equation and then multiplying by the inverse of the basis functions.

$$\begin{bmatrix} C_1 \\ C_2 \end{bmatrix} = \left(\begin{bmatrix} \phi_0\left(\zeta_{\max}\right) & \phi_1\left(\zeta_{\max}\right) \\ \phi_0\left(\zeta_{\min}\right) & \phi_1\left(\zeta_{\min}\right) \end{bmatrix}^{-1} \right) \left(\begin{bmatrix} F_1 \\ F_2 \end{bmatrix} - \begin{bmatrix} P_2\phi_2\left(\zeta_{\max}\right) + \cdots + P_r\phi_r\left(\zeta_{\max}\right) \\ P_2\phi_2\left(\zeta_{\min}\right) + \cdots + P_r\phi_r\left(\zeta_{\min}\right) \end{bmatrix} \right) \quad (4.9)$$

C_1 and C_2 are the first two coefficients in the polynomial chaos expansion for each moved mass test. $F_{\max}$ and $F_{\min}$ are the maximum and minimum output values for each test and P represents the polynomial chaos coefficients previously defined in the distribution test. It should be noted that this method will only work with finite distributions such as the uniform and beta distributions.

The polynomial chaos coefficients to define all the moved mass tests are given in the appendix. The beta distributions coefficients for the first test are given in the following table, Table 4.9.

Table 4.9: Polynomial Coefficient Values for Test 1

	Polynomial Coefficient Values Test 1				
Wheel Location	**1st order**	**2nd order**	**3rd order**	**4th order**	**5th order**
LF	449.63	6.986	0.25	0.05	0
RF	371.03	6.953	0.25	0	0
LR	509.3	4.93	0.5	0	0
RR	601.5	10.97	0.25	-0.1	0

To show the differences in the two distributions, the following plots were constructed to compare the uniform and beta distributions to the wheel load measured from the Longacre Computerscales DX.

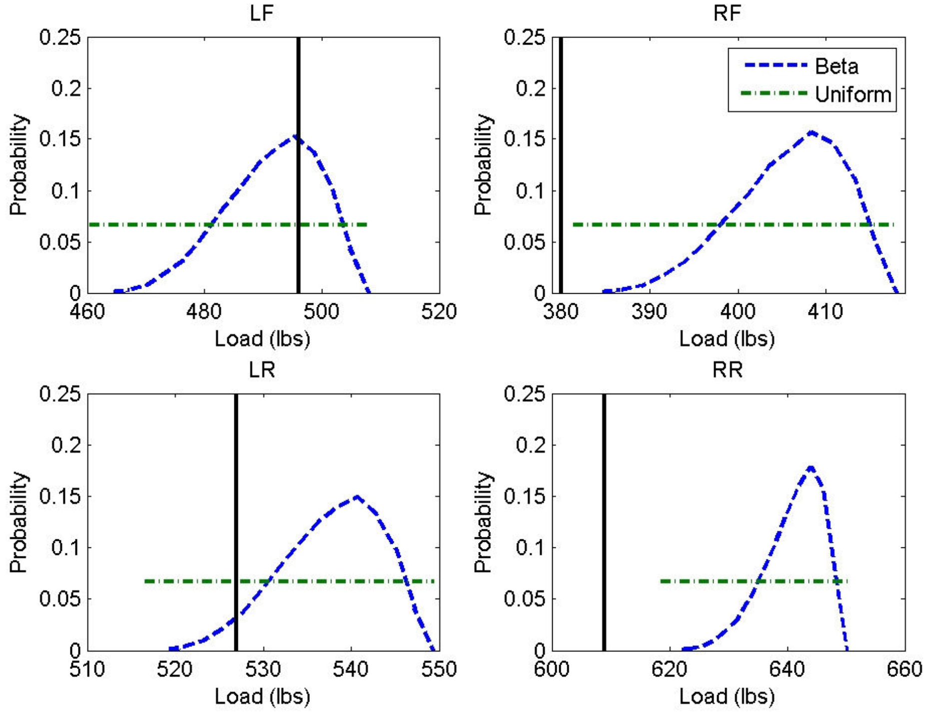

Figure 4.14: Estimated Distributions vs. Longacre Computerscales DX Wheel Load for Test 1

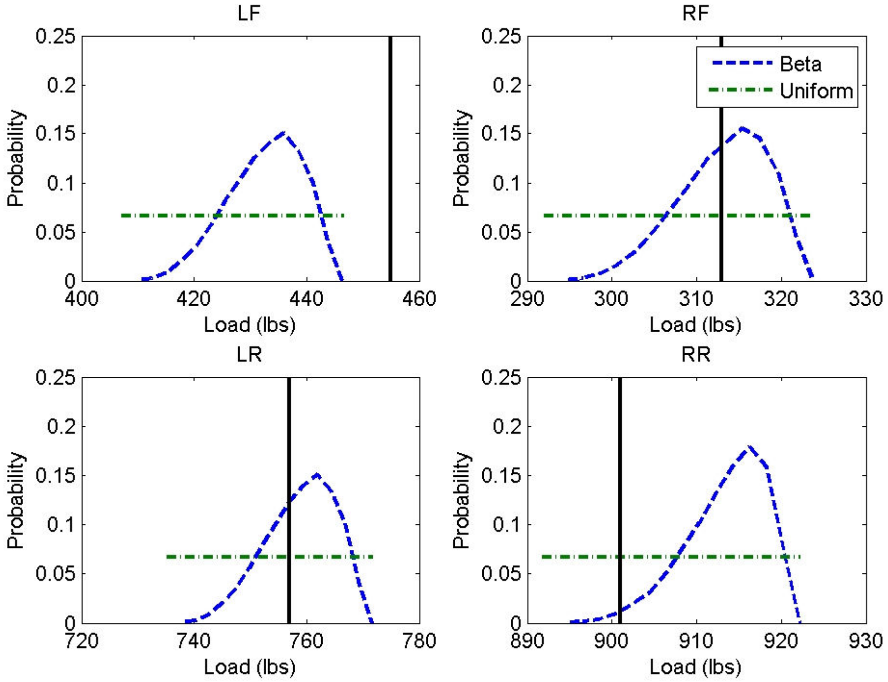

Figure 4.15: Estimated Distributions vs. Longacre Computerscales DX Wheel Load for Test 2

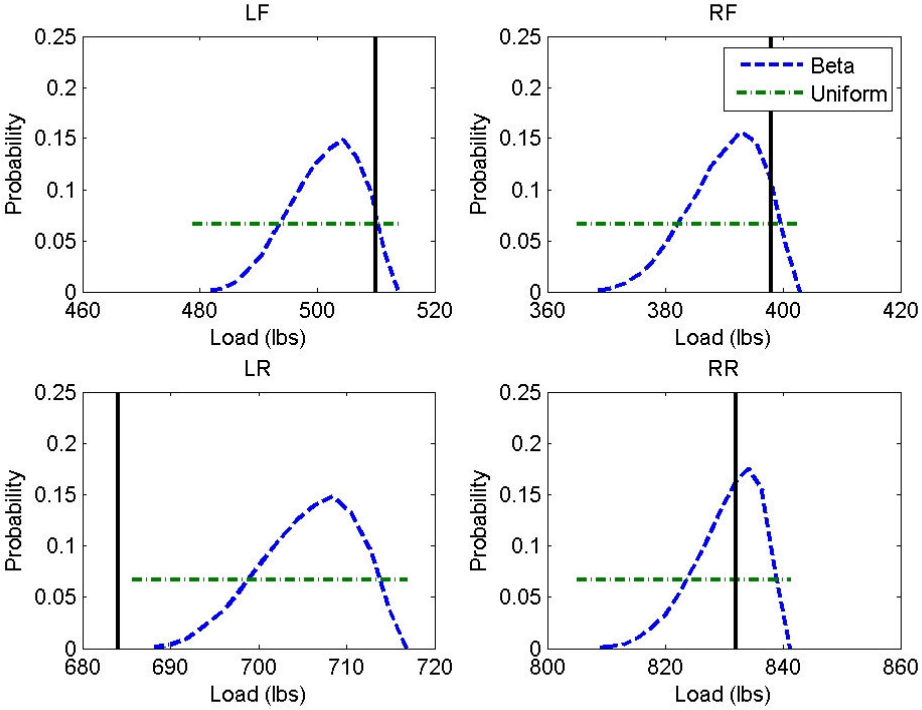

Figure 4.16: Estimated Distributions vs. Longacre Computerscales DX Wheel Load for Test 3

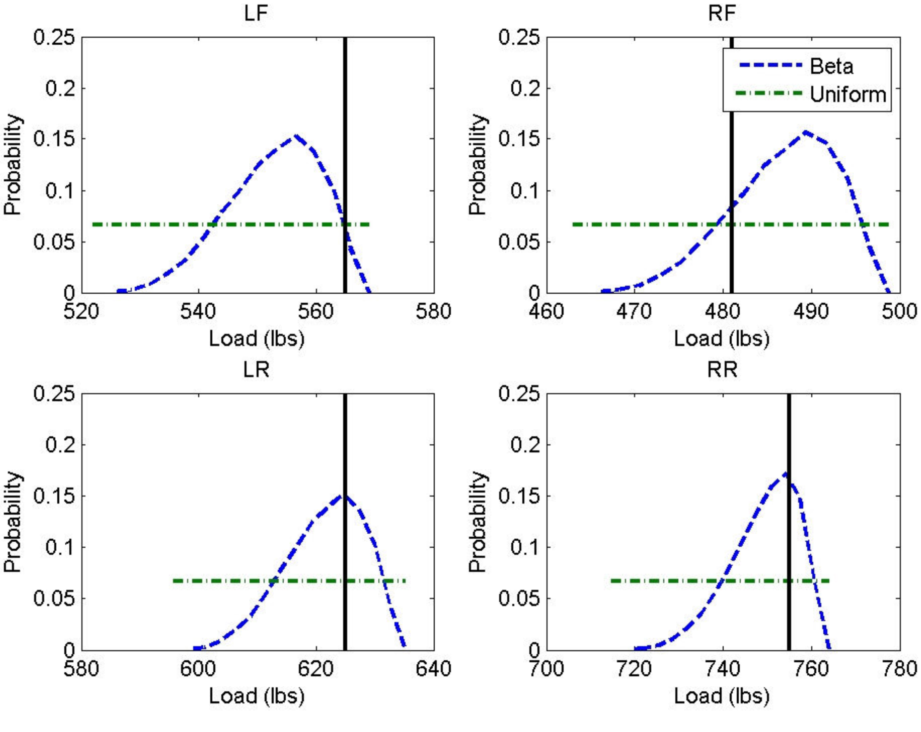

Figure 4.17: Estimated Distributions vs. Longacre Computerscales DX Wheel Load for Test 4

From the above figures, it can be seen that the distributions include the value from the scales for most the wheel loads. However, a few of the distributions do not include this value such as the RF and RR loads in test 1 and the LF in test 2. The cause of this is the uncertainty between the separate records. These uncertainties were previously described, but it can be seen in several cases that the large range between records distorts the test enough to place the average minimum and maximum off the value from the scale. As previously stated, the value from the scales may not be the true value since the errors from the aero loaders and stiction in the suspension of the vehicle are present on the scales as well. Since the scales do not prevent error from the aero loaders and the stiction in the suspension from occurring, it can not be seen as the “true” value.

The information from the scales in test four would appear to make the beta distribution is still applicable to the moved mass tests. However, this is not enough information to draw such a conclusion since the other tests are located throughout the distribution and in the zero probability area. These distributions will be used to in the PCE simulations in chapters five and six.

5. CALCULATION OF VEHICLE CENTER OF GRAVITY WITH ONE UNCERTAIN FORCE INPUT

This section analyzes the uncertainty caused from the input of one uncertain force on the calculation of the vehicle center of gravity using equation (3.4). Polynomial chaos expansion is the method used to analyze the process. Two cases will be examined, the case where F_1, *LR*, is uncertain and the case that F_2, *RR*, is uncertain. The results for the uniform and beta distributions are presented. Also, a comparison between the polynomial chaos and the Monte Carlo methods is performed to show the accuracy of the polynomial chaos expansions.

5.1 Polynomial Chaos Expansion Model with Uncertain Input F₁

To gain a full understanding of polynomial chaos, we will first look at the simplest case for our process. For our problem, only one input force is uncertain is the simplest case. We will define F_1 so it can represent any distribution.

$$\widehat{F_1}\left(\zeta_1\right)=\sum_{i=0}^{s}a_i\phi_i\left(\zeta_1\right) \tag{5.1}$$

ζ_1 is a random variable over some domain space representing a distribution, and $\widehat{F_1}$ represents the random variable of the force input. While $\widehat{F_1}$ is uncertain, the model itself is deterministic. $\widehat{F_1}$ is defined by polynomial chaos coefficients, a_i, and the orthogonal basis functions, $\phi_i\left(\zeta_1\right)$.

Any error or uncertainties in the result draw directly from $\widehat{F_1}$ as it propagates through the definite model. If this is the case, then the resulting uncertain distribution would be the same as the input distribution. It is found that the nonlinear effects within the equation cause the distribution to be skewed. Implementing $\widehat{F_1}$ into equation 4.2 yields the following equation:

$$x(\zeta_1) = \frac{(F_2 + F_3)L}{\left(\widehat{F}_1(\zeta_1) + F_2 + F_3 + F_4\right)}$$
$$y(\zeta_1) = \frac{(F_3 + F_4)W}{\left(\widehat{F}_1(\zeta_1) + F_2 + F_3 + F_4\right)} \tag{5.2}$$

$x(\zeta_1)$ and $y(\zeta_1)$ will also be represented by distributions. The polynomial chaos expansion can be implemented to solve for $x(\zeta_1)$ and $y(\zeta_1)$. This system analyses a static process. This is different from most polynomial chaos expansion (PCE) models which uses a PCE to find a parameter over time. Unlike many PCE's, this system has an uncertain input instead of an uncertain parameter.

There are two different methods to creating a polynomial-chaos model; The Galerkin projection and the collocation method. The Galerkin projection method solves for the solution analytically, while the collocation method uses certain solution points to run the simulation and interpolates between them [7,10]. This particular problem should be solved using a direct analytical approach to see how the force distribution impacts the final position of the center of gravity. The Galerkin approach can produce information about the distribution without having to plot the distribution.

Basis functions need to be set to create a polynomial chaos expansion. These basis functions are required to be orthogonal to each other over a certain range. There are many sets of polynomials that meet this demand such as, Jacobian, Legendre, Hermite; However, certain sets can more simply define specific distributions. For a uniform input distribution, Legendre polynomials work best [7, 8, 10]. Legendre polynomials are orthogonal over the range $[-1 \quad 1]$.

$$\phi_n(\zeta) = \left(\frac{1}{2^n (n!)}\right)\frac{\partial^n}{\partial \zeta^n}\left(\zeta^2 - 1\right)^n = \begin{cases} 1 & n = 0 \\ \zeta & n = 1 \\ \frac{1}{2}\left(3\zeta^2 - 1\right) & n = 2 \\ \vdots & \vdots \end{cases} \tag{5.3}$$

Equation (5.3) defines the Legendre polynomials used in the PCE model. The orthogonal basis functions to define the beta distributions from our experimental distribution test are Jacobian. These orthogonal basis functions were previously mentioned, but a detailed discussion is now presented. Jacobian polynomials are chosen based on the shape of the beta distribution. This means a beta (2,2) distribution would have different basis functions from a beta (3,4) distribution. Our data is best characterized by a beta (5,2) distribution. Its orthogonal basis functions are:

$$\phi_n = \begin{cases} 1 & n = 0 \\ (3/2)(1+3\zeta) & n = 1 \\ (1/4)\left(-1+30\zeta+55\zeta^2\right) & n = 2 \\ \vdots & \vdots \end{cases} \tag{5.4}$$

$\widehat{F_1}$ was previously defined by equation (5.1) for the case where the input distribution is defined by an s order basis function. The resulting center of gravity distributions is redefined as a series expansion of basis functions based on the Karhunen-Loeve Expansion. The basis functions are the same as those chosen to define the input distribution. These will need to be taken to a higher order since the resultant distribution may be of a higher order than the input distribution.

$$\begin{aligned} X(\zeta) &= \sum_{j=0}^{r} x_j \phi_j(\zeta) \\ Y(\zeta) &= \sum_{j=0}^{r} x_j \phi_j(\zeta) \end{aligned} \tag{5.5}$$

r defines the order of the resultant center of gravity basis functions. We can now create the PCE model since all the base variables have been redefined to the basis functions. This model be shown in just the longitudinal direction since the solution is nearly identical for both. Replacing $\widehat{F_1}$ and X with basis functions:

$$\left(\sum_{i=0}^{s} a_i\phi_i\left(\zeta_1\right)+F_2+F_3+F_4\right)\left(\sum_{j=0}^{r} x_j\phi_j\left(\zeta_1\right)\right)=\left(F_2+F_3\right)L \tag{5.6}$$

$$\sum_{i=0}^{s}\sum_{j=0}^{r} a_i x_j\phi_i\left(\zeta_1\right)\phi_j\left(\zeta_1\right)+\left(F_2+F_3+F_4\right)\left(\sum_{j=0}^{r} x_j\phi_j\left(\zeta_1\right)\right)=\left(F_2+F_3\right)L \tag{5.7}$$

Now we must project ϕ_n according to the Galerkin method being sure to take the appropriate inner product.

$$\begin{aligned}&\left\langle \phi_n\left(\zeta\right),\sum_{i=0}^{s}\sum_{j}^{r} a_i x_j\phi_i\left(\zeta_1\right)\phi_j\left(\zeta_1\right)\right\rangle+\left\langle \phi_n\left(\zeta_1\right),\left(F_2+F_3+F_4\right)\left(\sum_{j=0}^{r} x_j\phi_j\left(\zeta_1\right)\right)\right\rangle\\&=\left\langle \phi_n\left(\zeta_1\right),\left(F_2+F_3\right)L\right\rangle\end{aligned} \tag{5.8}$$

$$\begin{aligned}&\int_{-1}^{1}\sum_{i=0}^{s}\sum_{j=0}^{r} a_i x_j\phi_i\left(\zeta_1\right)\phi_j\left(\zeta_1\right)\phi_n\left(\zeta_1\right)w\left(\zeta_1\right)\partial\zeta+\cdots\\&\cdots\left(F_2+F_3+F_4\right)\int_{-1}^{1}\left(\sum_{j=0}^{r} x_j\phi_j\left(\zeta_1\right)\phi_n\left(\zeta\ \right)\right)w\left(\zeta_1\right)\partial\zeta=\left(F_2+F_3\right)L\int_{-1}^{1}\phi_n\left(\zeta_1\right)w\left(\zeta_1\right)\partial\zeta\end{aligned} \tag{5.9}$$

Bringing the constants out of the integral the equation is simplified to:

$$\begin{aligned}&\sum_{i=0}^{s}\sum_{j=0}^{r} a_i x_j\int_{-1}^{1}\phi_i\left(\zeta_1\right)\phi_j\left(\zeta_1\right)\phi_n\left(\zeta_1\right)w\left(\zeta_1\right)\partial\zeta+\cdots\\&\cdots\left(F_2+F_3+F_4\right)\sum_{j=0}^{r} x_j\int_{-1}^{1}\phi_j\left(\zeta_1\right)\phi_n\left(\zeta_1\right)w\left(\zeta_1\right)\partial\zeta=\left(F_2+F_3\right)L\int_{-1}^{1}\phi_n\left(\zeta_1\right)w\left(\zeta_1\right)\partial\zeta\end{aligned} \tag{5.10}$$

This leaves the integration to a matrix or array of integrals that can be calculated once. Since the basis functions are orthogonal, many of the integral matrices will be largely filled with zeros. The integral with two basis functions will be all zeros except along the diagonal where the basis function is multiplied by itself. The integrals with one or three basis functions require calculation at all points because it is not obvious where zeros will be located.

$$\delta_{ijn} = \int_{-1}^{1} \phi_i(\zeta)\phi_j(\zeta)\phi_n(\zeta)w(\zeta)\partial\zeta \tag{5.11}$$

$$\delta_{jn} = \int_{-1}^{1} \phi_j(\zeta)\phi_n(\zeta)w(\zeta)\partial\zeta \tag{5.12}$$

$$\delta_{in} = \int_{-1}^{1} \phi_i(\zeta)\phi_n(\zeta)w(\zeta)\partial\zeta \tag{5.13}$$

$$\delta_{n} = \int_{-1}^{1} \phi_n(\zeta)w(\zeta)\partial\zeta \tag{5.14}$$

Integrals are often solved numerically in computer models, but these were solved analytically using Matlab's symbolic toolbox. This provides an exact solution, and minimizes error due to computational error. This Matlab code can be found in Appendix A. The weighting function $w(\zeta)$ is different for different sets of basis functions. The weighting function for Legendre polynomials is 1, while the weighting function for Jacobian polynomials is given in equation (5.15).

$$w(\zeta) = (1-\zeta)^{\alpha}(1+\zeta)^{\beta} \tag{5.15}$$

We can think of these δ's as matrices with an order equal to the number of ϕ's within the integral. So, δ_{ijn} is a $i \times j \times n$, 3-dimensional matrix, δ_{jn} is a $j \times n$ matrix, and δ_n is a *n*-dimensional array.

To reduce the three dimensional matrix to two dimensions, a new matrix is created with ψ as a constant.

$$\begin{aligned}
\psi_{n0} &= \left(a_0\delta_{00n} + a_1\delta_{10n} + \cdots + a_s\delta_{s0n}\right) \\
\psi_{n1} &= \left(a_0\delta_{01n} + a_1\delta_{11n} + \cdots + a_s\delta_{s1n}\right) \\
&\vdots \\
\psi_{ns} &= \left(a_0\delta_{0rn} + a_1\delta_{1rn} + \cdots + a_s\delta_{srn}\right)
\end{aligned} \tag{5.16}$$

This can be placed in a matrix in the following order.

$$\psi_{nr} = \begin{bmatrix} \psi_{00} & \psi_{01} & \cdots & \psi_{0r} \\ \psi_{10} & \psi_{11} & & \vdots \\ \vdots & & \ddots & \vdots \\ \psi_{r0} & \cdots & \cdots & \psi_{rr} \end{bmatrix} \tag{5.17}$$

Now that equation (5.10), has been simplified, the equation can be written as matrices and arrays to be solved the problem with linear algebra.

$$\begin{bmatrix} \psi_{00} & \psi_{01} & \cdots & \psi_{0r} \\ \psi_{10} & \psi_{11} & & \vdots \\ \vdots & & \ddots & \vdots \\ \psi_{n0} & \cdots & \cdots & \psi_{nr} \end{bmatrix} \begin{Bmatrix} x_0 \\ x_1 \\ \vdots \\ x_r \end{Bmatrix} + \begin{bmatrix} \delta_{00} & 0 & 0 & 0 \\ 0 & \delta_{11} & 0 & 0 \\ 0 & 0 & \ddots & 0 \\ 0 & 0 & 0 & \delta_{rr} \end{bmatrix} \begin{Bmatrix} x_0 \\ x_1 \\ \vdots \\ x_r \end{Bmatrix} = \left(F_2 + F_3\right) L \begin{Bmatrix} \delta_0 \\ \delta_1 \\ \vdots \\ \delta_r \end{Bmatrix} \tag{5.18}$$

$$\left(\begin{bmatrix} \psi_{00} & \psi_{01} & \cdots & \psi_{0r} \\ \psi_{10} & \psi_{11} & & \vdots \\ \vdots & & \ddots & \vdots \\ \psi_{r0} & \cdots & \cdots & \psi_{rr} \end{bmatrix} + \begin{bmatrix} \delta_{00} & 0 & 0 & 0 \\ 0 & \delta_{11} & 0 & 0 \\ 0 & 0 & \ddots & 0 \\ 0 & 0 & 0 & \delta_{rr} \end{bmatrix} \right) \begin{Bmatrix} x_0 \\ x_1 \\ \vdots \\ x_r \end{Bmatrix} = \left(F_2 + F_3\right) L \begin{Bmatrix} \delta_0 \\ \delta_1 \\ \vdots \\ \delta_r \end{Bmatrix} \tag{5.19}$$

$$\begin{Bmatrix} x_0 \\ x_1 \\ \vdots \\ x_r \end{Bmatrix} = (F_2 + F_3) L \left(\left(\begin{bmatrix} \psi_{00} & \psi_{01} & \cdots & \psi_{0r} \\ \psi_{10} & \psi_{11} & & \vdots \\ \vdots & & \ddots & \vdots \\ \psi_{r0} & \cdots & \cdots & \psi_{rr} \end{bmatrix} + (F_2 + F_3 + F_4) \begin{bmatrix} \delta_{00} & 0 & 0 & 0 \\ 0 & \delta_{11} & 0 & 0 \\ 0 & 0 & \ddots & 0 \\ 0 & 0 & 0 & \delta_{rr} \end{bmatrix} \right)^{-1} \right) \left(\begin{Bmatrix} \delta_0 \\ \delta_1 \\ \vdots \\ \delta_r \end{Bmatrix} \right) \quad (5.20)$$

Equation (5.20) gives us the relationship for X with each basis function via the coefficient x described in equation (5.5). For this uncertain input the equation for Y is nearly identical.

$$\begin{Bmatrix} y_0 \\ y_1 \\ \vdots \\ y_r \end{Bmatrix} = (F_3 + F_4) T \left(\left(\begin{bmatrix} \beta_{00} & \beta_{01} & \cdots & \beta_{0r} \\ \beta_{10} & \beta_{11} & & \vdots \\ \vdots & & \ddots & \vdots \\ \beta_{r0} & \cdots & \cdots & \beta_{rr} \end{bmatrix} + (F_2 + F_3 + F_4) \begin{bmatrix} \delta_{00} & 0 & 0 & 0 \\ 0 & \delta_{11} & 0 & 0 \\ 0 & 0 & \ddots & 0 \\ 0 & 0 & 0 & \delta_{rr} \end{bmatrix} \right)^{-1} \right) \left(\begin{Bmatrix} \delta_0 \\ \delta_1 \\ \vdots \\ \delta_r \end{Bmatrix} \right) \quad (5.21)$$

The solution for x and y are the analytical equations that the Galerkin method supplies. This is the advantage of the Galerkin method compared to the collocation method. This equation can provide insight into the uncertainty without having to plot the PDF.

The simplest input case is F_1, so it would also be of interest to investigate the situation where F_2 is the uncertain input because it would increase the complexity of the problem. In this case, the uncertain input will be in the numerator and denominator of equation (3.4).

5.2 Polynomial Chaos Expansion Model with Uncertain Input $\mathbf{F_2}$

The case where F_2 is the uncertain input complicates the polynomial chaos expansion of equation (3.4) for the longitudinal CG coordinate. Since the majority of the steps in this calculation are the same as when F_1 is the uncertain input, not all of the PCE model derivation will be shown. Equation (5.22) defines the uncertain input, F_2 and is then inserted into equation (3.4) resulting in equation (5.24).

$$\widehat{F_2} = \sum_{i=0}^{s} b_i \phi_i \left(\zeta_2\right) \tag{5.22}$$

$$\begin{aligned} \hat{x}\left(\zeta_2\right) &= \frac{\left(\widehat{F_2}\left(\zeta_2\right) + F_3\right)L}{\left(F_1 + \widehat{F_2}\left(\zeta_2\right) + F_3 + F_4\right)} \\ \hat{y}\left(\zeta_2\right) &= \frac{\left(F_3 + F_4\right)W}{\left(F_1 + \widehat{F_2}\left(\zeta_2\right) + F_3 + F_4\right)} \end{aligned} \tag{5.23}$$

$$\begin{aligned} \hat{x}\left(\zeta_2\right) &= \frac{\left(\sum_{i=0}^{s} b_i \phi_i \left(\zeta_2\right) + F_3\right)L}{\left(F_1 + \sum_{i=0}^{s} b_i \phi_i \left(\zeta_2\right) + F_3 + F_4\right)} \\ \hat{y}\left(\zeta_2\right) &= \frac{\left(F_3 + F_4\right)W}{\left(F_1 + \sum_{i=0}^{s} b_i \phi_i \left(\zeta_2\right) + F_3 + F_4\right)} \end{aligned} \tag{5.24}$$

The x and y coordinates can be redefined to avoid the situation where one uncertain input is in the numerator and denominator. However, it is interesting to see how this situation impacts the distribution of the CG since it will not be avoidable as more uncertainties are added to the equations. Expanding the polynomial chaos and projecting x_n gives equation (5.25).

$$\begin{aligned}
&\sum_{i=0}^{s}\sum_{j=0}^{r} b_i x_j \int_{-1}^{1}\phi_i\left(\zeta_2\right)\phi_j\left(\zeta_2\right)\phi_n\left(\zeta_2\right)w\left(\zeta_2\right)\partial\zeta_2 + \cdots \\
&\cdots\left(F_1+F_3+F_4\right)\sum_{j=0}^{r} x_j \int_{-1}^{1}\phi_j\left(\zeta_2\right)\phi_n\left(\zeta_2\right)w\left(\zeta_2\right)\partial\zeta_2 = \cdots \\
&\cdots = L\left(\sum_{i=0}^{2} b_i\right)\int_{-1}^{1}\phi_i\left(\zeta_2\right)\phi_n\left(\zeta_2\right)w\left(\zeta_2\right)\partial\zeta + F_3 L\int_{-1}^{1}\phi_n\left(\zeta_2\right)w\left(\zeta_2\right)\partial\zeta_2
\end{aligned} \tag{5.25}$$

One more table needs to be precomputed for the integral. This δ_{in} is different from δ_{jn} because δ_{in} is a $r \times s$ matrix and δ_{jn} is a $r \times r$ matrix.

$$\delta_{in} = \int_{-1}^{1}\phi_i\left(\zeta_2\right)\phi_n\left(\zeta_2\right)w\left(\zeta_2\right)\partial\zeta_2 \tag{5.26}$$

We can rewrite equation (5.25) in linear algebra form to solve for x.

$$\begin{aligned}
&\begin{Bmatrix} x_0 \\ x_1 \\ \vdots \\ x_r \end{Bmatrix} = \left(\left(\begin{bmatrix} \psi_{00} & \psi_{01} & \cdots & \psi_{0r} \\ \psi_{10} & \psi_{11} & & \vdots \\ \vdots & & \ddots & \vdots \\ \psi_{r0} & \cdots & \cdots & \psi_{rr} \end{bmatrix} + \left(F_1+F_3+F_4\right)\begin{bmatrix} \delta_{00} & 0 & 0 & 0 \\ 0 & \delta_{11} & 0 & 0 \\ 0 & 0 & \ddots & 0 \\ 0 & 0 & 0 & \delta_{rr} \end{bmatrix}\right)^{-1}\right)\cdots \\
&\cdots\left(L\begin{bmatrix} \delta_{00} & 0 & 0 \\ 0 & \ddots & 0 \\ 0 & 0 & \delta_{ss} \\ 0 & 0 & 0 \end{bmatrix}\begin{bmatrix} b_0 \\ b_1 \\ \vdots \\ b_s \end{bmatrix} + F_3 L\begin{Bmatrix} \delta_0 \\ \delta_1 \\ \vdots \\ \delta_r \end{Bmatrix}\right)
\end{aligned} \tag{5.27}$$

Matlab is used to solve the linear algebra equations for x and y after precomputing the δ matrices. First, the order of the polynomial chaos function will be taken to a high order to ensure that the PCE model can capture the distribution. The resulting delta matrix for 8th order Legendre polynomials are:

$$\delta_{jn} = \begin{bmatrix} 2 & 0 & 0 & 0 & 0 & 0 & 0 & 0 \\ 0 & 0.6667 & 0 & 0 & 0 & 0 & 0 & 0 \\ 0 & 0 & 0.4000 & 0 & 0 & 0 & 0 & 0 \\ 0 & 0 & 0 & 0.2857 & 0 & 0 & 0 & 0 \\ 0 & 0 & 0 & 0 & 0.2222 & 0 & 0 & 0 \\ 0 & 0 & 0 & 0 & 0 & 0.1818 & 0 & 0 \\ 0 & 0 & 0 & 0 & 0 & 0 & 0.1538 & 0 \\ 0 & 0 & 0 & 0 & 0 & 0 & 0 & 0.1333 \end{bmatrix} \tag{5.28}$$

$$\delta_{in} = \begin{bmatrix} 2.0000 & 0 \\ 0 & 0.6667 \\ 0 & 0 \\ 0 & 0 \\ 0 & 0 \\ 0 & 0 \\ 0 & 0 \\ 0 & 0 \end{bmatrix} \tag{5.29}$$

$$\delta_{n} = \begin{bmatrix} 2 \\ 0 \\ 0 \\ 0 \\ 0 \\ 0 \\ 0 \\ 0 \end{bmatrix} \tag{5.30}$$

δ_{ijn} is an $i \times j \times n$ matrix. In many cases a third order PCE is sufficient. If this is the case, the order of the PCE model can be adjusted so the order matches the order required by the output polynomial chaos coefficients. After computing x_n and y_n, the distribution should be plotted.

5.3 Polynomial Chaos Probability Density Function Calculation

The end goal of using polynomial chaos expansions is to have a PDF of the uncertain parameter. In our case, the parameter is the vehicle's center of gravity coordinates. PCE Galerkin Method gives insight into the shape of the PDF without having to plot it. To truly see the distribution, it must be plotted.

The method used to plot the PDF of the PCE was the use random points of certain PDF's over a domain to represent ζ in the distribution of interest. Then bins are created to count all the possible CG locations within those bins. ζ is an array created via the *random* function in Matlab. ζ must have the same PDF as the distribution it represents. Equation (5.31) shows the example solution for the Legendre polynomials.

$$X(\zeta) = x_0 + x_1\zeta + x_2\left(1.5\zeta^2 - 0.5\right) + \cdots x_n\left(\left(\frac{1}{2^n\left(n!\right)}\right)\frac{\partial^n}{\partial\zeta^n}\left(\zeta^2 - 1\right)^n\right) \tag{5.31}$$

In any one direction, the probability of the Cg falling within a bin is:

$$p(x) = \frac{\text{Number of X}(\zeta)\text{ in bin}}{\text{Total Number of X}(\zeta)} \tag{5.32}$$

Another probability function that is important to know is the cumulative density function (CDF). This function is simply the integral of the PDF.

$$cdf(x) = \int_{-\infty}^{x} p(u)\partial u \tag{5.33}$$

These calculations become a bit more interesting as we expand to two dimensions. If $p(x)$ and $p(y)$ are independent of each other then

$$p(x,y) = p(x)\,p(y) \tag{5.34}$$

However, it is not certain that this is the case for our distribution. While the x and y in the CG calculations are not directly dependent on each other, they are dependent on the same uncertain input. Therefore, the assumption that $p(x)$ and $p(y)$ are independent can not be made and the probability must be calculated in the same way as equation (5.32) but using a two dimensional bin. The PDF and CDF in two dimensions is found with equations (5.35) and (5.36) respectfully.

$$p(x,y) = \frac{\text{Number of X}(\zeta)\text{ in bin}}{\text{Total Number of X}(\zeta)} \tag{5.35}$$

$$cdf(x,y) = \int_{-\infty}^{x}\int_{-\infty}^{y} p(u,v)\,\partial u \partial v \tag{5.36}$$

Another method to estimating the PDF is to model the uncertain parameter by selecting points that accurately represent the distributions CDF [10]. This method will only work for one uncertain input/parameter, but in that case it can greatly reduce the computations needed to accurately represent the distribution. It will only work for one uncertain parameter because combining multiple uncertainties with this method would create a strong coherence between them; Therefore, the model would not allow the independence of the multiple uncertainties. Monte Carlo's brute force method of randomly choosing numbers that represent the distribution provides randomness that supply add random error to the estimation for small data sets. Uniform distributions are simple to model since every point has equal likelihood of happening. A comparison of the methods used to model the distributions are shown below.

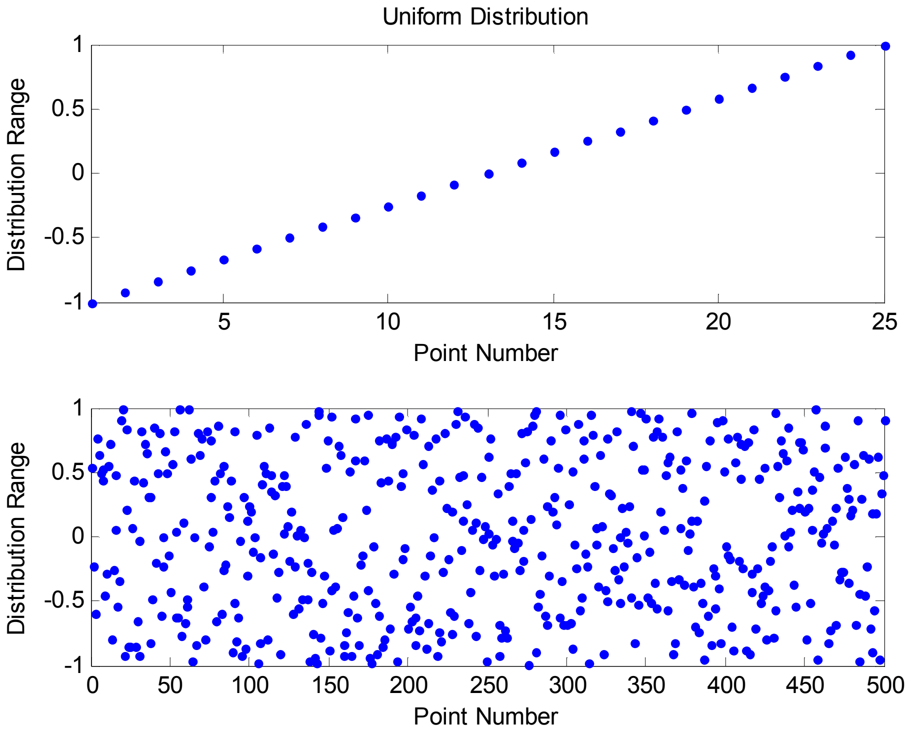

Figure 5.1: Methods for Representing Distribution

The top method uses the CDF to model the data and can efficiently be applied to one uncertain input. The bottom method is the Monte Carlo method which requires greater computations, but can be used for multiple uncertain inputs.

5.4 Polynomial Chaos Results for One Uncertain Input

This section covers the results for one uncertain input. First, a uniform uncertainty is varied over a broad range to observe the impact the uncertainty has on the center of gravity distribution. Then the uncertainty is varied from the results of the moved mass tests for a uniform distribution and a beta distribution.

5.4.1 Uncertain Input F_1: Uniform Distribution

The simplest uncertain input to model is a uniformly distributed F_1. The Monte Carlo method is also used in these simulations to compare to the PCE model. The initial test will show how uncertainty propagates through the base equation. A wide range of mean and range will be completed in the first test. Table 1 shows the mean and range used to define the uncertainty in each run.

Table 5.1: Simulation Runs for Uncertain Input F_1

	F1		F2		F3		F4	
Test	Mean	Range	Mean	Range	Mean	Range	Mean	Range
1	700	100	700	0	700	0	700	0
2	700	700	700	0	700	0	700	0
3	1200	100	700	0	700	0	700	0

These tests are run in order and the results are analyzed to determine the CG distribution changes with a simple uniform distribution. The NASCAR vehicle dimensions are used, $T = 60in$ and $L = 110in$, but none of the tests are meant to recreate the loads from real test results.

The first test places equal loads of 700 pounds. on all four wheels creating a perfect 50/50 weight distribution front to back and left to right. F_1 has a uniform distribution with a range of 100 pounds. Even though, 100 pounds may seem like a large range, it is not because the load sensors are designed to meet the requirements of many vehicles under dynamic loading. The four load sensors on the 8-post rig at the VIPER facility in Danville, VA are made to hold 10,000 pounds each. This means 100 pounds is 1% of the total capacity of the sensor.

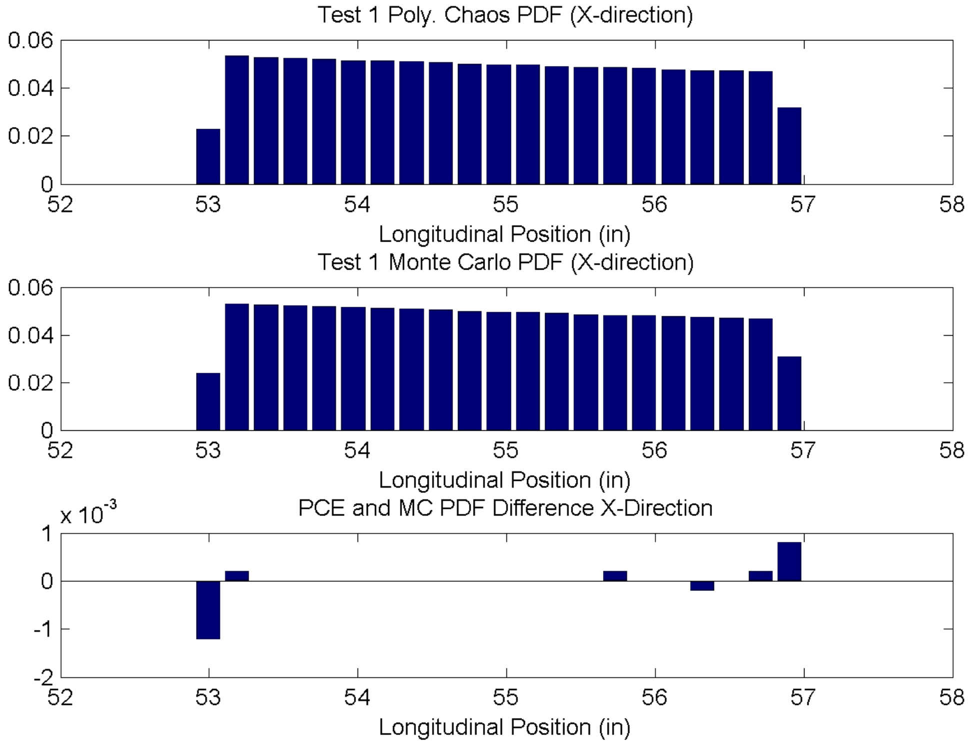

Figure 5.2: Longitudinal Results for Test 1 - F_1 Uniform Distribution

Plots of the y-direction will not be shown for uncertainty in F_1 since the equations in uniform distribution are the same except the y-direction uses the scaling of the track instead of the wheelbase. Since this is the case, it was expected that the two dimensional plots to be symmetrical along the diagonal. Figure 5.2 shows that the PCE and Monte Carlo results are nearly identical except for the fringes. It should be noted that the same random points were used for the two different distributions to remove random errors. This means the differences between the plots are a result of the differences in the Monte Carlo method and polynomial chaos expansion method.

Results for Test 1, as seen in Figure 5.3 show that the uniform input from F_1 does not produce a uniform result. The results appear to follow a linearly decaying probability. This is related to how a uniform distribution impacts equation 4.2. By analyzing the equation, if F_1 increases from the mean, the decrease in the center of gravity would be less than the CG increase if F_1 decreases the same amount from the mean. To quickly look at this we will examine a 50 pound increase and decrease of F_1 from the mean of 700 lbs.

$$\frac{\left(700lb+700lb\right)110in}{650lb+700lb+700lb+700lb}=56.00in$$
$$\frac{\left(700lb+700lb\right)110in}{750lb+700lb+700lb+700lb}=54.03in$$

Even though the differences from the mean of 55 inches are not significant, it does indicate why there is a higher probability for the lower center of gravity solutions. The initial test also shows that Monte Carlo and polynomial chaos expansion methods provide nearly identical results. The areas where the PDF difference shows the most error is at the corner of the distributions because the bins are not exactly the same between the Monte Carlo and polynomial chaos expansions. The main part of the distribution does not show significant error.

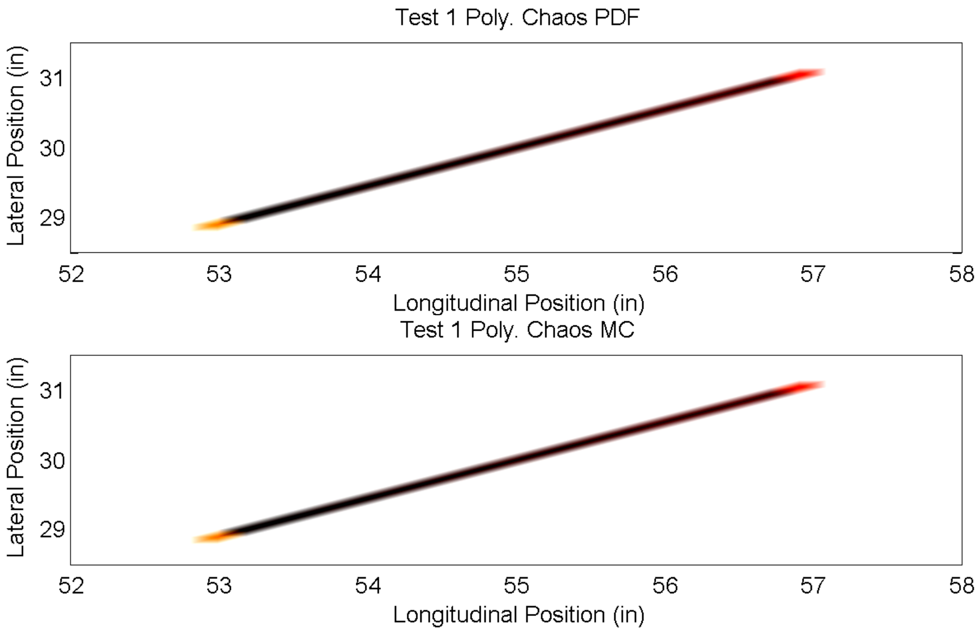

Figure 5.3: Longitudinal and Lateral 2-Dimensional Plot for Simulation Test 1

Figure 5.3 shows the 2-Dimensional results for Test 1. A circular PDF solution for the probability is expected, but for one uncertain parameter this is not the case. The reason for the distribution on the centerline of the vehicle is that the lateral and longitudinal CG positions are not independent of each other. They both depend on F_1, so the solutions are directly related. This creates a 1-dimensional line that travels along the diagonal of LF to RR as the range of uncertainty increases. With a range of uncertainty of 100 pounds, the length of the line is 4.5 inches. This would be significant in identifying the center of gravity of a vehicle, mostly for a light weight vehicle. It is clear that a 2-Dimensional plot is not as useful as 1-dimensional plot in the case of only one uncertain parameter. Therefore, the remaining plots for an uncertain F_1 will be 1-Dimensional.

Test 2 increases the range of the uncertainty from Test 1 to 700 pounds while maintaining the same mean. Range was limited to 700 pounds to not exceed the mean value of the distribution. As a result the CG of the vehicle was greatly increased. The following figure shows the resulting CG distribution.

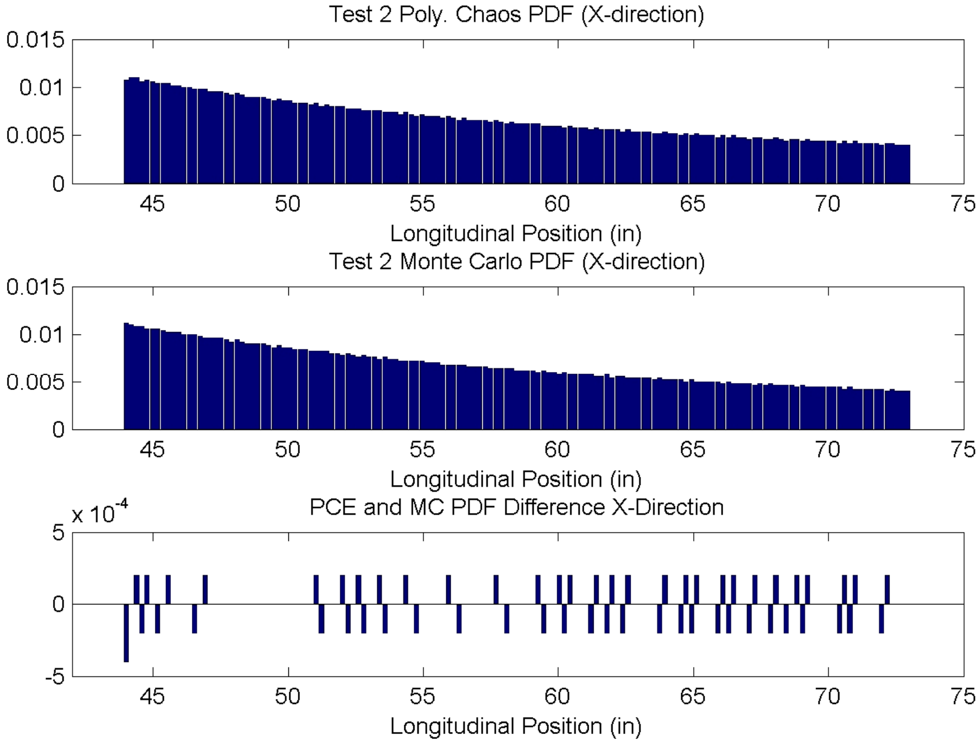

Figure 5.4: Longitudinal Results for Simulation Test 2 - F_1 Uniform Distribution

This figure shows that the probability is not linear decreasing as seen in Test 1. Since the range is much larger the shape of the distributions impact is much clearer. This shows that the CG probability behaves like the equation

$$y = \frac{1}{x} \tag{5.37}$$

This is how one would expect the probability to behave when observing the distributions resulting from equation (5.2). Upon closer look at the limits, it is seen that as F_1 increases to infinity the longitudinal CG location approaches a distance of zero. If F_1 is decreased to zero, the longitudinal CG location will increase to $73.\overline{33}$ inches, as seen in Figure 5.4. This is a result of the set weights at the other three wheel locations.

Test 3 was used to observe how the system would behave as the mean of the uncertainty was changed. Figure 5.5 shows that the mean of the distribution was shifted to around 46.5 inches from the original 55 inches. The range of the CG distribution was also decreased since the 100 lb input range is a smaller percentage of F_1's mean value.

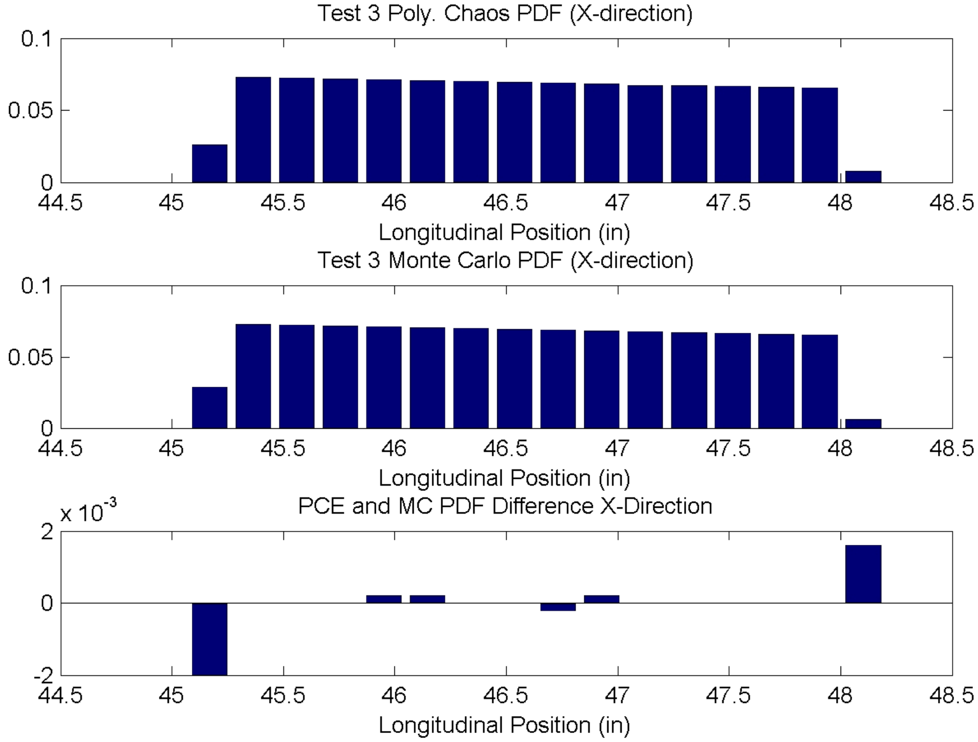

Figure 5.5: Longitudinal Results for Simulation Test 3 - F_1 Uniform Distribution

Polynomial chaos expansion also provides an advantage over Monte Carlo in that the derived coefficients in the solution provide information about the distribution without requiring a plot of the distribution. The information from these coefficients can aid in the determination of the mean or median value, the range of the distribution, or other information like the order polynomial, which is required to accurately recreate the distribution. Table 5.2 provides the polynomial coefficients to the 7th order polynomial.

Table 5.2: Polynomial Coefficients from Uncertain F₁ Uniform Simulation Tests

		Order of Polynomial Coefficients							
Direction	**Test**	**0**	**1**	**2**	**3**	**4**	**5**	**6**	**7**
X	**1**	55.0234	-1.9658	0.0468	-0.001	0	0	0	0
X	**2**	56.1908	-14.2898	2.4212	-0.3691	0.0536	-0.0074	0	0
X	**3**	46.681	-1.4149	0.0286	-0.0005	0	0	0	0
Y	**1**	30.0128	-1.0722	0.0255	-0.0005	0	0	0	0
Y	**2**	30.6495	-7.7944	1.3206	-0.2013	0.0292	-0.0041	0	0
Y	**3**	25.4623	-0.7718	0.0156	-0.0003	0	0	0	0

Table 5.2 clearly shows the impact of the mean and the range through the polynomial coefficients. The first two Legendre polynomial orders indicate the mean and range. By simply doubling the 1st order coefficient the range of the distribution is found. For example in the longitudinal direction test one, the mean of the distribution is 55.023 inches and the range is two times 1.966 inches or 3.932 inches. The impact of the higher order polynomials is not as clear, but they still provide relevant information. It shows that the distribution is not a simple first order distribution. It also shows the order of the polynomials that are required to accurately recreate the distribution. It can be seen that for a uniform input with a single uncertain parameter, a fifth order polynomial is large enough to capture the distribution. For more realistic uncertainties, a 3rd order polynomial is accurate enough..

It is interesting to see how the center of gravity distribution is impacted if the input uncertainty appeared in the numerator and denominator of the center of gravity equation. To analyze this, the previous tests were conducted with F_2 as the unknown distribution.

5.4.2 Uncertain Input F₂: Uniform Distribution

$$\begin{aligned} \hat{x}(\zeta_2) &= \frac{\left(\widehat{F_2}(\zeta_2) + F_3\right)L}{\left(F_1 + \widehat{F_2}(\zeta_2) + F_3 + F_4\right)} \\ \hat{y}(\zeta_2) &= \frac{(F_3 + F_4)W}{\left(F_1 + \widehat{F_2}(\zeta_2) + F_3 + F_4\right)} \end{aligned} \tag{5.23}$$

As seem in equation (5.23), F_2 is located in both the numerator and denominator of the longitudinal center of gravity equations. The direct impact of the uncertainty in the numerator and denominator is not easily known; Therefore, tests are necessary for this situation.

Table 5.3: Simulation Runs for Uncertain Input F_2

	F1		F2		F3		F4	
Test	Mean	Range	Mean	Range	Mean	Range	Mean	Range
1	700	0	700	100	700	0	700	0
2	700	0	700	700	700	0	700	0
3	700	0	1200	100	700	0	700	0

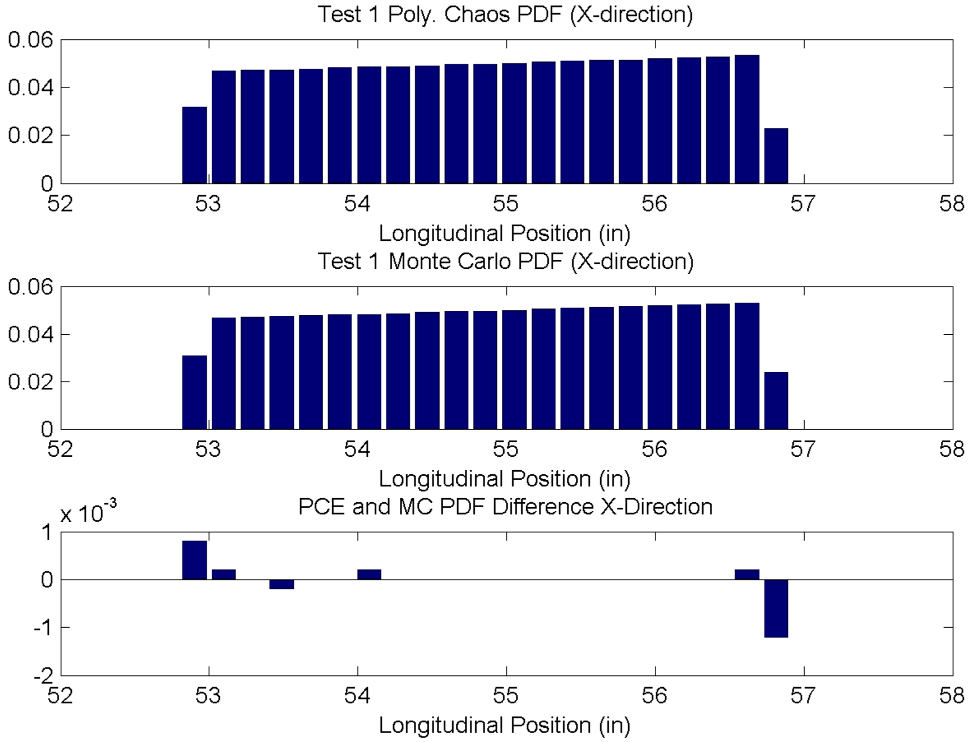

Figure 5.6: Longitudinal Results for Simulation Test 1 - F_2 Uniform Distribution

The results from simulation test 1 show that the graph is the opposite of the uncertain F_1 simulation. This is the solution that one would be arrived at if the coordinates were rearranged to avoid having F_2 in the numerator and denominator. It is not previously obvious that these two situations would arrive at the same solution since one situation has the uncertainty within the equation in the numerator and the denominator, while the other has the uncertainty solely in the denominator. Simulation tests two and three confirm that this is indeed the case.

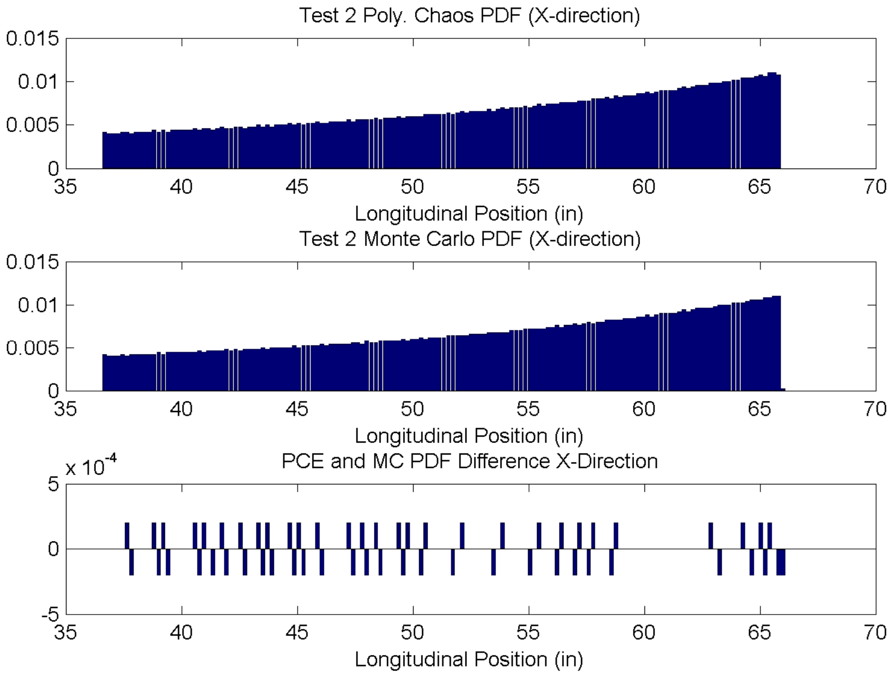

Figure 5.7: Longitudinal Results for Simulation Test 2 - F_2 Uniform Distribution

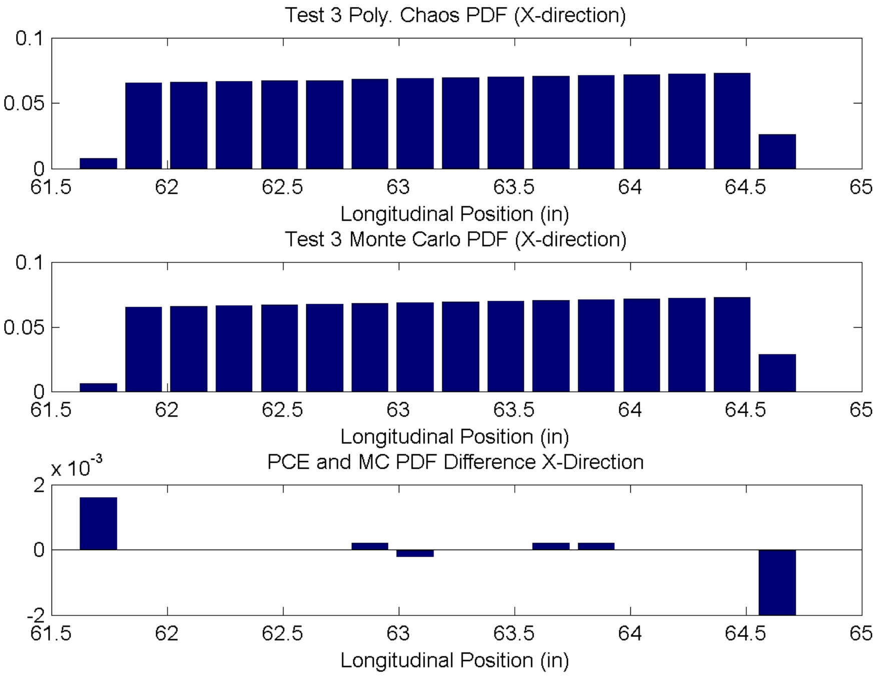

Figure 5.8: Longitudinal Results for Simulation Test 3 - F_2 Uniform Distribution

The coefficients from the polynomial chaos expansion also confirm that rearranging the coordinates does not make a difference. The 0th order coefficients for the longitudinal direction have flipped over the midpoint of the vehicle, 55 inches. Also, the other coefficients have changed signs since F_2 is at the front of the vehicle. This information can be seen by comparing Table 5.4 to Table 5.2

Table 5.4: Polynomial Coefficients from Uncertain F_2 Uniform Simulation Tests

		Order of Polynomial Coefficients							
Direction	**Test**	**0**	**1**	**2**	**3**	**4**	**5**	**6**	**7**
X	**1**	54.9766	-1.9658	-0.0468	0.001	0	0	0	0
X	**2**	53.8092	14.2898	-2.4212	0.3691	-0.0536	0.0074	0	0
X	**3**	63.319	1.4149	-0.0286	0.0005	0	0	0	0
Y	**1**	30.0128	-1.0722	0.0255	-0.0005	0	0	0	0
Y	**2**	30.6495	-7.7944	1.3206	-0.2013	0.0292	-0.0041	0	0
Y	**3**	25.4623	-0.7718	0.0156	-0.0003	0	0	0	0

5.4.3 Uncertain Input F_1: Estimated Distribution

The impact of a single uniform probability input distribution was detailed in the previous section. This section uses the PCE model to analyze the results from the data collected in the moved mass test. The results are presented from both the uniform and beta distribution results.

F_1's distribution is based on data collected from the four tests. The other three force values are based on the values taken from the scales. The average values from the load measurement system could also be used but they would add error not included in the F_1 distribution. The moved mass tests will first be analyzed using the uniform distribution and then the beta distribution. The moved mass tests are given in the following table.

Table 5.5: One Uncertain Input Moved Mass PCE Simulation Setup

	LF		**RF**		**LR**		**RR**	
Test	**Scale Value (lbs)**	**Range (lbs)**	**Scale Value (lbs)**	**Range (lbs)**	**Average (lbs)**	**Range (lbs)**	**Scale Value (lbs)**	**Range (lbs)**
1	496	0	380	0	533	32.8	609	0
2	455	0	313	0	753.4	36.4	901	0
3	510	0	398	0	701.2	31.2	832	0
4	565	0	481	0	615.4	39.6	755	0

The uniform distribution results are provided in Figure 5.9 and Figure 5.10.

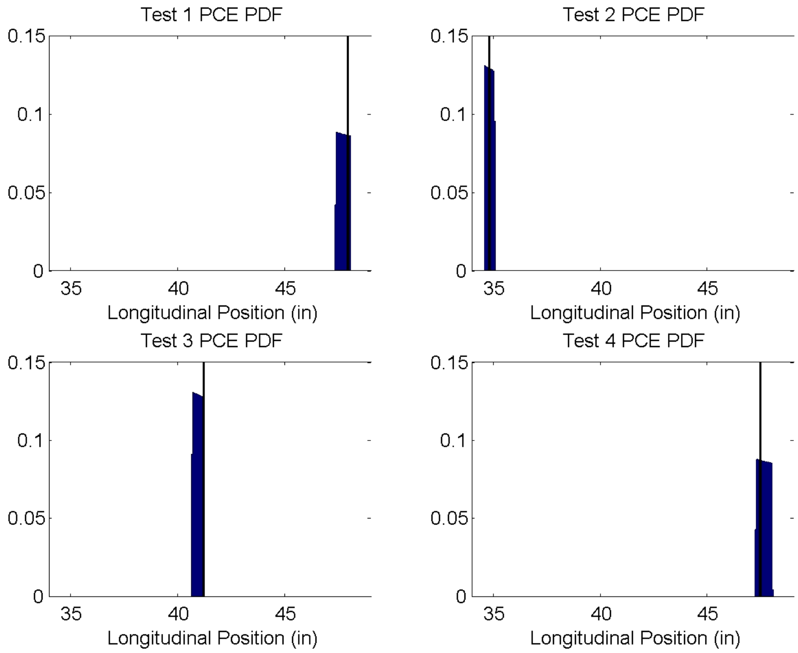

Figure 5.9: Center of Gravity Distribution from F_1 Uncertain Uniform Input Distribution – Longitudinal Direction

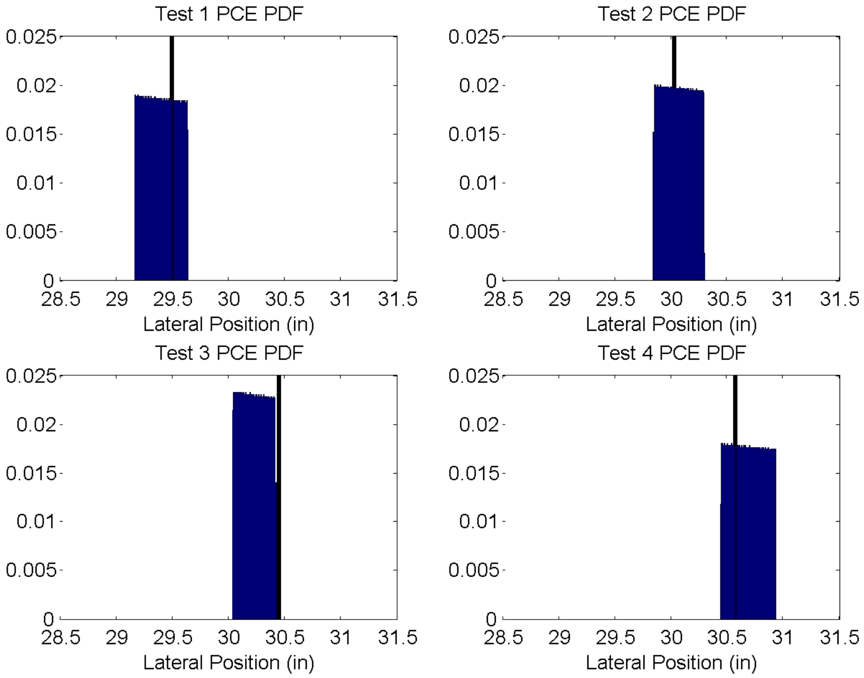

Figure 5.10: Center of Gravity Distribution from F_1 Uncertain Uniform Input Distribution – Lateral Direction

Figure 5.9 and Figure 5.10 show that the uncertainty from one uncertain force input creates a center of gravity uncertainty between half an inch to an inch in the longitudinal direction and half an inch in the lateral direction. The distribution includes the value from the Longacre Computerscales DX for all tests except test 3. As uncertainties from more wheels are added this occurrence should decrease. It can be seen that the distributions hold the same shape as those in the initial simulation, Figure 5.2.

This simulation can also be conducted with the beta distribution. The polynomial chaos coefficients for the left front wheel for each test are given in Table 5.6.

Table 5.6: Polynomial Chaos Coefficients for Beta Distribution for LR Wheelpan

	Polynomial Coefficient Values Left Rear				
Test	**1st order**	**2nd order**	**3rd order**	**4th order**	**5th order**
1	509.3	4.93	0.5	0	0
2	726.73	5.73	0.5	0	0
3	678.87	4.57	0.5	0	0
4	586.07	6.44	0.5	0	0

The distribution should have the same range as the uniform distribution, but merely shaped differently.

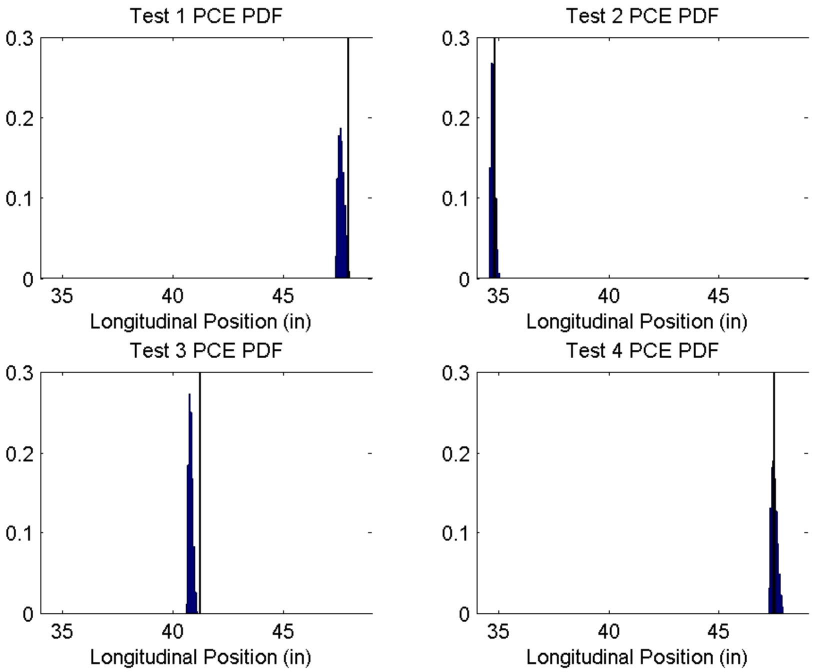

Figure 5.11: Center of Gravity Distribution from F_1 Uncertain Beta Input Distribution – Longitudinal Direction

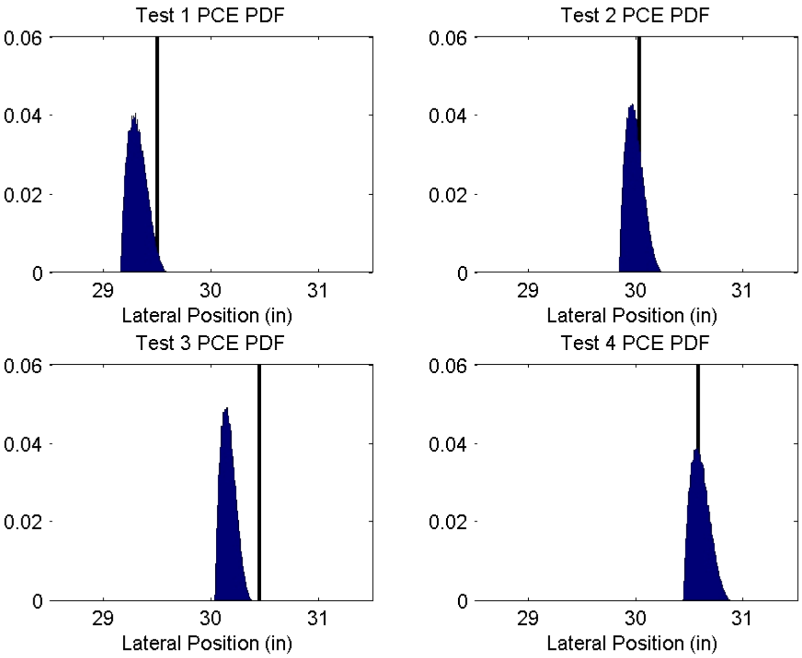

Figure 5.12: Center of Gravity Distribution from F_1 Uncertain Beta Input Distribution – Lateral Direction

It can be seen that the distributions have the same range. The range for the longitudinal direction is from half an inch to nearly an inch and approaches half an inch for the lateral direction. This range can be significant for a race vehicle, but it may not be of significant consequence for, other cars it. It can also be seen that the distribution shape reverses compared to F_1's distribution. This should be expected since a larger F_1 creates a center of gravity that is closer to F_1.

This test confirms that multiple distributions can be applied using polynomial chaos expansion. The uniform and beta distribution solution encompassed the same range, but their shapes were significantly different.

6. CALCULATION OF VEHICLE CENTER OF GRAVITY WITH MULTIPLE UNCERTAIN FORCE INPUTS

This section analyzes the uncertainty on the calculation of the vehicle center of gravity resulting from multiple uncertain force inputs. PCE methods are utilized during the analysis of this process. Two cases will be examined: the case where the distribution is an estimated distribution based on real data with two uncertain inputs and the case where four uncertain uniform inputs are used to estimate the center of gravity distribution.

6.1 Polynomial Chaos Expansion Model with Two Uncertain Inputs

Multiple uncertain input polynomial chaos expansion models are more complex than a single uncertain input. The increased complexity in the system results from several factors such as multiple uncertain inputs, which causes the solution to consist of a combination of their uncertainties. Therefore, the impact of both orthogonal basis functions must be considered. This is why the complexity of PCE models grows very quickly. Equation (6.1) defines how many basis functions are required given the order of the input basis functions and the number of uncertain inputs [7, 8, 9].

$$0 \le i_1 + \cdots + i_n \le P \Rightarrow S = \frac{(n+P)!}{n! \cdot P!} \tag{6.1}$$

P represents the number of uncertain inputs.

Table 6.1: Number of Polynomial Chaos Coefficients *r*

Order of Polynomials (s)	P=1	P=2	P=3	P=4
5	6	21	56	126
10	11	66	286	1001
20	21	231	1771	10626

The first problem to analyze will be a two degree of freedom polynomial chaos model. From there, the polynomial chaos model can easily be taken to multiple uncertain parameters.

6.1.1 Polynomial Chaos Model: Uncertain F1 and F4

The uncertain inputs will once again be defined as:

$$\begin{aligned} \widehat{F_1} &= \sum_{i=0}^{s} a_i \phi_i\left(\zeta_1\right) \\ \widehat{F_4} &= \sum_{i=0}^{s} d_i \phi_i\left(\zeta_4\right) \end{aligned} \tag{6.2}$$

Application of these definitions to the center of gravity equations results in the following equations.

$$\begin{aligned} X\left(\zeta_1,\zeta_4\right) &= \frac{\left(F_2+F_3\right)L}{\left(\widehat{F_1}+F_2+F_3+\widehat{F_4}\right)} \Rightarrow X\left(\zeta_1,\zeta_4\right) = \frac{\left(F_2+F_3\right)L}{\left(\sum_{i=0}^{s} a_i\phi_i\left(\zeta_1\right)+F_2+F_3+\sum_{i=0}^{s} d_i\phi_i\left(\zeta_4\right)\right)} \\ Y\left(\zeta_1,\zeta_4\right) &= \frac{\left(F_3+\widehat{F_4}\right)T}{\left(\widehat{F_1}+F_2+F_3+\widehat{F_4}\right)} \Rightarrow Y\left(\zeta_1,\zeta_4\right) = \frac{\left(F_3+\sum_{i=0}^{s} d_i\phi_i\left(\zeta_4\right)\right)T}{\left(\sum_{i=0}^{s} a_i\phi_i\left(\zeta_1\right)+F_2+F_3+\sum_{i=0}^{s} d_i\phi_i\left(\zeta_4\right)\right)} \end{aligned} \tag{6.3}$$

The CG locations, $X\left(\zeta_1,\zeta_4\right)$ and $Y\left(\zeta_1,\zeta_4\right)$ are redefined as polynomial chaos functions that are comprised of the polynomial chaos basis functions for each uncertain input. These basis functions need to be combined to achieve all possible combinations from the two possible basis functions. The grid in Figure 6.1 is used to explain this process.

$\Phi\left(\zeta_1,\zeta_4\right)=$

	$\phi_0\left(\zeta_1\right)$	$\phi_1\left(\zeta_1\right)$	$\phi_2\left(\zeta_1\right)$	$\phi_n\left(\zeta_1\right)$
$\phi_0\left(\zeta_4\right)$	$\Phi_0\left(\zeta_1,\zeta_4\right)$	$\Phi_1\left(\zeta_1,\zeta_4\right)$	$\Phi_3\left(\zeta_1,\zeta_4\right)$	
$\phi_1\left(\zeta_4\right)$	$\Phi_2\left(\zeta_1,\zeta_4\right)$	$\Phi_4\left(\zeta_1,\zeta_4\right)$		
$\phi_2\left(\zeta_4\right)$	$\Phi_5\left(\zeta_1,\zeta_4\right)$			
$\phi_n\left(\zeta_4\right)$				

Figure 6.1: Basis Function to n^{th} order

The basis functions for $X\left(\zeta_1,\zeta_4\right)$ and $Y\left(\zeta_1,\zeta_4\right)$ are the product of the basis functions for the two uncertain inputs [7]. For example:

$$\Phi_5\left(\zeta_1,\zeta_4\right)=\phi_0\left(\zeta_1\right)\phi_2\left(\zeta_4\right).$$

In order to maintain a certain polynomial power, the polynomial chaos functions are applied along the diagonal of the grid. The order of the polynomial basis functions does not matter as long as they are consistently chosen and known. Equation (6.4) shows the polynomial chaos basis functions for the Legendre polynomials to the 2nd power.

$$\Phi\left(\zeta_1,\zeta_4\right)=\begin{cases} \begin{array}{cc} 1 & \phi_0\left(\zeta_1\right)\phi_0\left(\zeta_4\right) \\ \zeta_1 & \phi_1\left(\zeta_1\right)\phi_0\left(\zeta_4\right) \\ \zeta_4 & \phi_0\left(\zeta_1\right)\phi_1\left(\zeta_4\right) \\ (1/2)\left(3\zeta_1^2-1\right) & \phi_2\left(\zeta_1\right)\phi_0\left(\zeta_4\right) \\ \zeta_1\zeta_4 & \phi_1\left(\zeta_1\right)\phi_1\left(\zeta_4\right) \\ (1/2)\left(3\zeta_4^2-1\right) & \phi_0\left(\zeta_1\right)\phi_2\left(\zeta_4\right) \end{array} \end{cases} \tag{6.4}$$

X and Y center of gravity locations can then be redefined with the new set of basis functions as seen in equation (6.5).

$$X\left(\zeta_1,\zeta_4\right)=\sum_{j=o}^{r}x_j\Phi_j\left(\zeta_1,\zeta_4\right)$$
$$Y\left(\zeta_1,\zeta_4\right)=\sum_{j=o}^{r}y_j\Phi_j\left(\zeta_1,\zeta_4\right) \tag{6.5}$$

This makes the definition of F_1 and F_4 complex. Even though the uncertainties in the forces are independent of each other, the definition in Equation (6.2) is not the easiest implementation of the basis functions into Equation (6.3). Another option is to define the forces with $\Phi\left(\zeta_1,\zeta_4\right)$, where coefficients are zero for all basis functions that are not each uncertain input's basis functions. To further lessen the computations that must be completed, $\Phi\left(\zeta_1,\zeta_4\right)$ can be ordered so the first Φ s directly correspond to the input basis functions. This can greatly reduce computations as higher order basis functions are applied.

$$F_1=\sum_{i=0}^{2s+1}a_i\Phi_i\left(\zeta_1,\zeta_4\right)\quad\begin{cases}a_{1,2,\cdots s} & \Phi_i=\phi\left(\zeta_1\right)_{1,2,\cdots s}\\ 0 & \Phi_i\neq\phi\left(\zeta_1\right)_{1,2\cdots s}\end{cases}$$
$$F_4=\sum_{i=0}^{2s+1}d_i\Phi_i\left(\zeta_1,\zeta_4\right)\quad\begin{cases}d_{1,2,\cdots s} & \Phi_i=\phi\left(\zeta_4\right)_{1,2\cdots s}\\ 0 & \Phi_i\neq\phi\left(\zeta_4\right)_{1,2\cdots s}\end{cases} \tag{6.6}$$

Using equation (6.6), equation 5.3 can be rewritten by moving the denominator to the other side thus to removing the division operation. The basis functions for F_1 and F_2 must be taken to the power $2s+1$ because the polynomial chaos functions for each must be unique; Therefore, the resulting equations are

$$\left(\sum_{i=0}^{2s+1}a_i\Phi_i\left(\zeta_1\right)+F_2+F_3+\sum_{i=0}^{s}d_i\Phi_i\left(\zeta_4\right)\right)\left(\sum_{j=0}^{r}x_j\Phi_j\left(\zeta_1,\zeta_4\right)\right)=\left(F_2+F_3\right)L$$
$$\left(\sum_{i=0}^{2s+1}a_i\Phi_i\left(\zeta_1\right)+F_2+F_3+\sum_{i=0}^{s}d_i\Phi_i\left(\zeta_4\right)\right)\left(\sum_{j=0}^{r}y_j\Phi_j\left(\zeta_1,\zeta_4\right)\right)=F_3T+T\left(\sum_{i=0}^{s}d_i\Phi_i\left(\zeta_4\right)\right) \tag{6.7}$$

The equation for the lateral CG location is more complex than the one for the longitudinal CG location because the uncertain inputs are in the numerator and denominator of center of gravity equation. However, it is impossible to choose a coordinate system for multiple uncertain inputs that does not place the uncertainty on both sides of the equation for either the lateral or the longitudinal CG equations. It is shown in section 5.4.2 this was not a issue because it did not increase the uncertainty in solving for the CG location. The derivation for the lateral direction is shown due to its relative complexity.

Multiplying through equation (6.7) results in

$$\begin{aligned}&\sum_{i=0}^{2s+1}\sum_{j=0}^{r} a_i y_j \Phi_i\left(\zeta_1\right)\Phi_j\left(\zeta_1,\zeta_4\right)+\sum_{i=0}^{2s+1}\sum_{j=0}^{r} d_i y_j \Phi_i\left(\zeta_1\right)\Phi_j\left(\zeta_1,\zeta_4\right)\cdots\\&\cdots+\left(F_2+F_3\right)\left(\sum_{j=0}^{r} y_j\Phi_j\left(\zeta_1,\zeta_4\right)\right)=F_3T+T\left(\sum_{i=0}^{2s+1} d_i\Phi_i\left(\zeta_4\right)\right)\end{aligned}\tag{6.8}$$

Applying Galerkin projection with the appropriate inner product on equation (6.8):

$$\begin{aligned}&\left\langle\Phi_n,\sum_{i=0}^{2s+1}\sum_{j=0}^{r} a_i y_j \Phi_i\left(\zeta_1\right)\Phi_j\left(\zeta_1,\zeta_4\right)\right\rangle+\left\langle\Phi_n,\sum_{i=0}^{2s+1}\sum_{j=0}^{r} d_i y_j \Phi_i\left(\zeta_1\right)\Phi_j\left(\zeta_1,\zeta_4\right)\right\rangle\cdots\\&\cdots+\left\langle\Phi_n,\left(F_2+F_3\right)\left(\sum_{j=0}^{r} y_j\Phi_j\left(\zeta_1,\zeta_4\right)\right)\right\rangle=\left\langle\Phi_n,F_3T+T\left(\sum_{i=0}^{2s+1} d_i\Phi_i\left(\zeta_4\right)\right)\right\rangle\end{aligned}\tag{6.9}$$

$$\begin{aligned}&\int_{-1}^{1}\int_{-1}^{1}\sum_{i=0}^{2s+1}\sum_{j=0}^{r} a_i y_j \Phi_i\left(\zeta_1\right)\Phi_j\left(\zeta_1,\zeta_4\right)\Phi_n\left(\zeta_1,\zeta_4\right)w\left(\zeta_1,\zeta_4\right)\partial\zeta_1\partial\zeta_4+\cdots\\&\cdots\int_{-1}^{1}\int_{-1}^{1}\sum_{i=0}^{2s+1}\sum_{j=0}^{r} d_i y_j \Phi_i\left(\zeta_1\right)\Phi_j\left(\zeta_1,\zeta_4\right)\Phi_n\left(\zeta_1,\zeta_4\right)w\left(\zeta_1,\zeta_4\right)\partial\zeta_1\partial\zeta_4+\cdots\\&\cdots\left(F_2+F_3\right)\int_{-1}^{1}\int_{-1}^{1}\sum_{j=0}^{r} y_j\Phi_j\left(\zeta_1,\zeta_4\right)\Phi_n\left(\zeta_1,\zeta_4\right)w\left(\zeta_1,\zeta_4\right)\partial\zeta_1\partial\zeta_4=\cdots\\&\cdots F_3T\int_{-1}^{1}\int_{-1}^{1}\Phi_j\left(\zeta_1,\zeta_4\right)w\left(\zeta_1,\zeta_4\right)\partial\zeta_1\partial\zeta_4+T\int_{-1}^{1}\int_{-1}^{1}\sum_{i=0}^{2s+1} d_i\Phi_i\left(\zeta_4\right)\Phi_n\left(\zeta_1,\zeta_4\right)w\left(\zeta_1,\zeta_4\right)\partial\zeta_1\partial\zeta_4\end{aligned}\tag{6.10}$$

These integrals can be precomputed using Matlab. In addition, multiple parts of this equation can be written in linear algebra form to be solved more efficiently. δ defines the precomputed integrals. δ is different from the δ used in one dimension in that it must integrate over multiple dimensions of ζ .

$$\delta_{ijn} = \int_{-1}^{1}\int_{-1}^{1} \Phi_i\left(\zeta_1\right)\Phi_j\left(\zeta_1,\zeta_4\right)\Phi_n\left(\zeta_1,\zeta_4\right)w\left(\zeta_1,\zeta_4\right)\partial\zeta_1\partial\zeta_4 \tag{6.11}$$

$$\delta_{jn} = \int_{-1}^{1}\int_{-1}^{1} \Phi_j\left(\zeta_1,\zeta_4\right)\Phi_n\left(\zeta_1,\zeta_4\right)w\left(\zeta_1,\zeta_4\right)\partial\zeta_1\partial\zeta_4 \tag{6.12}$$

$$\delta_{in} = \int_{-1}^{1}\int_{-1}^{1} \Phi_i\left(\zeta_1\right)\Phi_n\left(\zeta_1,\zeta_4\right)w\left(\zeta_1,\zeta_4\right)\partial\zeta_1\partial\zeta_4 \tag{6.13}$$

$$\delta_{n} = \int_{-1}^{1}\int_{-1}^{1} \Phi_n\left(\zeta_1,\zeta_4\right)w\left(\zeta_1,\zeta_4\right)\partial\zeta_1\partial\zeta_4 \tag{6.14}$$

The weighting function was first defined for one dimension. The weighting function for multiple dimensions is a bit different, but remains simplistic in form if the two distributions are independent of each other [7].

$$w\left(\zeta_1,\zeta_4\right) = w\left(\zeta_1\right)w\left(\zeta_4\right) \tag{6.15}$$

The load measurement uncertainties are assumed independent between different systems. The following equation shows the reduced form of equation 5.8.

$$\sum_{i=0}^{2s+1}\sum_{j=0}^{r} a_i y_j \delta_{ijn} + \sum_{i=0}^{2s+1}\sum_{j=0}^{r} d_i y_j \delta_{ijn} + \left(F_2 + F_3\right)\sum_{j=0}^{r} y_j \delta_{jn} = T\left(\sum_{i=0}^{2s+1} d_i \delta_{in} + F_3 \delta_{in}\right) \tag{6.16}$$

The first few terms in equation (6.16) can be condensed to take on a linear algebra form. This can be done in the same way it was done for the one-dimensional case in section 5.1.

$$\begin{aligned}
\psi_{n0} &= \left(a_0\delta_{00n} + a_1\delta_{10n} + \cdots + a_s\delta_{s0n}\right) & \tau_{n0} &= \left(d_0\delta_{00n} + d_1\delta_{10n} + \cdots + d_s\delta_{s0n}\right) \\
\psi_{n1} &= \left(a_0\delta_{01n} + a_1\delta_{11n} + \cdots + a_s\delta_{s1n}\right) & \tau_{n1} &= \left(d_0\delta_{01n} + d_1\delta_{11n} + \cdots + d_s\delta_{s1n}\right) \\
&\vdots & &\vdots \\
\psi_{nr} &= \left(a_0\delta_{0rn} + a_1\delta_{1rn} + \cdots + a_s\delta_{srn}\right) & \tau_{nr} &= \left(d_0\delta_{0rn} + d_1\delta_{1rn} + \cdots + d_s\delta_{srn}\right)
\end{aligned} \tag{6.17}$$

Converting this to linear algebra form:

$$\begin{aligned}
&\left(\begin{bmatrix} \psi_{00} & \psi_{01} & \cdots & \psi_{0r} \\ \psi_{10} & \psi_{11} & & \vdots \\ \vdots & & \ddots & \vdots \\ \psi_{r0} & \cdots & \cdots & \psi_{rr} \end{bmatrix} + \begin{bmatrix} \tau_{00} & \tau_{01} & \cdots & \tau_{0r} \\ \tau_{10} & \tau_{11} & & \vdots \\ \vdots & & \ddots & \vdots \\ \tau_{r0} & \cdots & \cdots & \tau_{rr} \end{bmatrix} + \left(F_2 + F_3\right) \begin{bmatrix} \delta_{00} & 0 & 0 & 0 \\ 0 & \delta_{11} & 0 & 0 \\ 0 & 0 & \ddots & 0 \\ 0 & 0 & 0 & \delta_{rr} \end{bmatrix}\right) \begin{Bmatrix} y_0 \\ y_1 \\ \vdots \\ y_r \end{Bmatrix} = \cdots \\
&\cdots T \left(F_3 \begin{Bmatrix} \delta_0 \\ \delta_1 \\ \vdots \\ \delta_r \end{Bmatrix} + \underbrace{\begin{bmatrix} \delta_{00} & 0 & 0 \\ 0 & \ddots & 0 \\ \vdots & 0 & \delta_{(2s+1)(2s+1)} \\ 0 & 0 & 0 \end{bmatrix}}_{r\times 2s+1} \begin{Bmatrix} b_0 \\ b_1 \\ \vdots \\ b_{2s+1} \end{Bmatrix} \right)
\end{aligned} \tag{6.18}$$

Solving for y_n, the lateral CG solution is given in equation (6.18).

$$\begin{aligned}
&\begin{Bmatrix} y_0 \\ y_1 \\ \vdots \\ y_r \end{Bmatrix} = T \left(\begin{bmatrix} \psi_{00} & \psi_{01} & \cdots & \psi_{0r} \\ \psi_{10} & \psi_{11} & & \vdots \\ \vdots & & \ddots & \vdots \\ \psi_{r0} & \cdots & \cdots & \psi_{rr} \end{bmatrix} + \begin{bmatrix} \tau_{00} & \tau_{01} & \cdots & \tau_{0r} \\ \tau_{10} & \tau_{11} & & \vdots \\ \vdots & & \ddots & \vdots \\ \tau_{r0} & \cdots & \cdots & \tau_{rr} \end{bmatrix} + \left(F_2 + F_3\right) \begin{bmatrix} \delta_{00} & 0 & 0 & 0 \\ 0 & \delta_{11} & 0 & 0 \\ 0 & 0 & \ddots & 0 \\ 0 & 0 & 0 & \delta_{rr} \end{bmatrix}\right)^{-1} \cdots \\
&\cdots \left(F_3 \begin{Bmatrix} \delta_0 \\ \delta_1 \\ \vdots \\ \delta_r \end{Bmatrix} + \underbrace{\begin{bmatrix} \delta_{00} & 0 & 0 \\ 0 & \ddots & 0 \\ \vdots & 0 & \delta_{(2s+1)(2s+1)} \\ 0 & 0 & 0 \end{bmatrix}}_{r\times 2s+1} \begin{Bmatrix} d_0 \\ d_1 \\ \vdots \\ d_{2s+1} \end{Bmatrix} \right)
\end{aligned} \tag{6.19}$$

The longitudinal center of gravity solution can be found in a similar way.

$$\begin{Bmatrix} x_0 \\ x_1 \\ \vdots \\ x_r \end{Bmatrix} = \left(F_2 + F_3\right) L \cdots$$

$$\cdots \left(\begin{bmatrix} \psi_{00} & \psi_{01} & \cdots & \psi_{0r} \\ \psi_{10} & \psi_{11} & & \vdots \\ \vdots & & \ddots & \vdots \\ \psi_{r0} & \cdots & \cdots & \psi_{rr} \end{bmatrix} + \begin{bmatrix} \tau_{00} & \tau_{01} & \cdots & \tau_{0r} \\ \tau_{10} & \tau_{11} & & \vdots \\ \vdots & & \ddots & \vdots \\ \tau_{r0} & \cdots & \cdots & \tau_{rr} \end{bmatrix} + \left(F_2 + F_3\right) \begin{bmatrix} \delta_{00} & 0 & 0 & 0 \\ 0 & \delta_{11} & 0 & 0 \\ 0 & 0 & \ddots & 0 \\ 0 & 0 & 0 & \delta_{rr} \end{bmatrix} \right)^{-1} \begin{Bmatrix} \delta_0 \\ \delta_1 \\ \vdots \\ \delta_r \end{Bmatrix} \tag{6.20}$$

The δ matrices can be precomputed and are dependent on the choosen orthogonal basis functions. δ_{ijn} is a three dimensional matrix of dimensions $s \times r \times r$. The other δ's were described in chapter 5.

$X_n \text{ and } Y_n$ can now be solved for equations (6.19) and (6.20). Since $X_n \text{ and } Y_n$ are known, they can be plotted using methods described in section 5.3.

6.2 Polynomial Chaos Expansion Model with Four Uncertain Inputs

The previous derivations were all taking steps to attain the final derivation for the polynomial chaos expansion for the center of gravity equation. This is the case where all four wheel loads are uncertain and is the real world situation. This section will provide the polynomial chaos expansion for four uncertain inputs.

The Karhunen-Love expansion can redefine the four uncertain parameters as

$$\begin{aligned}\widehat{F}_1 &= \sum_{i=0}^{s} a_i\phi_i\left(\zeta_1\right)\\ \widehat{F}_2 &= \sum_{i=0}^{s} b_i\phi_i\left(\zeta_2\right)\\ \widehat{F}_3 &= \sum_{i=0}^{s} c_i\phi_i\left(\zeta_3\right)\\ \widehat{F}_4 &= \sum_{i=0}^{s} d_i\phi_i\left(\zeta_4\right)\end{aligned} \tag{6.21}$$

Application of these definitions to the center of gravity equations results in the following equation:

$$\begin{gathered} X\left(\zeta_1,\zeta_2,\zeta_{3,}\zeta_4\right)=\frac{\left(\widehat{F}_2+\widehat{F}_3\right)L}{\left(\widehat{F}_1+\widehat{F}_2+\widehat{F}_3+\widehat{F}_4\right)}\Rightarrow X\left(\zeta_1 ...\right)=\cdots \\ \cdots\frac{\left(\sum_{i=0}^{s} b_i\phi_i\left(\zeta_2\right)+\sum_{i=0}^{s} c_i\phi_i\left(\zeta_3\right)\right)L}{\left(\sum_{i=0}^{s} a_i\phi_i\left(\zeta_1\right)+\sum_{i=0}^{s} b_i\phi_i\left(\zeta_2\right)+\sum_{i=0}^{s} c_i\phi_i\left(\zeta_3\right)+\sum_{i=0}^{s} d_i\phi_i\left(\zeta_4\right)\right)} \\ Y\left(\zeta_1,\zeta_2,\zeta_{3,}\zeta_4\right)=\frac{\left(\widehat{F}_3+\widehat{F}_4\right)T}{\left(\widehat{F}_1+\widehat{F}_2+\widehat{F}_3+\widehat{F}_4\right)}\Rightarrow Y\left(\zeta_1,...\right)=\cdots \\ \cdots\frac{\left(\sum_{i=0}^{s} c_i\phi_i\left(\zeta_3\right)+\sum_{i=0}^{s} d_i\phi_i\left(\zeta_4\right)\right)T}{\left(\sum_{i=0}^{s} a_i\phi_i\left(\zeta_1\right)+\sum_{i=0}^{s} b_i\phi_i\left(\zeta_2\right)+\sum_{i=0}^{s} c_i\phi_i\left(\zeta_3\right)+\sum_{i=0}^{s} d_i\phi_i\left(\zeta_4\right)\right)} \end{gathered} \tag{6.22}$$

As preformed in the previous section, the CG locations, $X\left(\zeta_1,\zeta_{2,}\zeta_3,\zeta_4\right)$ and $Y\left(\zeta_1,\zeta_2,\zeta_3,\zeta_4\right)$ are then redefined as a polynomial chaos functions. The difference now is the presence of four uncertain inputs rather than just two. Therefore more uncertain inputs will cause the basis functions to escalate at a rate defined by equation 6.1. Since the uncertainties are independent of each other, the basis functions for X and Y are the product of the basis functions for the two uncertain inputs [7]. For example:

$$\Phi\left(\zeta_1,\zeta_2,\zeta_3,\zeta_4\right)=\phi\left(\zeta_1\right)\phi\left(\zeta_2\right)\phi\left(\zeta_3\right)\phi\left(\zeta_4\right) \tag{6.23}$$

In order to maintain a defined polynomial power, the polynomial chaos functions are applied along the diagonal of the grid. Figure 6.1 shows the polynomial chaos functions to the 2nd power. *X* and *Y* center of gravity locations can then redefined with the new set of basis functions.

$$
\begin{aligned}
X\left(\zeta_1,\zeta_2,\zeta_3,\zeta_4\right) &= \sum_{j=o}^{r} x_j \Phi_j\left(\zeta_1,\zeta_2,\zeta_3,\zeta_4\right) \\
Y\left(\zeta_1,\zeta_2,\zeta_3,\zeta_4\right) &= \sum_{j=o}^{r} y_j \Phi_j\left(\zeta_1,\zeta_2,\zeta_3,\zeta_4\right)
\end{aligned}
\tag{6.24}
$$

Again F_1, F_2, F_3 and F_4 should be adapted to the multiple uncertain parameter equation thus causing the basis functions to be changed to match the output basis functions as seen in the following system of equations.

$$
\begin{aligned}
F_1 &= \sum_{i=0}^{4s+1} a_i \Phi_i\left(\zeta_1,\zeta_2,\zeta_3,\zeta_4\right) \quad \begin{cases} a_{1,2,\cdots s} & \Phi_i = \phi\left(\zeta_1\right)_{1,2,\cdots s} \\ 0 & \Phi_i \neq \phi\left(\zeta_1\right)_{1,2\cdots s} \end{cases} \\
F_2 &= \sum_{i=0}^{4s+1} b_i \Phi_i\left(\zeta_1,\zeta_2,\zeta_3,\zeta_4\right) \quad \begin{cases} b_{1,2,\cdots s} & \Phi_i = \phi\left(\zeta_2\right)_{1,2,\cdots s} \\ 0 & \Phi_i \neq \phi\left(\zeta_2\right)_{1,2\cdots s} \end{cases} \\
F_3 &= \sum_{i=0}^{4s+1} c_i \Phi_i\left(\zeta_1,\zeta_2,\zeta_3,\zeta_4\right) \quad \begin{cases} c_{1,2,\cdots s} & \Phi_i = \phi\left(\zeta_3\right)_{1,2,\cdots s} \\ 0 & \Phi_i \neq \phi\left(\zeta_3\right)_{1,2\cdots s} \end{cases} \\
F_4 &= \sum_{i=0}^{4s+1} d_i \Phi_i\left(\zeta_1,\zeta_2,\zeta_3,\zeta_4\right) \quad \begin{cases} d_{1,2,\cdots s} & \Phi_i = \phi\left(\zeta_4\right)_{1,2\cdots s} \\ 0 & \Phi_i \neq \phi\left(\zeta_4\right)_{1,2\cdots s} \end{cases}
\end{aligned}
\tag{6.25}
$$

By moving the denominator to the other side to eliminate the division operation, Equation (6.22) can be rewritten as

$$
\begin{aligned}
\left(\sum_{i=0}^{4s+1} a_i\Phi_i + \sum_{i=0}^{4s+1} b_i\Phi_i + \sum_{i=0}^{4s+1} c_i\Phi_i + \sum_{i=0}^{4s+1} d_i\Phi_i\right)\left(\sum_{j=0}^{r} x_j\Phi_j\left(\zeta_1,\zeta_4\right)\right) &= L\left(\sum_{i=0}^{4s+1} b_i\Phi_i + \sum_{i=0}^{4s+1} c_i\Phi_i\right) \\
\left(\sum_{i=0}^{4s+1} a_i\Phi_i + \sum_{i=0}^{4s+1} b_i\Phi_i + \sum_{i=0}^{4s+1} c_i\Phi_i + \sum_{i=0}^{4s+1} d_i\Phi_i\right)\left(\sum_{j=0}^{r} y_j\Phi_j\left(\zeta_1,\zeta_4\right)\right) &= T\left(\sum_{i=0}^{4s+1} c_i\Phi_i + \sum_{i=0}^{4s+1} d_i\Phi_i\right)
\end{aligned}
\tag{6.26}
$$

These equations are similar in form so the derivation of one will show the methodology used solve the other. The longitudinal equation will be solved from this point forward. Multiplying through equation (6.26) results in.

$$\begin{aligned}&\sum_{i=0}^{4s+1}\sum_{j=0}^{r} a_i x_j \Phi_i \Phi_j + \sum_{i=0}^{4s+1}\sum_{j=0}^{r} b_i x_j \Phi_i \Phi_j + \sum_{i=0}^{4s+1}\sum_{j=0}^{r} c_i x_j \Phi_i \Phi_j + \sum_{i=0}^{4s+1}\sum_{j=0}^{r} d_i x_j \Phi_i \Phi_j \cdots \\ &\cdots = L\left(\sum_{i=0}^{4s+1} b_i x_j \Phi_i + \sum_{i=0}^{4s+1} c_i x_j \Phi_i\right)\end{aligned} \tag{6.27}$$

Application of the Galerkin projection using the appropriate inner product:

$$\begin{aligned}&\left\langle \Phi_n, \sum_{i=0}^{4s+1}\sum_{j=0}^{r} a_i x_j \Phi_i \Phi_j \right\rangle + \left\langle \Phi_n, \sum_{i=0}^{4s+1}\sum_{j=0}^{r} b_i x_j \Phi_i \Phi_j \right\rangle + \left\langle \Phi_n, \sum_{i=0}^{4s+1}\sum_{j=0}^{r} c_i x_j \Phi_i \Phi_j \right\rangle + \cdots \\ &\left\langle \Phi_n, \sum_{i=0}^{4s+1}\sum_{j=0}^{r} d_i x_j \Phi_i \Phi_j \right\rangle = \left\langle \Phi_n, T\left(\sum_{i=0}^{4s+1} b_i x_j \Phi_i + \sum_{i=0}^{4s+1} c_i x_j \Phi_i\right)\right\rangle\end{aligned} \tag{6.28}$$

$$\begin{aligned}&\iiint\int_{-1}^{1}\sum_{i=0}^{4s+1}\sum_{j=0}^{r} a_i x_j \Phi_i \Phi_j w \partial\zeta_{1,2,3,4} + \iiint\int_{-1}^{1}\sum_{i=0}^{4s+1}\sum_{j=0}^{r} b_i x_j \Phi_i \Phi_j w \partial\zeta_{1,2,3,4} \cdots \\ &+\iiint\int_{-1}^{1}\sum_{i=0}^{4s+1}\sum_{j=0}^{r} c_i x_j \Phi_i \Phi_j w \partial\zeta_{1,2,3,4} + \iiint\int_{-1}^{1}\sum_{i=0}^{4s+1}\sum_{j=0}^{r} d_i x_j \Phi_i \Phi_j w \partial\zeta_{1,2,3,4} \cdots \\ &= L\left(\iiint\int_{-1}^{1}\sum_{i=0}^{4s+1}\sum_{j=0}^{r} b_i x_j \Phi_i \Phi_j w \partial\zeta_{1,2,3,4} + \iiint\int_{-1}^{1}\sum_{i=0}^{4s+1}\sum_{j=0}^{r} c_i x_j \Phi_i \Phi_j w \partial\zeta_{1,2,3,4}\right)\end{aligned} \tag{6.29}$$

$$\partial\zeta_{1,2,3,4} = \partial\zeta_1 \partial\zeta_2 \partial\zeta_3 \partial\zeta_4$$

By assuming the uncertainties are independent results in the following weighting function

$$w = w(\zeta_1, \zeta_2, \zeta_3, \zeta_4) = w(\zeta_1) w(\zeta_2) w(\zeta_3) w(\zeta_4). \tag{6.30}$$

The integrals from equation (6.29) can be precomputed as δ. δ is the same as in equation (6.11) through (6.14) except they are quadruple integrals instead of double.

Computing quadruple integrals is a computational intensive task, especially when it is repeated $r \times r \times (4s+1)$ times. Fortunately, this task can be computed once and used as a precomputed table. Simplification of equation (6.29) using δ results in.

$$\begin{aligned}
&\sum_{i=0}^{4s+1}\sum_{j=0}^{r} a_i x_j \delta_{ijn} + \sum_{i=0}^{4s+1}\sum_{j=0}^{r} b_i x_j \delta_{ijn} + \sum_{i=0}^{4s+1}\sum_{j=0}^{r} c_i x_j \delta_{ijn} + \sum_{i=0}^{4s+1}\sum_{j=0}^{r} d_i x_j \delta_{ijn} = \cdots \\
&\cdots L\left(\sum_{i=0}^{4s+1} b_i x_j \delta_{in} + \sum_{i=0}^{4s+1} c_i x_j \delta_{in}\right)
\end{aligned} \tag{6.31}$$

Transformation of equation 6.29 into a matrix form uses the same method as shown in Equation (6.17). This creates a solvable system of matrices.

$$\begin{aligned}
&\left(\begin{bmatrix} \psi_{00} & \psi_{01} & \cdots & \psi_{0r} \\ \psi_{10} & \psi_{11} & & \vdots \\ \vdots & & \ddots & \vdots \\ \psi_{r0} & \cdots & \cdots & \psi_{rr} \end{bmatrix} + \begin{bmatrix} \gamma_{00} & \gamma_{01} & \cdots & \gamma_{0r} \\ \gamma_{10} & \gamma_{11} & & \vdots \\ \vdots & & \ddots & \vdots \\ \gamma_{r0} & \cdots & \cdots & \gamma_{rr} \end{bmatrix} + \begin{bmatrix} \chi_{00} & \chi_{01} & \cdots & \chi_{0r} \\ \chi_{10} & \chi_{11} & & \vdots \\ \vdots & & \ddots & \vdots \\ \chi_{r0} & \cdots & \cdots & \chi_{rr} \end{bmatrix} + \begin{bmatrix} \tau_{00} & \tau_{01} & \cdots & \tau_{0r} \\ \tau_{10} & \tau_{11} & & \vdots \\ \vdots & & \ddots & \vdots \\ \tau_{r0} & \cdots & \cdots & \tau_{rr} \end{bmatrix}\right)\begin{Bmatrix} x_0 \\ x_1 \\ \vdots \\ x_r \end{Bmatrix} = \cdots \\
&\cdots L\left(\underbrace{\begin{bmatrix} \delta_{00} & 0 & 0 \\ 0 & \ddots & 0 \\ \vdots & 0 & \delta_{(4s+1)(4s+1)} \\ 0 & 0 & 0 \end{bmatrix}}_{r\times 4s+1}\begin{Bmatrix} b_0 \\ b_1 \\ \vdots \\ b_{4s+1} \end{Bmatrix} + \underbrace{\begin{bmatrix} \delta_{00} & 0 & 0 \\ 0 & \ddots & 0 \\ \vdots & 0 & \delta_{(4s+1)(4s+1)} \\ 0 & 0 & 0 \end{bmatrix}}_{r\times 4s+1}\begin{Bmatrix} c_0 \\ c_1 \\ \vdots \\ c_{4s+1} \end{Bmatrix}\right)
\end{aligned} \tag{6.32}$$

The longitudinal center of gravity polynomial chaos model is

$$\begin{aligned}
&\begin{Bmatrix} x_0 \\ x_1 \\ \vdots \\ x_s \end{Bmatrix} = L\left(\begin{bmatrix} \psi_{00} & \psi_{01} & \cdots & \psi_{0r} \\ \psi_{10} & \psi_{11} & & \vdots \\ \vdots & & \ddots & \vdots \\ \psi_{r0} & \cdots & \cdots & \psi_{rr} \end{bmatrix} + \begin{bmatrix} \gamma_{00} & \gamma_{01} & \cdots & \gamma_{0r} \\ \gamma_{10} & \gamma_{11} & & \vdots \\ \vdots & & \ddots & \vdots \\ \gamma_{r0} & \cdots & \cdots & \gamma_{rr} \end{bmatrix} + \begin{bmatrix} \chi_{00} & \chi_{01} & \cdots & \chi_{0r} \\ \chi_{10} & \chi_{11} & & \vdots \\ \vdots & & \ddots & \vdots \\ \chi_{r0} & \cdots & \cdots & \chi_{rr} \end{bmatrix} + \begin{bmatrix} \tau_{00} & \tau_{01} & \cdots & \tau_{0r} \\ \tau_{10} & \tau_{11} & & \vdots \\ \vdots & & \ddots & \vdots \\ \tau_{r0} & \cdots & \cdots & \tau_{rr} \end{bmatrix}\right)^{-1} \cdots \\
&\cdots\left(\underbrace{\begin{bmatrix} \delta_{00} & 0 & 0 \\ 0 & \ddots & 0 \\ \vdots & 0 & \delta_{(4s+1)(4s+1)} \\ 0 & 0 & 0 \end{bmatrix}}_{r\times(4s+1)}\begin{Bmatrix} b_0 \\ b_1 \\ \vdots \\ b_{4s+1} \end{Bmatrix} + \underbrace{\begin{bmatrix} \delta_{00} & 0 & 0 \\ 0 & \ddots & 0 \\ \vdots & 0 & \delta_{(4s+1)(4s+1)} \\ 0 & 0 & 0 \end{bmatrix}}_{r\times(4s+1)}\begin{Bmatrix} c_0 \\ c_1 \\ \vdots \\ c_{4s+1} \end{Bmatrix}\right)
\end{aligned} \tag{6.33}$$

The lateral center of gravity polynomial chaos model is shown in equation (6.34).

$$\begin{gathered}\left\{\begin{matrix} y_0 \\ y_1 \\ \vdots \\ y_r \end{matrix}\right\} = T\left(\begin{bmatrix} \psi_{00} & \psi_{01} & \cdots & \psi_{0r} \\ \psi_{10} & \psi_{11} & & \vdots \\ \vdots & & \ddots & \vdots \\ \psi_{r0} & \cdots & \cdots & \psi_{rr} \end{bmatrix} + \begin{bmatrix} \gamma_{00} & \gamma_{01} & \cdots & \gamma_{0r} \\ \gamma_{10} & \gamma_{11} & & \vdots \\ \vdots & & \ddots & \vdots \\ \gamma_{r0} & \cdots & \cdots & \gamma_{rr} \end{bmatrix} + \begin{bmatrix} \chi_{00} & \chi_{01} & \cdots & \chi_{0r} \\ \chi_{10} & \chi_{11} & & \vdots \\ \vdots & & \ddots & \vdots \\ \chi_{r0} & \cdots & \cdots & \chi_{rr} \end{bmatrix} + \begin{bmatrix} \tau_{00} & \tau_{01} & \cdots & \tau_{0r} \\ \tau_{10} & \tau_{11} & & \vdots \\ \vdots & & \ddots & \vdots \\ \tau_{r0} & \cdots & \cdots & \tau_{rr} \end{bmatrix}\right)^{-1} \cdots \\ \cdots\left(\underbrace{\begin{bmatrix} \delta_{00} & 0 & 0 \\ 0 & \ddots & 0 \\ \vdots & 0 & \delta_{(4s+1)(4s+1)} \\ 0 & 0 & 0 \end{bmatrix}}_{r\times(4s+1)} \left\{\begin{matrix} c_0 \\ c_1 \\ \vdots \\ c_{4s+1} \end{matrix}\right\} + \underbrace{\begin{bmatrix} \delta_{00} & 0 & 0 \\ 0 & \ddots & 0 \\ \vdots & 0 & \delta_{(4s+1)(4s+1)} \\ 0 & 0 & 0 \end{bmatrix}}_{r\times(4s+1)} \left\{\begin{matrix} d_0 \\ d_1 \\ \vdots \\ d_{4s+1} \end{matrix}\right\}\right)\end{gathered} \tag{6.34}$$

X_n and Y_n now are in analytical expressions that can be used to find distribution of the center of gravity. From this analytical expression critical information can be determined without plotting the distribution, which can prevent excess computational time. The distribution is often of interest though, so it can be plotted using the same method as before.

6.3 Polynomial Chaos Results for Multiple Uncertain Inputs

The polynomial chaos model can now be applied to the 8-post rig. This section will apply results from the moved lump mass test in chapter 3 to two different models to create PCE simulation results. The first will be a two uncertain input beta distribution model. The second will be a four uncertain input uniform distribution model.

6.3.1 Simulation Results – 2 Uncertain Inputs

The data collected in the moved mass tests can be analyzed with either a uniform or a beta distribution. The uniform distribution is used in the case where no information other than the range of the distribution is known. The beta distribution is used if it is necessary to use the distribution used in the first distribution test. This distribution is not likely to be the case for the moved lumped mass test since the test conditions are different. The beta distribution and the uniform distribution will be used for this simulation to show that the PCE model can work for any distribution.

The uncertain force inputs that are used for this test are the same ones used in the example from section 6.1.1, F_1 and F_4. First, the polynomial chaos coefficients must be input into the model. The method for finding these coefficients from real data was discussed in section 4.4. The coefficients used for this test are given in the following table.

Table 6.2: Beta Distribution Polynomial Chaos Coefficients for Moved Lump Mass Tests

	Polynomial Coefficient Values Test 1				
Wheel Location	**Zero order**	**1st order**	**2nd order**	**3rd Order**	**4th order**
LR (F1)	509.3	4.93	0.5	0	0
RR (F4)	601.5	10.97	0.25	-0.1	0

	Polynomial Coefficient Values Test 2				
Wheel Location	**Zero order**	**1st order**	**2nd order**	**3rd Order**	**4th order**
LR (F1)	726.73	5.73	0.5	0	0
RR (F4)	875.1	10.71	0.25	-0.1	0

	Polynomial Coefficient Values Test 3				
Wheel Location	**Zero order**	**1st order**	**2nd order**	**3rd Order**	**4th order**
LR (F1)	678.87	4.57	0.5	0	0
RR (F4)	786.37	12	0.25	-0.1	0

	Polynomial Coefficient Values Test 4				
Wheel Location	**Zero order**	**1st order**	**2nd order**	**3rd Order**	**4th order**
LR (F1)	586.07	6.44	0.5	0	0
RR (F4)	691.57	14.93	0.25	-0.1	0

The force from the more accurate scales was used in the estimation of the other two force inputs, F_2 and F_3. This eliminates the uncertainty in the other forces from these simulations and distortion in the simulation results. It should be noted that these load measurements may not be the true values due to stiction in the shocks and the aero loaders.

The polynomial chaos expansion model was ran with these inputs. The results were plotted in a two dimensions since the distribution can now be placed on more than a line. The polynomial chaos and Monte Carlo simulation are shown in the following plots. The polynomial chaos model was taken to the fifth order for a total of twenty one polynomials in the expanded series.

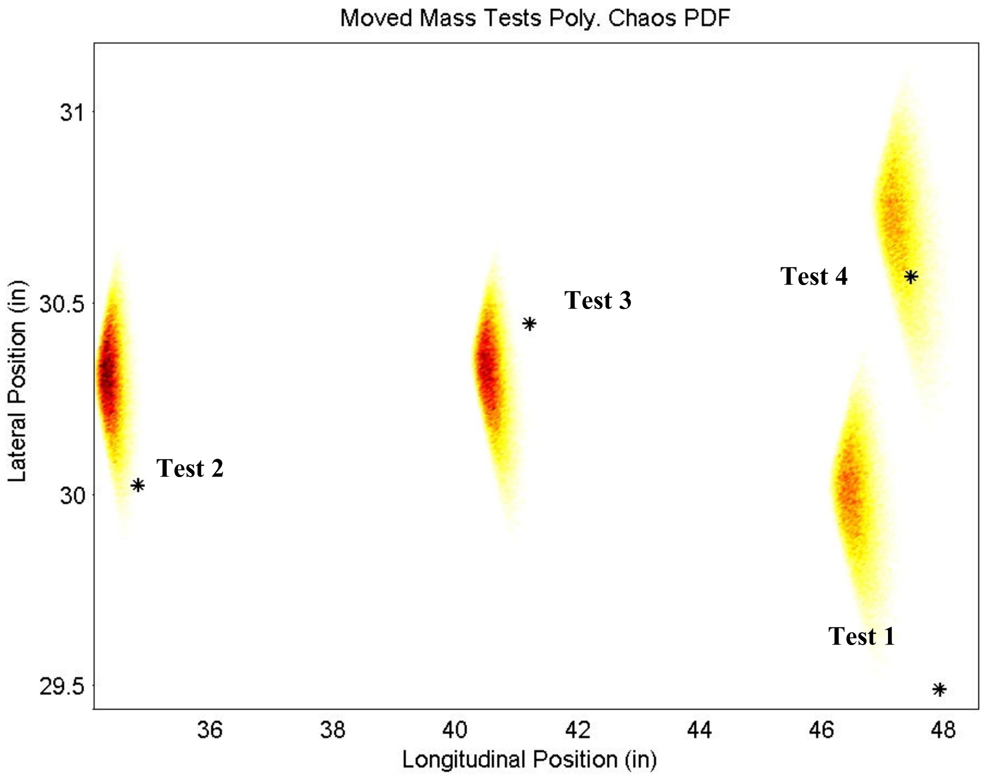

Figure 6.2: Polynomial Chaos Moved Lump Mass Test - Beta Distribution

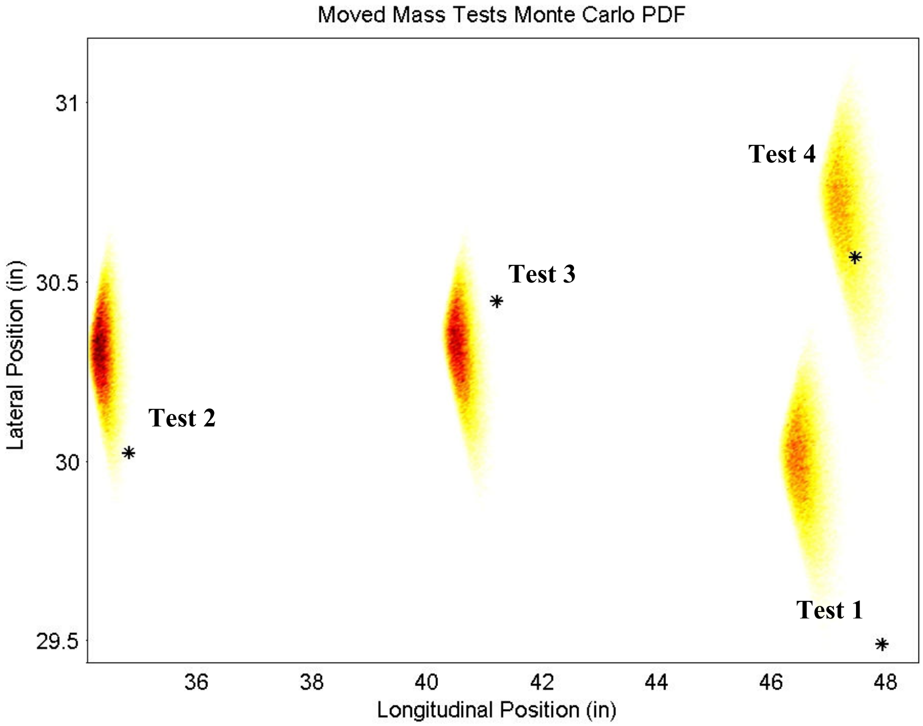

Figure 6.3: Polynomial Chaos Moved Lump Mass Test - Beta Distribution

The polynomial chaos and Monte Carlo distributions are nearly the same, once again confirming that polynomial chaos Galerkin method provides a correct distribution of the data by following the standard Monte Carlo. Figure 6.2 shows that the center of gravity from the Longacre Computerscales DX does not fall within the polynomial chaos distribution for tests 1, 2, or 3. Clearly there is more uncertainty in the system than has been accounted for in the polynomial chaos model. This is to be expected since the aero loaders and shock stiction effects were not considered in the range. Given this information, the range is not too far from the scales center of gravity estimate. Therefore, if the polynomial chaos estimate was created to estimate the total uncertainties in the vehicle, aero loader, and load measurement system this error could be accounted for.

An advantage of the Galerkin method is the analytical equation it provides. provides information without requiring the distribution to be plotted. The first ten of twenty-one coefficients for the longitudinal direction and the lateral direction are given in the following table.

Table 6.3: Polynomial Chaos Coefficients Beta Distribution

n	Xn	Yn
1	48.5033	35.64981
2	-0.120089	-0.086021
3	-0.01171	-0.007182
4	0.000107	6.36E-05
5	5.95E-06	3.03E-06
6	-1.01E-07	-5.00E-08
7	-0.266905	-0.160665
8	-0.003939	-0.002694
9	0.002509	0.001541
10	-5.04E-05	-2.53E-05

These coefficients show the impact from each polynomial coefficient which can be seen by multiplying them by the expanded polynomials. This allows the determination of necessary information such as the range in either direction without plotting the distribution. This is done the same way as the range was used to determine the coefficients in chapter four, by using the boundary conditions.

It is useful to compare the beta distribution results to the uniform distribution results. The uniform distribution is shown in Figure 6.4.

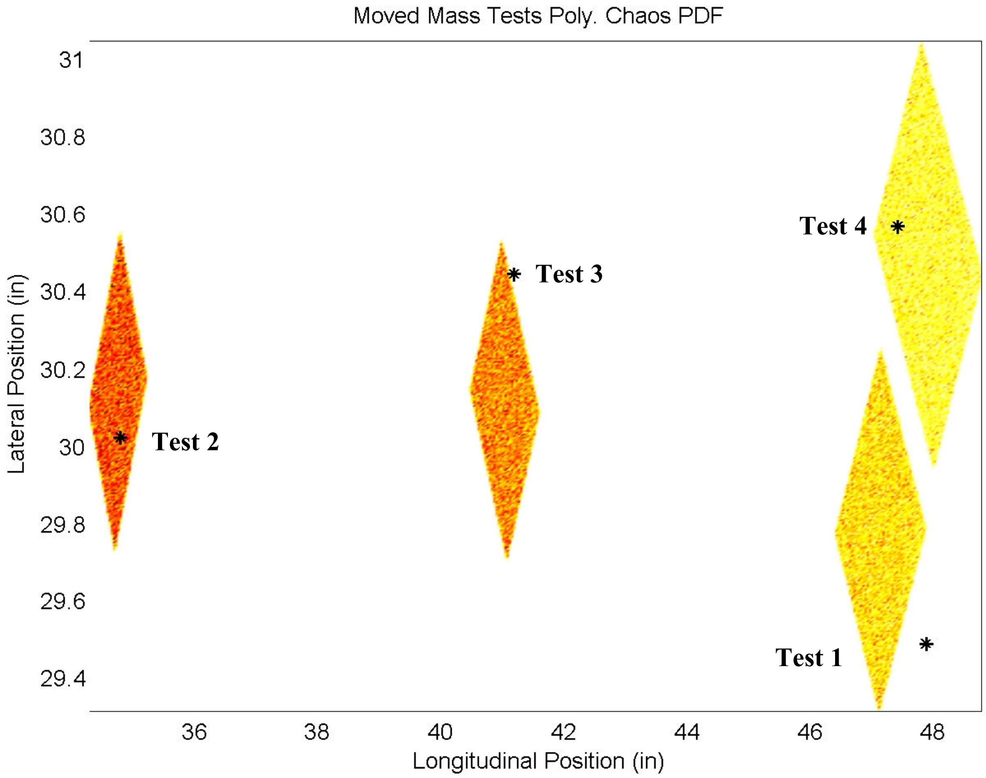

Figure 6.4: Polynomial Chaos Moved Mass Test – Uniform Distribution

The uniform distribution may provide a better estimate of the distribution than the beta distribution for the moved mass test because it is not making any assumptions about the shape of the distribution. Therefore it simply finds the area of probability. The results from the scales in test two and four stay within the area given in the uniform distribution. Test one is still roughly a quarter inch outside the distribution in the longitudinal direction and test three is millimeters outside the distribution. These errors could be accounted for if the uncertainties from the other two wheels were included. The center of gravity uncertainty in the longitudinal direction varies two inches while the CG uncertainty in the lateral direction is one inch. These are within 2% of the total wheelbase or track for either direction.

The center of gravity distribution area from the two uncertain input's is shaped like a rhombus. The edges of the rhombus are parallel to the lines that connect the wheels diagonal to each other. This is due to a change in wheel load in a specific wheel impacts the center of gravity along that diagonal line. Since there are two uncertain inputs, a rhombus shape is created. A more realistic center of gravity distribution is created when all four wheel loads are uncertain

6.3.2 Simulation Results – 4 Uncertain Inputs

This section compares the experimental data to the PCE models. First the distribution data is used through the Monte Carlo method and compared to uniform and beta distributions of the PCE model. Then the PCE model is used to model the moved mass test.

6.3.2.1 Distribution Test Results- Experimental Data versus PCE Model

The ultimate goal is a PCE simulation with all four wheel inputs uncertain. A polynomial chaos model with a uniform wheel load distribution was created to accomplish this task. Since the distribution is uniform, only the average and range values are required to define the uncertainty distribution of the load cells.

The experimental data collected in the distribution test is directly compared to the polynomial chaos expansion model. Monte Carlo method is used to present the experimental data. A uniform distribution will be used to model the distribution data for the polynomial chaos model; the PCE coefficients are given in the following table.

Table 6.4: PC Coefficients to Define Uniform Distribution for Experimental Data

	Order of PC Coefficients	
Wheel	**0**	**1**
LF	498	12
RF	548	6
LR	833	30
RR	746	18

The zeroth order coefficient is based on the average and the first order coefficient is based on the range for each wheel distribution. The results of the four uniformly distributed inputs are shown in Figure 6.5.

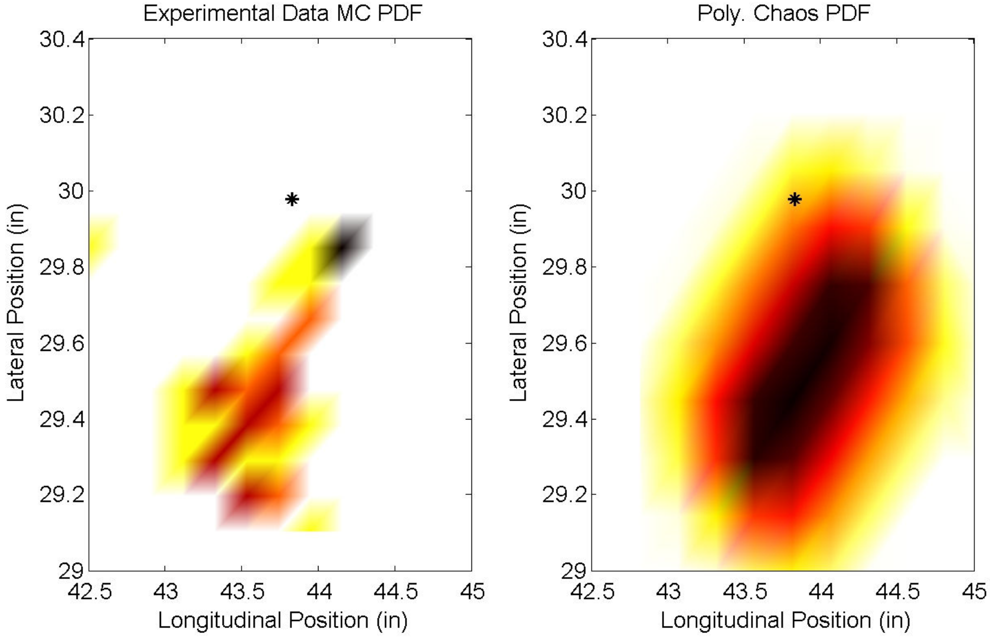

Figure 6.5: Experimental Data PDF versus Uniform Polynomial Chaos Model

The experimental data is shown on the left of Figure 6.5. Fifty experimental data points were used to create the Monte Carlo from the distribution test presented in section 4.2. This creates a rough distribution, but a trend can be attained. The black point represents the CG location measured from the portable scales. The experimental data shows that the highest probability is along the center of the diagonal. There also seems to be a general higher probability in the lower left end around the location (43.6”, 29.4”). At the upper right end of this distribution (44.2”, 29.9”) is the highest probability location. This is due to the bimodal RF and LR data collected in the distribution test shown in Figure 4.7: Experiment Data vs Polynomial Chaos Estimated Distributions The experimental data has one outlier at (42.5”, 29.9”). The distribution on the right is created from the polynomial chaos model with uniform load inputs. This distribution follows the real data in that the highest probability is down the center of the diagonal. The polynomial chaos expansion model appears to have a higher uncertainty area. Since there are four uncertain inputs, fifty data points is not enough to draw a conclusive distribution for the many possible combinations of the uncertain inputs.

In section 4.2 a beta distribution was chosen to represent the experimental data with the coefficients given in Table 4.3. This distribution is also compared to the experimental data in Figure 6.6.

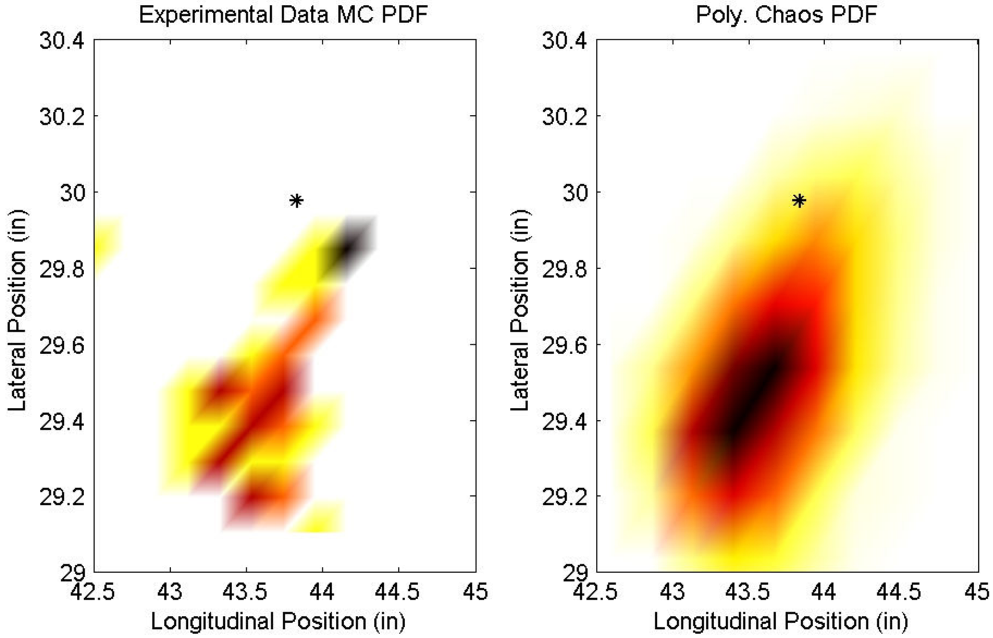

Figure 6.6: Experimental Data PDF versus Beta Distributed Polynomial Chaos

The beta distribution has some of the same characteristics as the experimental data. The PCE model has greater uncertainty in the lower left end of the diagonal centered at (43.5”, 29.5”). If the high probability location at (44.2”, 29.9”) is considered mostly random chance, the beta distribution better represents the experimental data. This assumption resulted from choosing the beta distribution as seen in section 4.2.

The main goal of this section is to show that the PCE model can accurately represent experimental data. This goal was accomplished in the distribution results presented in Figure 6.5 and Figure 6.6. The moved mass tests are presented in the following sections to show that the PCE model can be also be applied to that situation.

6.3.2.2 Moved Mass Test Results- PCE Model

This section applies the PCE model to the moved mass distributions to show that the model can be applied to multiple loads producing accurate results. The PCE model is derived in chapter 6.2. The two equations used in the PCE model for moved mass tests are equations (6.33) and (6.34). The inputs are first order polynomials since the distribution is assumed to be uniform and the outputs are third order polynomials. Four parameters to the third order create thirty-five polynomials as calculated from equation (6.1). The result is a hundred thousand point probability distribution, shown in the following plot.

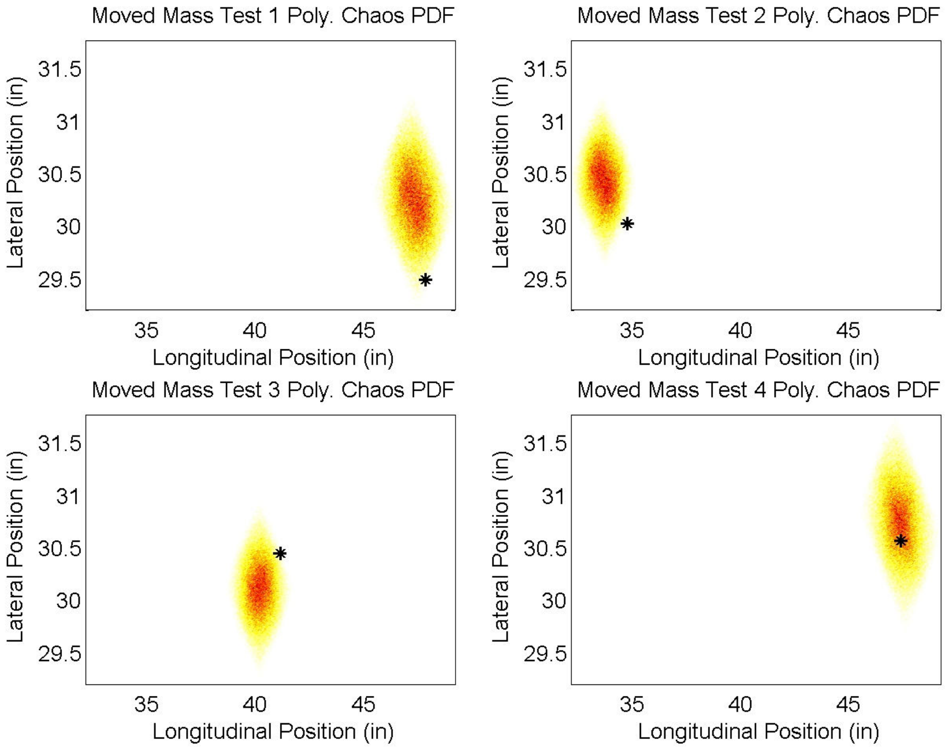

Figure 6.7: Polynomial Chaos Simulation for Moved Mass Test – 4 Uniform Uncertain Inputs

Figure 6.7 shows that the distributions for four uniform uncertain inputs create a more natural probability distribution than those shown from two-uncertain parameters. The center of the distribution has the highest probability, and the probability decreases as it approaches the outside. It can also be seen that the center of gravity found by the Longacre Computerscales DX either falls within or just outside the four moved mass distributions. All the center of gravity points from the Longacre Computerscales DX would be included in the distribution if the uncertainty between records was included in the polynomial chaos code. These uncertainties were averaged out, but this was not done for the Longacre Computerscales DX because only one record was taken for each moved mass distribution using these scales. Therefore, it is possible that the stiction in the vehicle shocks or differences in the aero loaders from test to test could cause these to be at error as well.

In section 6.3.1, it was presented that the edges of the two uncertain parameters are parallel to the lines that connect the wheels diagonal to each other. It can also be shown that for four uncertain parameters there is an area where there is a chance that the CG can lay within a rhombus shaped area. The distribution for four uncertain parameters has the greatest probability in the center and decreases towards the outside as shown in Figure 6.8. This distribution is circular in the center, but the area of the probability is rhombus shaped.

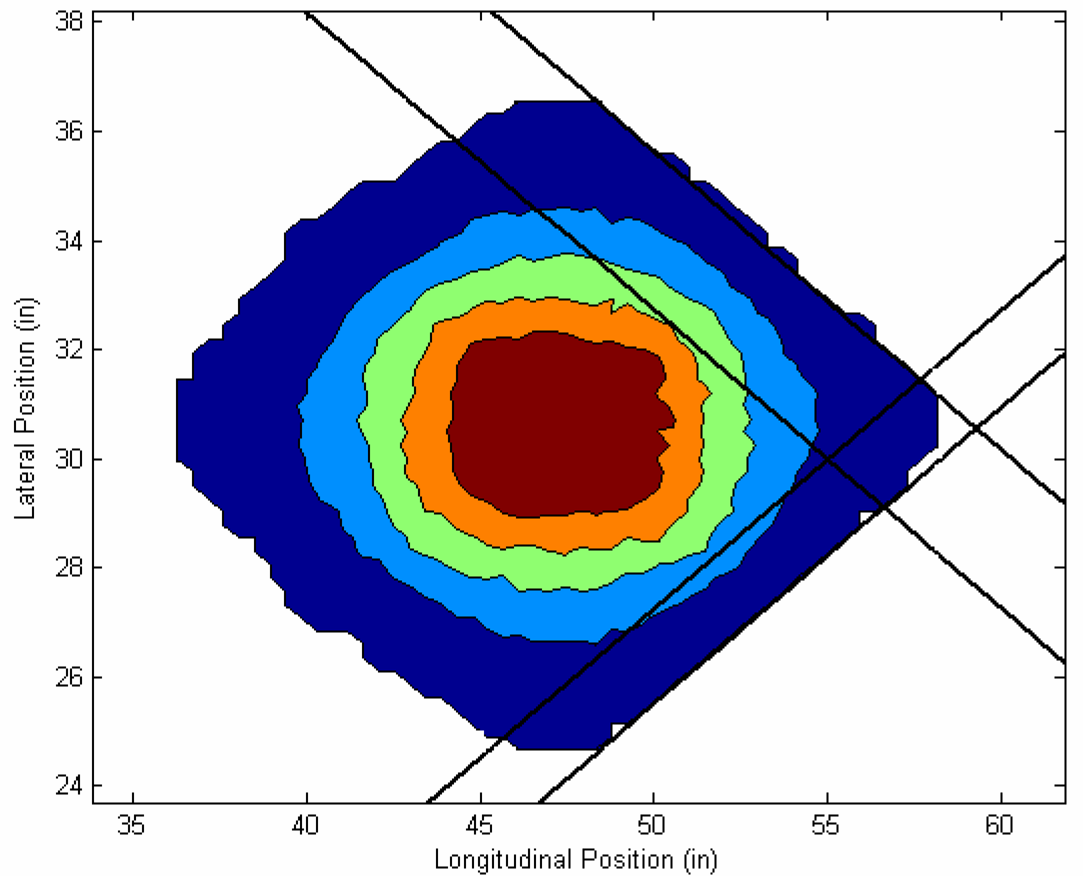

Figure 6.8: PDF with Diagonal Edge Lines

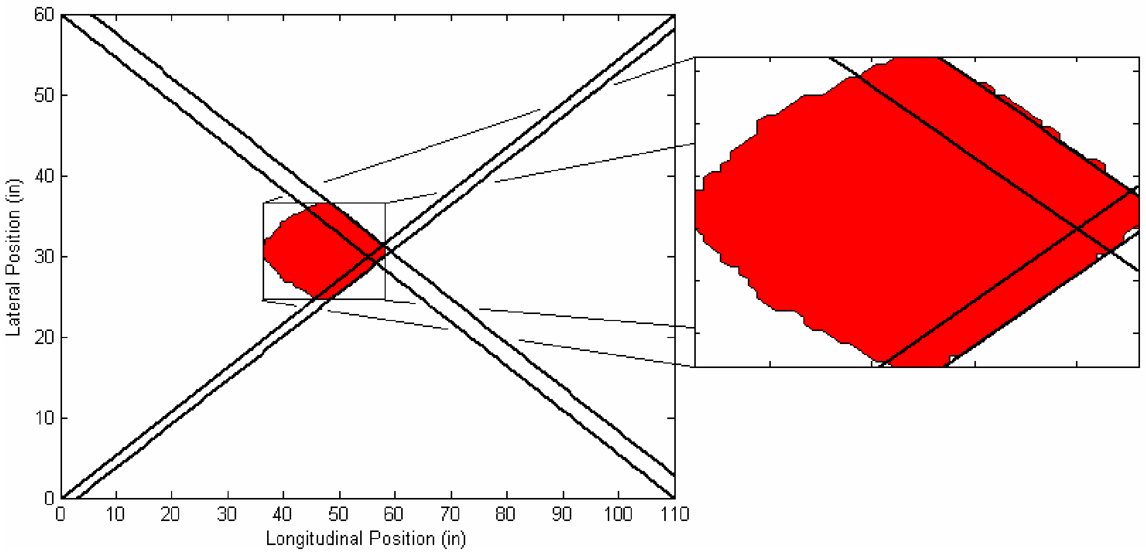

Figure 6.9: Area of Probability Edges versus Diagonal Wheel Line

The red rhombus area in Figure 6.9 shows the probability area in a stretched PCE model. For each diagonal direction there are two lines. The first is a line that connects the diagonal wheels together and the other black line shows the edge of the rhombus. It is seen that this diagonal line is parallel to the other diagonal line. This effect is directly related to the center of gravity equations and the impact of the uncertainties.

7. CONCLUSIONS AND RECOMMENDATIONS

7.1 Conclusions

The goal of this thesis was to present how polynomial chaos expansion (PCE) can be used to analyze the uncertainty in calculating the lateral and longitudinal center of gravity for a vehicle from static load cell measurements. This uncertainty is propagated through the center of gravity equation and impacts the uncertainty of the CG location. It has been shown that the uncertainty in the load measurement system and methods can cause significant error in determining the center of gravity of a vehicle. Derived from the Galerkin method, the center of gravity equation provides an analytical set of equations to define the distribution through polynomials.

The center of gravity distribution has also been plotted and compared to the Monte Carlo simulation. It has been shown that the polynomial chaos model and Monte Carlo methods provide nearly identical solutions. In addition, the polynomial chaos model provides an analytical solution for the model. This allows the determination of which sources of uncertainty have the largest impact on the solution by analyzing the equation. The Monte Carlo simulation would require multiple simulations to determine a subjective view of each uncertainties impact on the process and final solution.

The uncertainty in the load measurement system was defined in the distribution test. From this test, it was shown that the beta distribution most accurately defines the uncertainty distribution. However, the aero loaders impacted the distribution for the moved mass tests. How? ; therefore, the assumptions of the beta distribution could not used for the moved mass test. A method for adjusting a distribution from test to test was proposed based on the range of the output. This method can be applied to many types of distributions because it requires the minimum and maximum value of the collected data, the corresponding range of the random variable and a previously determined uncertainty distribution. This method allows one to adapt a distribution that maintains most of its shape but may vary over its useful range.

7.2 Recommendations

This study did not fully identify the sources of the uncertainty in the distribution. The amount of uncertainty caused by the aero loaders, shocks in the vehicle, shift in the load cell system between wheel pan loadings and general load cell measurement system was not determined. A test that could isolate various sources of the uncertainty would need to be conducted to determine these uncertainties. To find uncertainties in the load cell measurement system, a known mass should be used to determine the variance under normal loading. This mass could be moved around the wheel pan to show the impact the loading has on the four load sensors within each wheel pan. This mass would need to be of significant amount, greater than 400 pounds, to compare to the load a vehicle would create. The advantage of this test is that it would remove the aero loaders, and the possible shift in the weight distribution of a vehicle due to the vehicle's suspension. This would determine if the lack of repeatability in some of the load cell measurements is a result of the load measurement system, if it's from the vehicle shifting weight or the aero loaders.

This study has derived the polynomial chaos expansion using the Galerkin method. A PCE model using the collocation method should be derived if a faster model is required. A collocation model can use fewer points to represent the distribution and find a solution than the Galerkin method or Monte Carlo methods. It can greatly reduce the computational time to resolve the problem. However, it does not provide an analytical solution to the center of gravity equation, and leaves the possibility of an incorrect solution to be found if the collocation points are chosen incorrectly.

8. REFERENCES

1. Milliken W. F., Milliken D. L., *Race Car Vehicle Dynamics,* Society of Automotive Engineers Inc., Warrendale, PA, 1995.
2. Bixel R., Heydinger G., Durisek N., Guenther D., Novak J., “Developments in Vehicle Center of Gravity and Inertial Parameter Estimation and Measurement,” *SAE Technical Paper Series, No. 950356*, Warrendale, PA, 1995.
3. Shapiro S., Dickerson C., Arndt S., Arndt M., Mowry G., “Error Analysis of Center-of-Gravity Measurement Techniques,” *SAE Technical Paper Series, No. 950027*, Warrendale, PA, 1995.
4. Mango N., “Measurement & Calculation of Vehicle Center of Gravity Using Portable Wheel Scales,” *SAE Technical Paper Series, No. 2004-01-1076*, 2004.
5. Xintong Z., Hongzhou J, Shutao Z., Junwei H., “Development of High Precision Gravity Center Position Measurement System for Large Heavy Vehicles,” *International Society for Optical Engineering*, 2005.
6. Gillespie T., *Fundamentals of Vehicle Dynamics,* Society of Automotive Engineers Inc., Warrendale PA, 1992.
7. Sandu A., Sandu C., Ahmadian M., “Modeling Multibody Systems with Uncertaintes. Part I: Theoretical and Computational Aspects,” *Multibody System Dynamics*, Vol 15, No. 4, May 2006.
8. Ghanem R., Spanos P., *Stochastic Finite Elements: A Spectral Approach*, Dover Publications, Inc., Mineola, NY, 1991.
9. Xiu D., Karniadakis G., “The Weiner-Askey Polynomial Chaos for Stochastic Differential Equations,” *SIAM J. Sci. Comput*., 2002.
10. Southward S.C., “Real-Time Parameter ID Using Polynomial Chaos Expansions,” *ASME*, November 2007.
11. Ghanem R., Spanos R., “Spectral Stochastic Finite-Element Formulation for Reliability Analysis,” *Journal of Engineering Mechanics*, Vol 117, No. 10, October 1991.

12. Bulychev Y., Bulycheva Y., “Efficient Realization of the Galerkin Method in View of New Properties of Chebyshev Polynomials,” *Cybernetics and Systems Analysis,* Vol. 40, No. 6, 2004.
13. Stefanou G., Papadrakakis M., “Assessment of Spectral Representation and Karhunen-Loeve Expansion Methods for the Simulation of Gaussian Stochastic Fields,” *Comput. Methods Appl. Mech. Engrg.*, Jan 2007.
14. Blanchard E., Sandu A., Sandu C., “A Polynomial-Chaos-Based Bayesian Approach for Estimating Uncertain Parameters of Mechanical Systems,” *ASME International Design Technical Conferences, No. DETC2007-34600*, 2007.
15. Huang S., Mahadevan S., Rebba R., “Collocation-based Stochastic Finite Element Analysis for Random Field Problems,” *Probablistic Engineering Mechanics*, 2007.
16. Matthies G., Keese A., “Galerkin Methods for Linear and Nonlinear Elliptic Stochastic Partial Differential Equation,” *Computer Method in Appl. Mech. Engrg.*, May 2004.
17. Kallenbach R., “Identification Methods for Vehicle System Dynamics,” *Vehicle System Dynamics*, 1987.
18. Sachdeva S., Nair P., Keane A., “Hybridization of Stochastic Reduced Basis Methods with Polynomial Chaos Expansions,” *Probablistic Engineering Mechanics*, September 2005.
19. Longacre, http://www.longacreracing.com/, website, Monroe, WA, 2008.

APPENDIX

Appendix A - Analytical Integration Matlab Code

```
function [deltan,deltaijn,deltakn,deltain]=delta2leg(s,order)
%s=order of inputs
%order=order of output

syms x1 x2  %symbolic
x=[x1,x2];

%Legendre polynomials
for i=1:2
phi(i,:)=[1, x(i), (3/2*(x(i).^2)-1/2), (5/2)*(x(i).^3)-(3/2*x(i)),
(1/8)*(35*(x(i).^4)-30*(x(i).^2)+3)...
    (1/8)*(63*(x(i).^5)-70*(x(i).^3)+15*x(i)), (1/16)*(231*x(i).^6-
315*(x(i).^4)+105*(x(i).^2)-5),...
    (1/16)*(429*x(i).^7-693*x(i).^5+315*x(i).^3-35*x(i))...
    (1/128)*(6435*x(i).^8-12012*x(i).^6+6930*x(i).^4-1260*x(i).^2+35)];
end
phi1=phi(1,:);
phi2=phi(2,:);

x=[x1,x2];



%Defining PHI from phi1 and phi2
PHI(1:order+1)=phi1(1:order+1);
PHI(order+2:2*order+1)=phi2(2:order+1);

k=2*order+1;
for j=2:order+1
    for i=2:order+1
        if ((i+j)<=(order+2))
            k=k+1;
            PHI(1,k)=phi1(i).*phi2(j);
        end
    end
end

r=length(PHI);

%Computing deltas
w1=1; %weighting function 1
w2=1; %weighting function 2
w=w1*w2; %total weighting function
for n=1:r
    for i=1:2*s+1
        for j=1:r
            phiijn(i,j,n)=PHI(i)*PHI(j)*PHI(n)*w;
```

```
            deltaijn(i,j,n)=int(int(phiijn(i,j,n),x(1),-1,1),x(2),-
1,1);
        end
    end
end

for i=1:r;
    PHIkn(i,i)=PHI(i)*PHI(i)*w;
    deltakn(i,i)=int(int(PHIkn(i,i),x(1),-1,1),x(2),-1,1);
end

%Integral of phi1(i)*phi1(n)
% deltain=zeros(length(phi3),r);
for i=1:r
    for n=1:2*s+1
        PHIin(i,n)=PHI(i)*PHI(n)*w;
        deltain(i,n)=int(int(PHIin(i,n),x(1),-1,1),x(2),-1,1);
    end
end

%Integral of PHI(n)
for i=1:r;
    deltan(i,1)=int(int(PHI(i)*w,x(1),-1,1),x(2),-1,1);
end

deltan=double(deltan);
deltaijn=double(deltaijn);
deltakn=double(deltakn);
deltain=double(deltain);

return
```

Appendix B – Legendre and Jacobian Polynomials

$$\phi_n(\zeta) = \left(\frac{1}{2^n\left(n!\right)}\right)\frac{\partial^n}{\partial\zeta^n}\left(\zeta^2 - 1\right)^n = \begin{cases} 1 & n=0 \\ \zeta & n=1 \\ \frac{1}{2}\left(3x^2 - 1\right) & n=2 \\ \frac{1}{2}\left(5x^3 - 3x\right) & n=3 \\ \frac{1}{8}\left(35x^4 - 30x^2 + 3\right) & n=4 \\ \frac{1}{8}\left(63x^5 - 70x^3 + 15x\right) & n=5 \\ \frac{1}{16}\left(231x^6 - 315x^4 + 105x^2 - 5\right) & n=6 \\ \frac{1}{16}\left(429x^7 - 693x^5 + 315x^3 - 35x\right) & n=7 \end{cases}$$

Figure B 1: Legendre Polynomials

$$\phi_n\left(\zeta\right) = \begin{cases} 1 & n=0 \\ \frac{3}{2}\left(1+3\zeta\right) & n=1 \\ \frac{1}{4}\left(-1+30\zeta+55\zeta^2\right) & n=2 \\ \frac{1}{4}\left(-7-11\zeta+99\zeta^2+143\zeta^3\right) & n=3 \\ \frac{3}{16}\left(-1-68\zeta-78\zeta^2+364\zeta^3+455\zeta^4\right) & n=4 \\ \frac{7}{8}\left(2-65\zeta^2-65\zeta^3+195\zeta^4+221\zeta^5\right) & n=5 \\ \frac{7}{16}\left(1+38\zeta+15\zeta^2-460\zeta^3-425\zeta^5+969\zeta^6\right) & n=6 \\ \frac{9}{16}\left(-3+5\zeta+165\zeta^2+85\zeta^3-1105\zeta^4-969\zeta^5+1615\zeta^6+1615\zeta^7\right) & n=7 \end{cases}$$

Figure B 2: Jacobian Polynomials for Beta (5,2) Distribution

Appendix C – PCE Coefficients for Moved Mass Test

Table C 1: Moved Mass Polynomial Coefficients

	Polynomial Coefficient Values Test 1				
Wheel Location	**1st order**	**2nd order**	**3rd order**	**4th order**	**5th order**
LF	449.63	6.986	0.25	0.05	0
RF	371.03	6.953	0.25	0	0
LR	509.3	4.93	0.5	0	0
RR	601.5	10.97	0.25	-0.1	0

	Polynomial Coefficient Values Test 2				
Wheel Location	**1st order**	**2nd order**	**3rd order**	**4th order**	**5th order**
LF	399.17	5.164	0.25	0.05	0
RF	283.23	5.87	0.25	0	0
LR	726.73	5.73	0.5	0	0
RR	875.1	10.71	0.25	-0.1	0

	Polynomial Coefficient Values Test 3				
Wheel Location	**1st order**	**2nd order**	**3rd order**	**4th order**	**5th order**
LF	472.23	4.19	0.25	0.05	0
RF	354.23	7.22	0.25	0	0
LR	678.87	4.57	0.5	0	0
RR	786.37	12	0.25	-0.1	0

	Polynomial Coefficient Values Test 4				
Wheel Location	**1st order**	**2nd order**	**3rd order**	**4th order**	**5th order**
LF	511.43	6.85	0.25	0.05	0
RF	452.9	6.78	0.25	0	0
LR	586.07	6.44	0.5	0	0
RR	691.57	14.93	0.25	-0.1	0

Appendix D – X and Y PCE Coefficients for 4-Uncertain Uniform Input Model

Table D 1: X_n Basis Functions for Moved Mass Simulations

Xn	Basis Functions Test 1	Basis Functions Test 2	Basis Functions Test 3	Basis Functions Test 4
0	47.3962	33.7441	40.2657	47.4163
1	-0.3789	-0.2564	-0.2612	-0.3943
2	0.7264	0.6272	0.5076	0.6177
3	0.5586	0.5062	0.5482	0.4705
4	-0.3651	-0.2156	-0.3031	-0.4919
5	-0.0014	-0.0027	-0.0014	-0.0012
6	0	0	0	0
7	-0.0056	-0.0034	-0.0025	-0.0041
8	0.0001	0	0	0
9	0	0	0	0
10	0	0	0	0
11	-0.0011	-0.0021	-0.0015	-0.0009
12	0	0	0	0
13	-0.013	-0.0083	-0.008	-0.0093
14	0.0001	0.0001	0.0001	0.0001
15	0.0002	0.0001	0.0001	0.0001
16	-0.0033	-0.0022	-0.0029	-0.0024
17	0	0	0	0
18	0.0001	0.0001	0.0001	0.0001
19	0	0	0	0
20	0.002	0.0013	0.0011	0.0022
21	0.0058	0.0033	0.0039	0.0082
22	0	0	0	-0.0001
23	-0.0014	-0.0022	-0.0016	-0.0016
24	0	0	0	-0.0001
25	0.0001	0	0	0.0001
26	-0.001	-0.0018	0	0
27	0	0	0	0
28	0.0001	0.0001	0.0001	0.0001
29	0	0	0	0
30	0.0019	0.0009	0.0015	0.0034
31	0	0	0	0.0001
32	0	0	0	0
33	0	0	0	0
34	0	0	0	0

Table D 2: Y_n Basis Functions for Moved Mass Simulations

Yn	Basis Functions Test 1	Basis Functions Test 2	Basis Functions Test 3	Basis Functions Test 4
0	30.2478	30.4338	30.1183	30.7472
1	-0.2419	-0.2313	-0.1954	-0.2557
2	-0.351	-0.2503	-0.2192	-0.3035
3	0.2654	0.1963	0.2349	0.2199
4	0.2292	0.1889	0.2249	0.3035
5	0.0056	0.0038	0.0028	0.005
6	0	0	0	0
7	0.0027	0.0014	0.0011	0.002
8	-0.0001	0	0	0
9	0	0	0	0
10	0	0	0	0
11	0	0	0	0.0001
12	0	0	0	0
13	0	0	0	0.0001
14	0	0	0	0
15	0	0	0	0
16	-0.0016	-0.009	-0.0012	-0.0011
17	0	0	0	0
18	0	0	0	0
19	0	0	0	0
20	0.0013	0.0012	0.0008	0.0014
21	0	0	0	0.0001
22	0	0	0	0
23	0	0	0	0.0002
24	0	0	0	-0.0001
25	0	0	0	0
26	-0.0041	-0.0025	-0.0035	-0.0046
27	0	0	0	0
28	0	0	0	0
29	0	0	0	0
30	-0.0012	-0.0008	-0.0011	-0.0021
31	0	0	0	0
32	0	0	0	0
33	0	0	0	0
34	0	0	0	0